Shaping Inputs to Reduce Vibration in Flexible Space Structures

Kenneth Wonuk Chang

This blank page was inserted to preserve pagination.

SHAPING INPUTS TO REDUCE VIBRATION IN FLEXIBLE SPACE STRUCTURES

by

KENNETH WONUK CHANG

B.S., Mechanical Engineering
Stanford University
(June 1990)

Submitted to the Department of Mechanical Engineering
in Partial Fulfillment of the Requirements for the Degree of

MASTER OF SCIENCE
IN MECHANICAL ENGINEERING

at the

MASSACHUSETTS INSTITUTE OF TECHNOLOGY
MAY 1992

iv

SHAPING INPUTS TO REDUCE VIBRATION IN FLEXIBLE SPACE STRUCTURES

by

Kenneth Wonuk Chang

ABSTRACT

Future NASA plans to launch large space structures solicit the need for effective vibration control schemes which can solve the unique problems associated with unwanted residual vibration in flexible spacecraft. In this work, a type of input command shaping called impulse shaping is examined. These shapers require only a simple model of the system and are fairly insensitive to parameter variations.

A theoretical background of impulse shaping is presented along with some insight into the methods of calculating multiple mode sequences. The Middeck Active Control Experiment (MACE), an MIT/NASA space shuttle experiment, is then described as the testbed for the experiments. A nonlinear simulation is used to verify the effectiveness of these shapers on a model of MACE. Finally, hardware experimental results are presented and analyzed.

Some conclusions were derived from the results of testing. First, it was found that the shaper was effective in canceling the slowest frequency of the structure, but was less successful in the higher modes. Second, large angle movements decreased the effective vibration cancellation. The nonlinearity involved with large angle movements causes the shaper to lose some of its effectiveness. Third, although methods exist which can increase the robustness of an impulse shaper, none were found to aid in canceling the effects of nonlinearities caused by large angle moves. Fourth, the bandwidth of the controller was found to be linked to the effectiveness of the shaper. A higher bandwidth produced more favorable results.

Although many of the inadequacies of impulse shapers when applied to complex nonlinear systems are discussed, it remains a very effective tool in controlling vibration in flexible space structures.

Thesis Supervisor: Warren P. Seering
                       Professor of Mechanical Engineering

ACKNOWLEDGMENTS

I have many things to be thankful for. Much of what I have received in the past two years has been directed through the talents of the people I'm surrounded by. This page can only act as a small symbol of the gratitude I feel for the people mentioned.

I have to start with my thesis advisor, Warren Seering. Thank you very much, Warren, for providing me with the right balance of supervision and autonomy I needed to finish my degree. You always seem to know exactly what to say when I need to hear it. I've learned much from you.

My education experience would have been cheated had it not been for the wacky group of guys in my research group at the AI lab. Brian Avery, Mike Caine, Andy Christian, Jim Hyde, Sarath Krishnaswamy, Whit Rappole, Lukas Ruecker, Tim Tuttle, and Erik Vaaler; thanks. Thanks for putting up with all my stupid questions and thanks for usually answering them. You're quite a bunch.

I am also in debt to the MACE research group at the Space Engineering Research Center. Prof. Ed Crawley, Dr. Dave Miller, Dr. Mathieu Mercadal, Erik Saarmaa, Mark Campbell, Dan Rey, Carlos Padilla, and Marco Quadrelli; thanks for taking me in and taking care of me. You guys really know what you're doing.

My family has been a constant source of faith and support throughout my years at school. I wouldn't be near where I am today without them. Mom, Dad, Bro, Sis, Bro-in-Law and my beautiful baby niece; I hope you realize how grateful I am to all of you. Hey Eryn, you're in the first chapter! Umma, Appa, I love you and this is for you. I also need to thank my friends John, Jooyee, and Agnes for helping me with the rough transition to Boston. Thanks guys, I wouldn't have made it without you.

TABLE OF CONTENTS

CHAPTER 5

CHAPTER 6

LIST OF FIGURES

7

8

LIST OF TABLES

INTRODUCTION

Chapter 1

1.1 Background

It's a common problem that we see all the time. From bad suspensions that make us carsick to the annoying blinds that flutter when the windows are open, vibration is present everywhere in our world. If we had the ability, we would all know how to control the vibration in these systems. Humans are amazingly good at manipulating things with an uncanny knowledge of the vibrational characteristics of structures. Watching my baby niece, I realized that even she knew how to shake her rattle to cause maximum vibration of the beads inside. If she could understand me, she could probably shake the rattle such that there would be no vibration inside also. The point is that humans have a basic knowledge of how to make things vibrate and how to stop them from vibrating. The only remaining hurdle is to build the tools to implement this knowledge.

With the advent of robotic manipulators in industrial applications and in space, control of vibration has become a focal point of much research in the engineering community. For a robot designed to do assembly in a manufacturing line, control of vibration is critical in both precision and in the amount of time required to do its job. A solution to the problem could save a company large sums of money on an annual basis. An example of vibration problems in space is the shuttle Remote Manipulator System which has its fundamental bending frequency in the 0.5Hz region. Having to wait for this vibration to settle after every move is a tremendous loss of time and money for the space program. As the links in manipulators become lighter and more flexible due to cost saving reasons, the need for efficient vibration control schemes looms larger.

In space structures, this is becoming more and more the case. With the high cost per unit of weight of sending payloads into outer space, the materials used in the space structures tend to be lighter, and thus more flexible. Moreover there are currently plans by NASA for building large space structures. The Space Station and the Earth Observing Satellite are two examples. The vibrations in these systems are a problem on a larger scale. The structural integrity becomes an issue when vibration is present. Nurre et al. [15] have given a comprehensive overview of the issues involved in controlling large spacecraft. They start with a definition of a large flexible space structure and go on to survey some of the modeling, frequency identification, and control issues in large structure dynamics. Vibration control of large space structures is the goal of the work presented here.

1.2 Input Shaping

There are two branches in the field of vibration control research. The first is feedback control where the algorithm uses the state of the current system to calculate the input. This is a well-researched field where new ideas are seen on a regular basis. The other type of vibration control is what I would call input shaping. These are generally open loop methods of vibration control that carefully manipulate the inputs into a system to reduce the resulting vibration. We are interested in the latter in this paper.

Input shaping can be further divided into two subcategories: those that work in real time, and those that do not. The latter type tends to be more computationally complex and have smoother profiles. Many examples of this type of shaping are given in the literature review below. These methods generate predetermined inputs which are designed to move a system from one point to another without exciting vibration. The ones that work in real time tend to be less computationally complex and can work for any arbitrary input. Some examples of this include lowpass filters, digital notch filters, and the subject of this thesis, impulse shaping.

The most common, and some may even say the best, method of input shaping is to use slow commands. Usually, this will erase most of the vibration incurred during faster moves. This would be a valid method always if time was not an issue. But it is. All the attempts at input shaping described below try to minimize the time it takes to move a system to a certain point without leaving any residual vibration. An input shaping algorithm always has to be measured against the cost in time delay as well as

its effectiveness. The bottom line for an input shaper is the time it takes for the system to settle down to an acceptable vibration level.

1.3 Literature Review

Some of the early work in input shaping includes Swigert [23], who showed ways to calculate torques on simple rotational structures which resulted in zero residual vibration. He started with a simple state space model and found waveforms that met the zero vibration terminal boundary conditions. He also included a penalty on residual amplitude that allowed limited errors in plant frequency identification. Aspinwall [2] used sine series to create forcing functions that cancel vibration in single degree of freedom undamped systems. By using a finite Fourier series expansion, he was able to find the coefficients to the sine series that minimize the frequency content over a wide range of frequencies. This was an effective method but was only considered for undamped systems and the forcing functions were lengthy. Farrenkopf [8] used Calculus of Variations to solve the optimal slewing profile problem with initial and final boundary conditions set. He found that on a simple one mode system, it is difficult to not excite the structural mode when $\omega t < 5$, where ω is the modal frequency and t is the total time of the move.

Meckl [12] did some similar work in generating smooth force profiles that are shaped to reduce energy levels at the modal frequencies. He used the sum of ramped sinusoids and chose the coefficients by minimizing the spectral magnitudes over a range of frequencies and the time of the move. He also developed profiles that are fundamental versine curves which can be

applied to velocity limited systems. A closed loop implementation of these methods was described where the force profiles are double integrated to generate reference position commands and fed forward.

Eisler, Segalman, and Robinett [6] have used recursive quadratic programming and a finite element model to generate approximate minimum time trajectories for a two link flexible robot. Boundary conditions were set on the end position, energy, straight-line tracking, and motor torque limits to optimize the parameters of the move. Their results showed good accuracy in tip tracking, and it was found interestingly that the calculated torque profiles were similar even for large variances in plant configuration and modal frequencies. Turner and Junkins [25] have looked at optimal single-axis reorientations of a structure with flexible arms. Necessary conditions stemming from Pontryagin's principle were applied to arrive at the move profiles. Also, an extension of the algorithm to include kinematic nonlinearities was presented.

Inverse dynamics is another method of input shaping that has been researched. Many recent textbooks describe the method of inverting the system model to calculate the required inputs for a given desired trajectory. Asada, Ma, and Tokumaru [1] present a technique that reduces the computation complexity. They use what they term a virtual rigid link coordinate system to simplify the boundary conditions that need to be set.

Prucz, Soong, and Reinhorn [18] present an interesting twist on the use of impulses in vibration control. In "Pulse Control," impulses are input into the system to limit the system response to a certain threshold level at all times. They propose an efficient algorithm to calculate the optimal times and amplitudes of these impulses to keep the vibration level low.

The pioneer of the impulse shaping method may arguably have been Smith [22]. Way back in 1958, he proposed what he called "Posicast Control." It requires that a step input be divided into two equal parts, the second half being delayed in time by half the period of the modal frequency. By doing this, the plant can be moved without exciting its resonant frequency. He also proposed a closed loop implementation of posicast control that could work to reject disturbances in the system. This, however, requires an exact model of the system and is not very robust to errors in system identification.

Singer [20] wrote the first authoritative work on the modern technology referred to as impulse shaping. He discovered a way to use the mathematics behind the response of second order systems to impulses to create real time filters that produce vibration reducing inputs. By setting the residual vibration amplitude to go to zero, he was able to generate sequences of impulses that did not excite the modal frequencies. Real time implementation was achieved through convolution of these impulses with any arbitrary input. The breakthrough in this technology was the ability to operate in the presence of errors in system parameter identification. He derived his method in both the frequency and time domains and presented experimental results that showed the method to be extremely effective in simple structures. He also did a thorough comparison study of the method to digital notch filters. He found that the impulse shaping method was superior in decreasing the amount of vibration and was also more robust to system parameter variations.

Hyde [10] introduced a method of calculating multiple mode impulse sequences through a direct solution method which decreases the total time length of Singer's sequences. Though more complex in computation, these

sequences had fewer impulses than the previous multiple mode sequences and had a time savings of 20-30%. He verified his results in both linear and non-linear simulations. Singhose [21] also proposed an extension to Singer's original method. He showed that more robustness can be obtained by specifying a tolerance level in vibration amplitude. By releasing the zero vibration constraint, a larger region of insensitivity can be achieved by modifying the basic three impulse sequence for one mode developed by Singer.

There have been a handful of papers written since the advent of impulse shaping by people who have successfully implemented the method. Christian [4] built a two link flexible robot, called the "Flexbot," which was specifically designed to study vibration control. He compared impulse shaping to slow acceleration moves and showed that impulse filtering is a more effective way to reduce vibration in systems with constant vibrational frequencies. Tzes, Englehart, and Yurkovich [26, 27] have experimented with an adaptive form of impulse shaping that uses frequency domain information from the plant to control systems with time varying frequencies. They use a real time frequency identification scheme to compute modal frequencies and update the spacing between impulses. By doing this, they were able to use the shorter two impulse sequences and achieved good robustness to variances in plant frequencies. Murphy and Watanabe [15] offer a digital analysis of the impulse shaping formulation and show that the digitized form is a class of notch filters that place zeroes to cancel the plant modal roots. They also propose an arbitrary sampling rate digital shaping filter that allows the implementation of these filters in varying frequency systems.

1.4 Overview of Thesis

The goal of my work is to answer some of the implementation issues involved in impulse shaping. Most of the past research has concentrated on theory and application to simple systems. Simulations have been done on more complex systems, but there still isn't enough experimental data to raise the necessary questions of implementation. A theoretician can be very confident about her design on paper, but there will always be unmodeled factors that arise when working in real hardware. This thesis will answer some of the questions that have to do with implementing impulse shaping on a complex structure.

A comprehensive overview of the impulse shaping theory is given in Chapter 2. I will go over Singer's equations and then cover the modifications made by Hyde and Singhose. Then, I will present a comparison of the different methods of computing multiple mode sequences. Some tradeoffs will be shown between Singer's convolution method and Hyde's direct solution method. I will end the chapter with some considerations in choosing the most efficient sequence for a multiple mode system.

Chapter 3 will reveal the testbed on which the experiments will take place. The Middeck Active Control Experiment (MACE) is a planned space shuttle mission project that will be shown to be an ideal platform on which to generate valuable data about the effectiveness of impulse shaping on complicated structures. I will describe the current hardware for the project and detail some control algorithms for the gimbal actuator.

Nonlinear simulation will be the topic of Chapter 4. DISCOS (Dynamics Interaction Simulation of Controls and Structures) will be used as the tool

for modeling and simulating an early version of the MACE hardware. Impulse shaping results for both open loop and closed loop runs will be shown.

Experimental results from the hardware will be presented in Chapter 5. A description of the flight objectives for impulse shaping will be explained to define the problem. In both frequency domain results and time domain results, impulse shaping will be shown to be very effective for small angle moves. Insensitivity curves will be compared from experimental to theoretical data. A further analysis will be presented concerning the non-linearities associated with large angle movements. Also, the involvement of the controller bandwidth in the effectiveness of shapers will be shown. I will show through these experiments that although impulse shaping can work very well in certain configurations, it does have its shortcomings as non-linearities arise.

Finally, in Chapter 6, I will reach some conclusions about all the data presented and look to the future with suggestions for both the MACE project and further research on impulse shaping.

THE TECHNOLOGY: IMPULSE SHAPING

Chapter 2

2.1 Introduction

This chapter deals with the theoretical basis of impulse shaping. The objective of this type of input shaping is to use a series of impulses to suppress the residual vibration of a dynamic system. By solving for a set of vibration constraint equations based on the response of systems to impulses, a sequence of unique impulses can be formulated which, when convolved with the input to a system, will suppress the resonant mode vibration. The following sections are meant to give a comprehensive overview of the algorithm for generating the sequences and to lend some insight into the method. The authors cited should be consulted for more detailed explanations.

THE TECHNOLOGY: IMPULSE SHAPING

Chapter 2

2.1   Introduction

This chapter deals with the theoretical basis of impulse shaping. The objective of this type of input shaping is to use a series of impulses to suppress the residual vibration of a dynamic system. By solving for a set of vibration constraint equations based on the response of systems to impulses, a sequence of unique impulses can be formulated which, when convolved with the input to a system, will suppress the resonant mode vibration. The following sections are meant to give a comprehensive overview of the algorithm for generating the sequences and to lend some insight into the method.   The authors cited should be consulted for more detailed explanations.

2.2   Implementing the Sequences

One first needs to understand how these impulse sequences are used. Impulses are not actually input into the system, as that would be hard on the amplifiers, and it would not achieve any desired move. Instead, the impulse sequence is used as a filter to "shape" an arbitrary move. This is accomplished by performing a convolution of the original input with the impulse sequence. By doing this, we are projecting the vibration reducing attributes of the impulse sequence onto an arbitrary move. This presents one of the many advantages of impulse shaping, which is that it can be used in real time, with any type of input. An example of what a "shaped" input looks like is shown in figure 2.1.

Command   Three impulse filter   Shaped Command
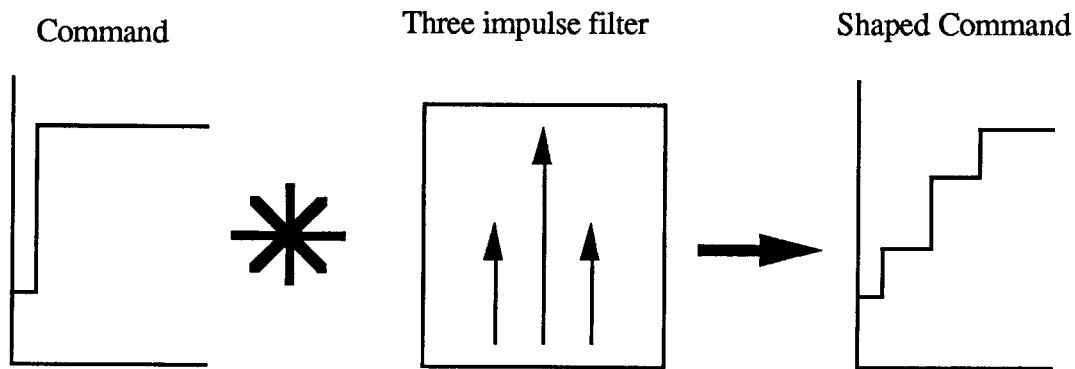
FIGURE 2.1: An example of how a step input is convolved with an impulse sequence to generate a shaped command.

2.3 Calculating Single Mode Sequences

Much like Smith's posicast control, impulse shaping delays parts of the original input based on the natural frequency of the plant. A good way to visualize what is happening is shown in figure 2.2. A simple pendulum on

a string is chosen as the plant to be controlled. The desired move is to go from point A to point B without causing the mass to swing at the end of the move. The pendulum motion is the resonant vibration of this system. The move is split into two parts. The pendulum is first moved half the distance to point B. Then, after the mass has swung all the way to the other side, the other half of the move is completed. The desired move has been achieved without any residual vibration. It is a very simple idea but it is the foundation for a very sophisticated vibration control strategy that has many important applications.
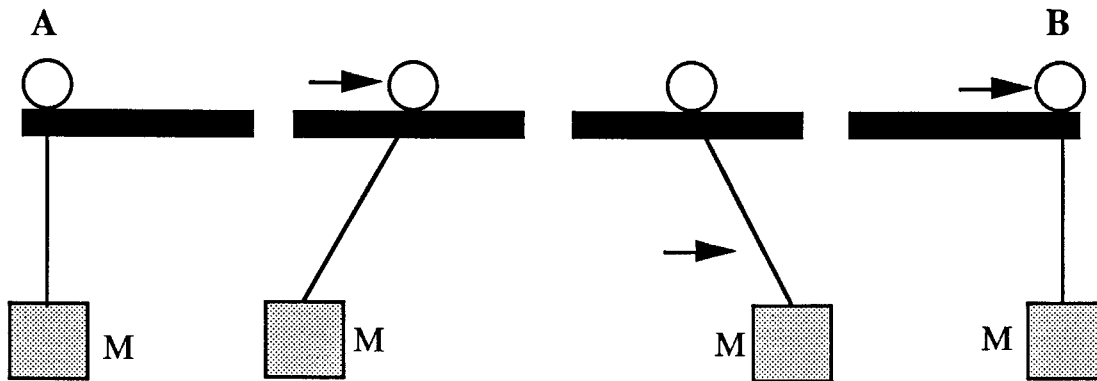
FIGURE 2.2: Example of posicast control, or a two-impulse shaper.

The modern technology that we call impulse shaping is a few generations removed from Smith's posicast control idea. The original work done in this area by Singer starts with the assumption that most dynamic systems can be modeled as a sum of second order linear systems. The response of a second order system to an impulse is governed by the following equation:

$$y(t) = A\, e^{-\zeta\omega(t-t_0)} \sin\left(\omega \sqrt{1-\zeta^2}\,(t-t_0)\right), \tag{2.1}$$

where ω is the undamped natural frequency of the system, ζ is the damping ratio of the system, t_0 is the time of the impulse, and A is the amplitude of the impulse.   By superposition, we can then conclude that the response to a series of impulses will be the sum of the responses to each of the impulses. We can then write:

$$y(t) = \sum_{i=1}^{n} A_i\, e^{-\zeta\omega(t-t_i)} \sin\left(\omega \sqrt{1-\zeta^2}\ (t-t_i)\right), \qquad (2.2)$$

where n is the number of impulses. From this we can derive an equation for the amplitude of vibration at the time of the last impulse. This equation describes the residual vibration amplitude envelope.

$$\text{Amp} = \sqrt{\left(\sum_{i=1}^{n} B_i \cos \phi_i\right)^2 + \left(\sum_{i=1}^{n} B_i \sin \phi_i\right)^2}$$

$$B_i = A_i\, e^{-\zeta \omega (t_n - t_i)}$$

$$\phi_i = \omega \sqrt{1 - \zeta^2}\ t_i \qquad (2.3)$$

To obtain a vibration-free impulse sequence, we want this expression to equal zero.   This requires that both squared terms in equation 2.3 independently go to zero, yielding the following constraint equations:

$$\sum_{i=1}^{n} A_i\, e^{-\zeta\omega(t-t_i)} \sin\left(\omega \sqrt{1-\zeta^2}\ (t-t_i)\right) = 0$$

$$\sum_{i=1}^{n} A_i\, e^{-\zeta\omega(t-t_i)} \cos\left(\omega \sqrt{1-\zeta^2}\ (t-t_i)\right) = 0 \qquad (2.4)$$

Given that we know ω and ζ, the undetermined variables are the impulse amplitudes A_i and the impulse times t_i. More constraint equations are added. We realize that only the relative amplitudes are important and that the starting time of the impulse sequence is arbitrary, so we list two more constraints:

$$t_i = 0$$
$$\sum_{i=1}^{n} A_i = 1 \tag{2.5}$$

The time of the first impulse is set to be zero and the amplitudes are normalized to maintain the same final steady state value of the original input during implementation. We now have four equations and, since each impulse has two variables (time and amplitude), two impulses can be found that will satisfy these equations. The resulting two impulse sequence, when implemented with a step input, is not unlike Smith's posicast control.

The breakthrough in impulse shaping is its robustness factor. By robustness we mean that the method should be fairly effective even for slight errors in system parameter identification (ω and ζ). This robustness constraint is modeled by taking the first derivative of equation 2.4 with respect to ω and setting it to zero. Singer proves that the derivative of 2.4 with respect to ω is the same as the derivative with respect to ζ. So the following derivative constraints require that the impulse train have little residual vibration for errors in both the system natural frequency and damping ratio.

$$\sum_{i=1}^{n} A_i\, t_i\, e^{-\zeta\omega(t_n-t_i)}\, \sin\left(t_i\, \omega\, \sqrt{1-\zeta^2}\right) = 0$$

$$\sum_{i=1}^{n} A_i\, t_i\, e^{-\zeta\omega(t_n-t_i)}\, \cos\left(t_i\, \omega\, \sqrt{1-\zeta^2}\right) = 0$$

(2.6)

We now have six equations which can be satisfied by three impulses. This is a basic three impulse sequence for one mode that is fairly robust to system parameter uncertainty. To gain more robustness, we can add another constraint by taking a second derivative, yielding a fourth impulse. We can actually go on and on by adding more and more derivative constraints. The tradeoff, however, is the length of the impulse train. Every additional derivative constraint adds an additional length to the sequence that is equal to half the period of the frequency being controlled. The longer the impulse train, the longer the delay will be in implementation. An example of a three impulse sequence for a 10Hz resonant system is shown in figure 2.3. Figure 2.4 shows an insensitivity curve for the three impulse sequence. The insensitivity curve is way to graphically portray the robustness of an impulse sequence by showing the residual vibration amplitude as a function of frequency. The curve is a calculation of the residual vibration amplitude response for each frequency to the given impulse sequence, and plotted on a linear scale as a percentage of the residual vibration amplitude for a unit impulse. The plot is thus a measurement of how much vibration amplitude a certain impulse sequence can cancel at each frequency for a given range.
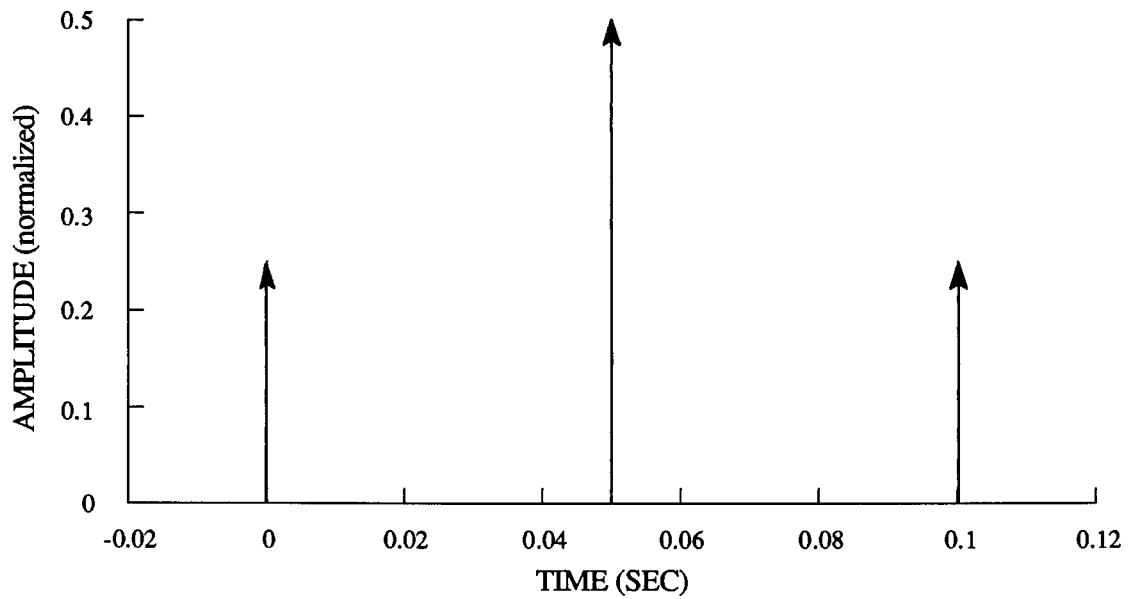
FIGURE 2.3: Three impulse sequence for ω=10Hz, ζ=0.
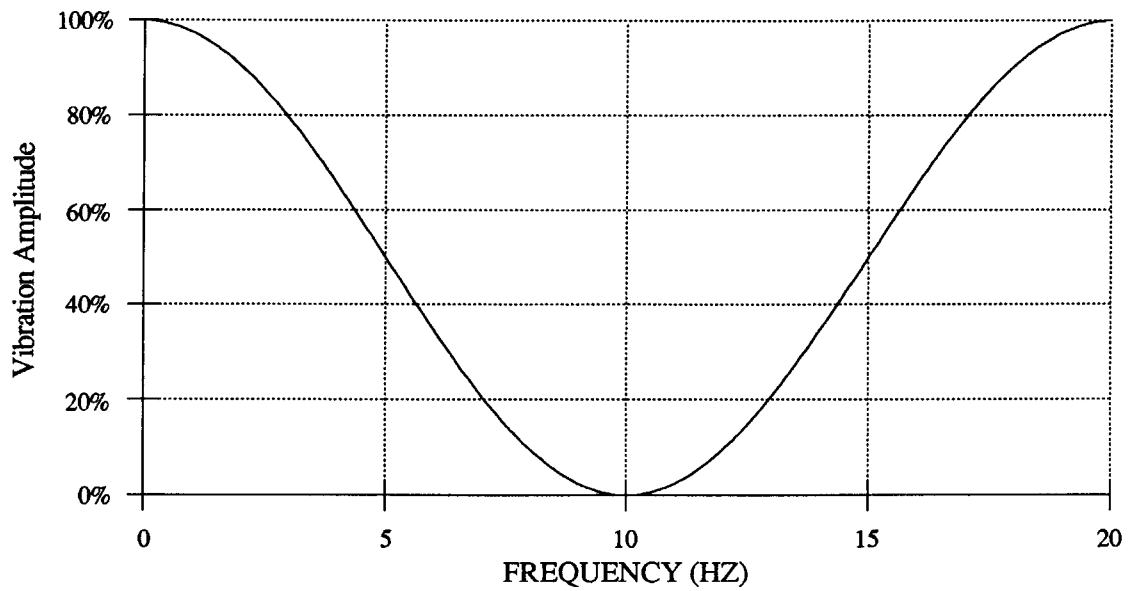
FIGURE 2.4: Insensitivity curve for three impulse sequence; ω=10Hz, ζ=0.

2.4   Calculating Multiple Mode Sequences

2.4.1   Convolution

This algorithm is now ready to be extended to multiple mode problems. The method suggested by Singer is to convolve the impulse sequences for each of the individual modes. Mathematically, this involves performing an outer sum of the impulse times and an outer product of the impulse amplitudes. The resulting sequence has $\prod_{i=1}^{m} n_i$ impulses, and a length of $\sum_{i=1}^{m} l_i$, where m is the number of modes, n is the number of impulses for each mode, and l is the length of each sequence. An easier way to think of convolution is to picture a one mode impulse shaper as a black box filter which splits an input into three parts, delaying the latter two. Convolution puts these black boxes in series such that the "filtered" output from the first shaper is used as input into the second shaper and so forth. The resulting impulse sequence is the output from the last shaper in the series. Figure 2.5 shows the type of sequence that would result from convolving two 3-impulse shapers.

Convolved sequences are easy to calculate since they involve only finding the sequences for one mode problems and some simple math in joining them. They are also easy to implement in computer code by using this black box idea and programming the individual one mode shapers in series. This results in less code and also less calculations for the computer, which is an advantage when systems are working at high servo rates. The disadvantage to convolving is the length of the resulting sequence. As will be shown in the next section, shorter sequences can be found to satisfy the same vibration constraint equations.
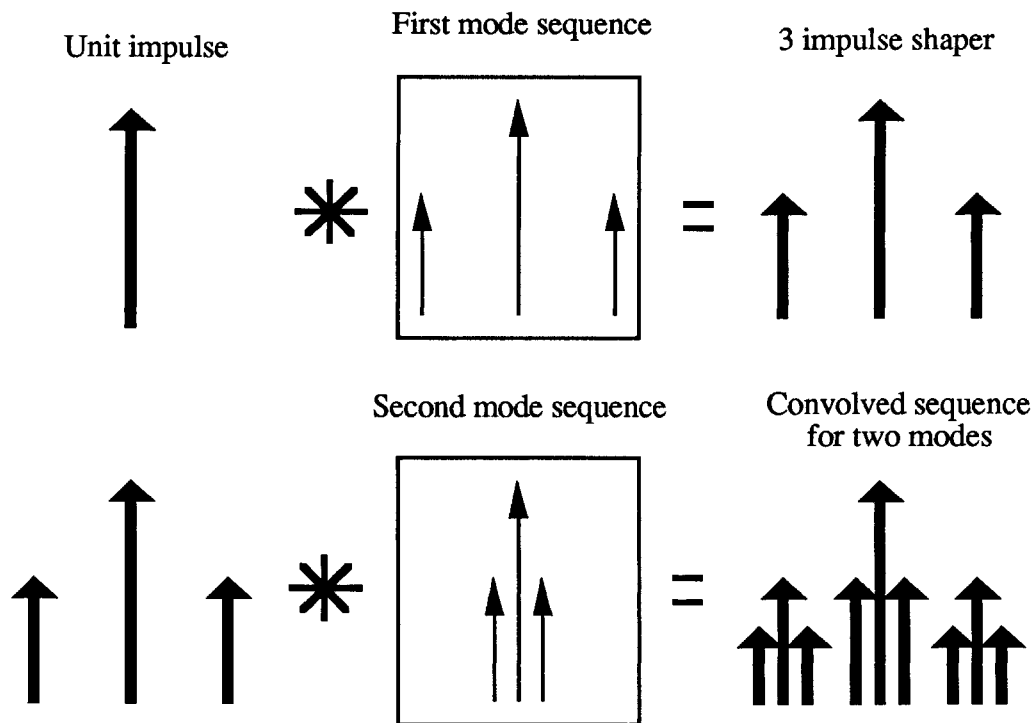
FIGURE 2.5: An illustration of convolving a two mode sequence

2.4.2   Direct Solution

Hyde has detailed a direct solution method for finding impulse sequences for multiple mode problems. The algorithm basically lays out the vibration constraint equations for all the modes and solves them simultaneously. For example, if we are solving for 3 impulse sequences, we can generate the constraint equations for an arbitrary number of modes m:

$$\sum_{i=1}^{n} A_i \, e^{-\zeta_j \omega_j (t_n - t_i)} \, \sin\left(\omega_j \sqrt{1 - \zeta_j^2} \, (t_n - t_i)\right) = 0$$

$$\sum_{i=1}^{n} A_i \, e^{-\zeta_j \omega_j (t_n - t_i)} \, \cos\left(\omega_j \sqrt{1 - \zeta_j^2} \, (t_n - t_i)\right) = 0$$

$$\sum_{i=1}^{n} A_i \, t_i \, e^{-\zeta_j \omega_j (t_n - t_i)} \, \sin\left(\omega_j \sqrt{1 - \zeta_j^2} \, (t_n - t_i)\right) = 0$$

$$\sum_{i=1}^{n} A_i \, t_i \, e^{-\zeta_j \omega_j (t_n - t_i)} \, \cos\left(\omega_j \sqrt{1 - \zeta_j^2} \, (t_n - t_i)\right) = 0 \tag{2.6}$$

$$t_i = 0$$

$$\sum_{i=1}^{n} A_i = 1$$

where the top four equations are repeated for each mode *j*. We now have a system of $4m + 2$ equations, which is satisfied by $2m + 1$ impulses. So for a two mode case, the direct solution method results in five impulses where convolution would come up with nine. The calculated sequence not only has fewer impulses than the convolved sequence, but also is shorter in length. The savings in length is not always predictable but experience has shown that, for three impulse sequence modes of less than five modes, the savings can be up to 30%. When we're dealing with slow modes, the savings in time can be a big factor.

The method does have its shortcomings, however. So far, an easy way to solve the nonlinear constraint equations has not been found. Currently, linear approximations generated through optimization are used for non-linear solving routines. The procedure is complex, time-consuming, and does not always find an exact solution. The author has many times experienced the frustration of spending much time for a multiple-mode problem only to find that the solver does not converge. Contributions from

current research on developing closed-form solutions to multiple mode problems could make this method much more attractive. The robustness of the convolution method is lost also in the direct solutions as is shown in the following section.

2.4.3 Convolution vs. Direct Solution

The two approaches to solving multiple mode problems produce somewhat different insensitivity curves. Although they satisfy the same zero vibration constraint equations, the robustness of the two types of sequences varies considerably. Insensitivity curves are usually plotted as a function of a normalized frequency. This means the robustness is a function of a percentage of the frequency, not absolute frequency (Hz, for example). So a 1Hz mode sequence may have 5% residual vibration robustness between .85Hz and 1.15Hz, but a 10Hz mode sequence will have the same robustness between 8.5Hz and 11.5Hz, an interval ten times greater than that of the 1Hz sequence. So, in absolute terms, we can say that the 10Hz sequence is ten times more robust than the 1Hz sequence. This is a fortunate feature of impulse shaping since the higher modes are generally harder to identify precisely and they tend to move around more.

In comparing the insensitivity curves for convolved and direct solution sequences, we notice a vast difference in robustness for the higher modes. The convolved sequence maintains the same robustness in the multiple mode sequence as in the one mode sequence. This means that if we compare the insensitivity curve in the area of 20Hz for a one mode sequence for 20Hz and a two mode convolved sequence for 10Hz and 20Hz, they are the
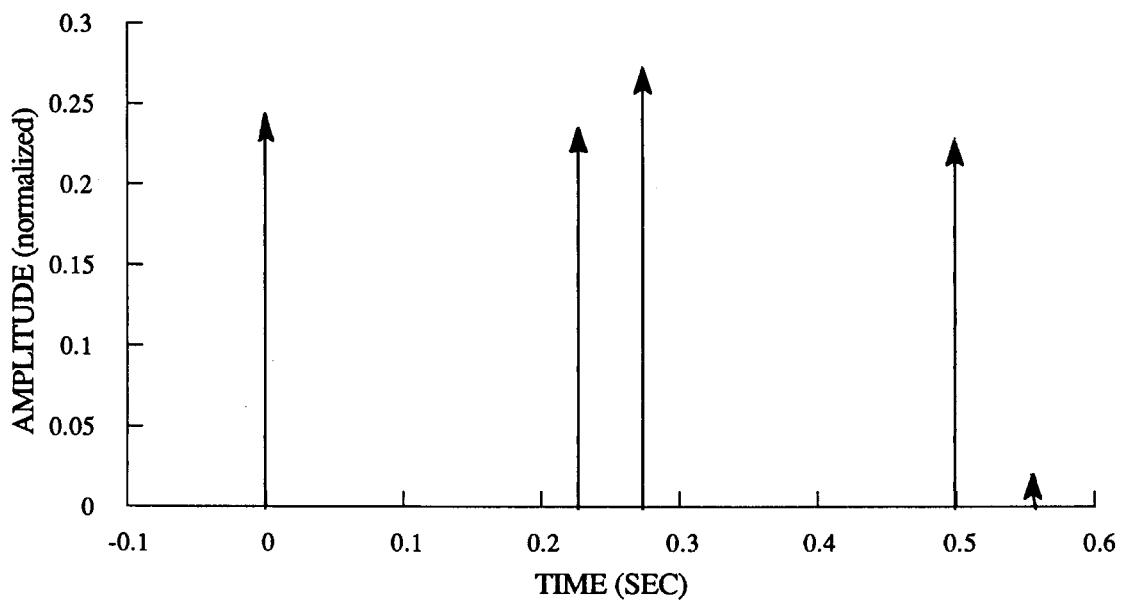
FIGURE 2.6: Direct solution sequence for two modes, three
impulses per mode (2, 20Hz).
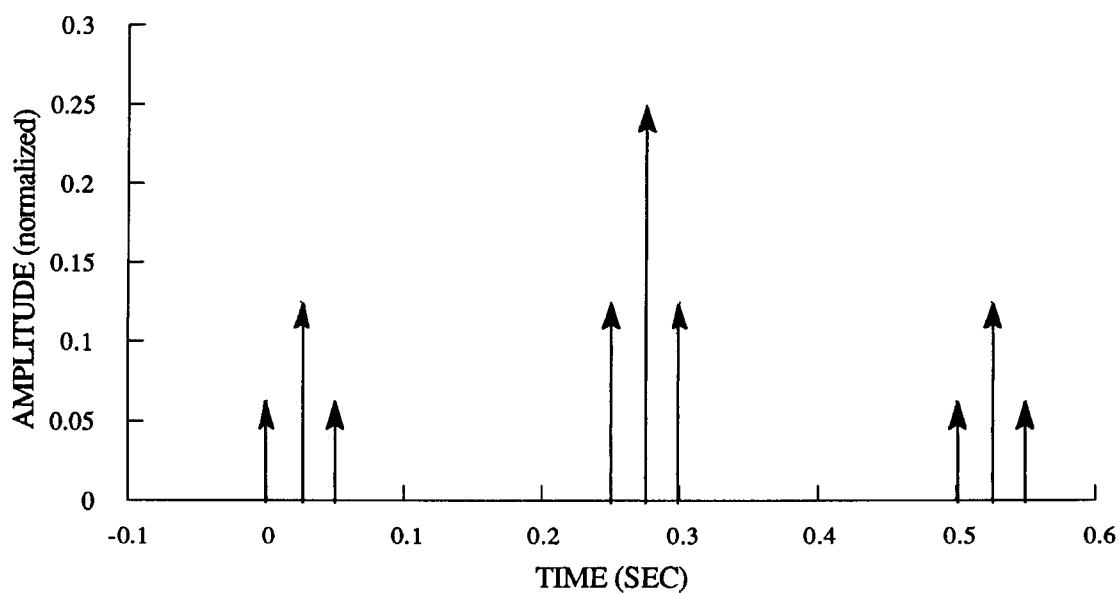
FIGURE 2.7: Convolved sequence for two modes, three
impulses per mode (2, 20Hz).
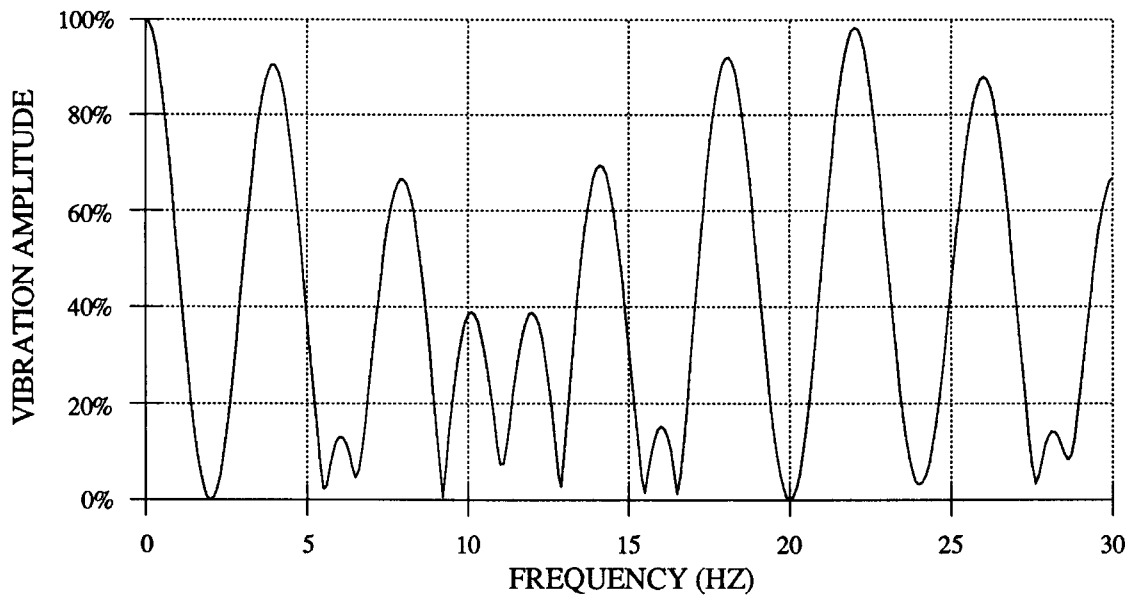
FIGURE 2.8: Insensitivity curve for direct solution two mode sequence;
ω_1=2Hz ζ_1=0, ω_2=20Hz, ζ_2=0.
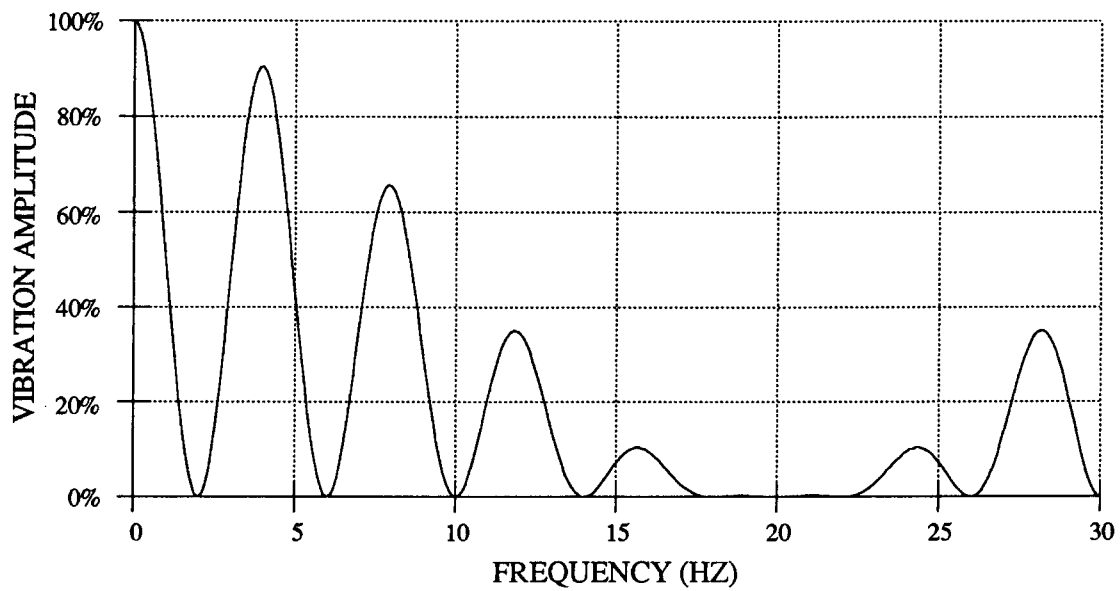
FIGURE 2.9: Insensitivity curve for convolved two mode sequence;
ω_1=2Hz ζ_1=0, ω_2=20Hz ζ_2=0.

same. However, in the direct solution sequences, the higher modes seem to inherit the robustness curve shape of the slowest mode that is shaped. So if we compare the same two sequences solved by the direct solution method, we find that the insensitivity curve in the area of 20Hz for the two mode case is only as robust as the 10Hz region, about half as much as the convolved sequence. Figures 2.6 and 2.7 show the impulse sequences using both the convolution and direct solution method for a two mode problem using three impulses per mode. The two modes are placed an order of magnitude apart to magnify the difference between the two methods. Figures 2.8 and 2.9 show the corresponding insensitivity curves for the two sequences. Notice the difference in insensitivities for both sequences in the 20Hz region.

A peculiar feature of this combination of modes is that the direct solution method yields a longer sequence than the convolved sequence. This has to do with the fact that the ratio of the two frequencies is rather large. There is no current method to predict when this will happen, but we do know that for a two mode sequence, a ratio of frequencies that is greater than 3 will yield a longer direct solution sequence. Further investigation into closed form solutions for the direct solution method may reveal what causes this to happen. For most cases, however, the direct solution method displays a significant savings in length.

To summarize, we can say that there are certain advantages and disadvantages to each method. Convolution is simple to calculate, easy to program and implement, and maintains high robustness. Direct solution produces a shorter sequence, but is more complex in calculation, harder to implement, and loses some robustness. Different applications will call for different methods. When reducing the time lag in the move is critical,

direct solution is the best choice. An application with high modes which tend to move around a lot will call for convolution. And in many cases, a combination of the two is ideal. A list of the qualities of both methods is given in table 2.1.

	Convolution	Direct Solution
Number of impulses	$\displaystyle\prod_{i=1}^{m} n_i$	$\displaystyle\sum_{i=1}^{m} (n_i-1) + 1$
Length of sequence	$\displaystyle\sum_{i=1}^{m} l_i$	$\displaystyle ?<\sum_{i=1}^{m} l_i$
Calculation complexity	Simple	Complex
Robustness	Very robust	Less robust

TABLE 2.1: A comparison of multiple mode shaping methods.
m is the number of modes, n is the number of impulses per mode,
and l is the length of each sequence.

2.5   Finding the Most Efficient Sequence

There needs to be some sort of strategy in finding the "best" sequence for a particular application. Ideally what we would like to do is to somehow minimize the length of the sequence while maximizing the robustness of the insensitivity curve. There are some variables to consider. We've already considered direct solution versus convolution. The other two variables are the number of modes to shape. and the number of derivative constraints to use

In determining the number of modes to be shaped, the first thing to realize is the repeating nature of impulse shaping. Because we are using

impulses at half periods of the frequency, we also happen to cancel modes which are odd harmonics of the original frequency. By sheer coincidence, this can often eliminate the need to shape for certain higher modes, resulting in shorter, less complicated sequences.

Also, as mentioned earlier, higher mode sequences are much more robust than lower mode sequences. This can also be used in our favor. If two fairly fast resonant peaks are close together, usually, a sequence for one of the modes, or a sequence for the frequency in between the two modes will suffice. The higher the modes, the more this applies. These are two inherent features of impulse shaping that we can use in our favor to simplify our algorithm.

The addition of a derivative constraint adds one more impulse to the tail end of a one mode sequence. It also tends to lengthen the sequence for multiple mode problems. In the recent research done on impulse shaping, a three impulse sequence has been found to be adequate for most applications. However, the number of derivative constraints for a mode should depend on the uncertainty of the plant or the tendency of that mode to change.

We can also use less derivative constraints when modes are close to one another. Singhose has proposed a method which takes advantage of modes which are close together to yield shorter sequences. His method is actually equivalent to a direct solution sequence for two modes without derivative constraints. The argument centers around the fact than when 2 shaped modes are close together, their robustness tend to "overlap." Whereas a single two impulse shaper is not very robust, if two 2-impulse sequences are

placed close to each other in frequency, the region in between the two modes is still pretty robust. Given a certain tolerance level, the two modes can be placed an optimal distance apart to gain maximum robustness. This is used in place of three-impulse sequences for both modes or one three-impulse sequence for the frequency in between the two modes. The resulting insensitivity curve may look something like figure 2.7. It shows a three impulse sequence that has been solved for two modes around 10Hz (9Hz and 11Hz). The figure may be compared against a similar three impulse sequence for the 10Hz mode alone.
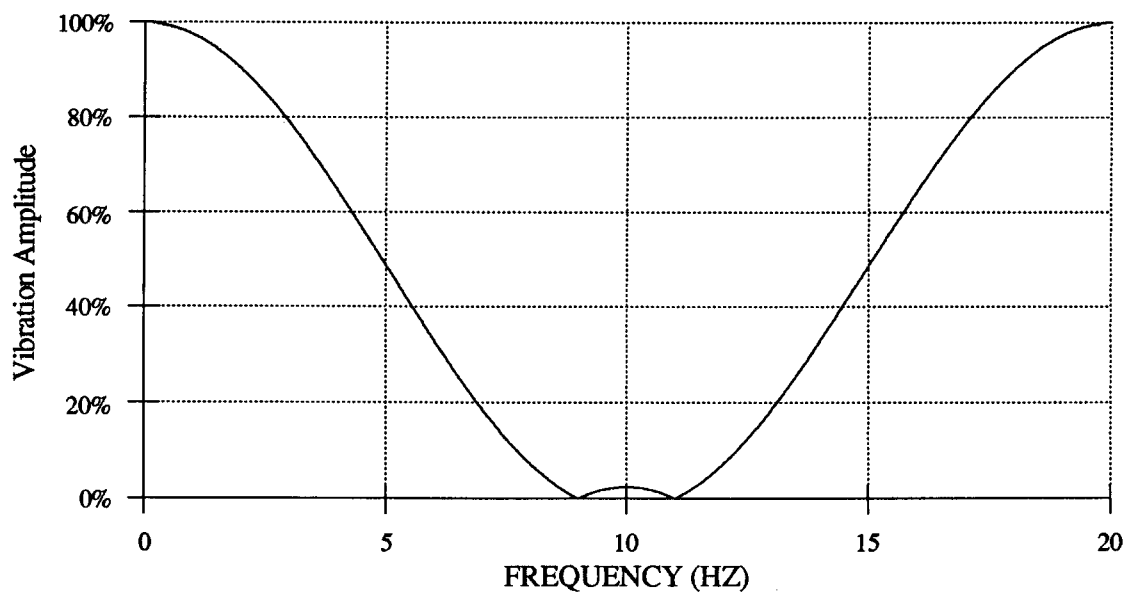
FIGURE 2.10: Insensitivity curve for three impulse sequence for two
modes at 9Hz and 11Hz.

We have covered three variables we can control to come up with the most efficient impulse sequence: convolution vs. direct solution, the number of modes to shape, and the number of derivative constraints. These variables

can be used in our favor to optimize the tradeoff between robustness and time delay. The robustness factor and the ability to implement the shapers in real time are the main advantages of impulse shaping technology. The tools are now in place to exploit these factors to produce more efficient sequences.

THE TESTBED: MACE

Chapter 3

3.1   Introduction

One of the most suitable applications of impulse shaping is in space structures. Residual vibration is a common problem in large flexible space-borne systems and has been the focus of extensive recent research effort in the aerospace and mechanical engineering communities. For this reason, the Middeck Active Control Experiment (MACE) has been chosen as the testbed for verification of the issues concerning impulse shaping presented in this work. This chapter will describe the MACE project and detail some of the work done in control derivation.

3.2   Project Motivation and Agenda

NASA initiated efforts in 1988 to investigate the behavior of on-orbit closed loop dynamic systems which utilize Controlled Structures

Technology (CST). CST refers to the use of active control techniques in highly flexible structures with closely coupled modes within the controller bandwidth. One of the products of this effort was the MACE project, a proposed Space Shuttle middeck experiment. The goal of the project was to provide a platform for analyzing closed loop behavior in a zero gravity environment. This project is on-going at the MIT Space Engineering Research Center and managed by the NASA Langley Research Center. The launch date is currently set for the summer of 1994.

A multibody platform was chosen as the template for the MACE design. It was desired that the results of the experiment be useful to planned future space missions. The design, therefore, takes after a scaled down version of a larger functional proposed design such as the Earth Observing System (EOS), the Geostationary Platform (GEOS), or other exploratory or military designs. The multibody configuration is conducive to studying many issues associated with active control:

- Three dimensional behavior
- Disturbance isolation
- Time varying dynamics
- Multiple interacting control systems

These features allow MACE to be the subject of various types of analysis whose findings can be useful in future space flights.

The experiments will be run on the Space Shuttle middeck because of the low relative cost of running experiments there and the ease of access to the facility. The middeck dimensions are mission specific because of
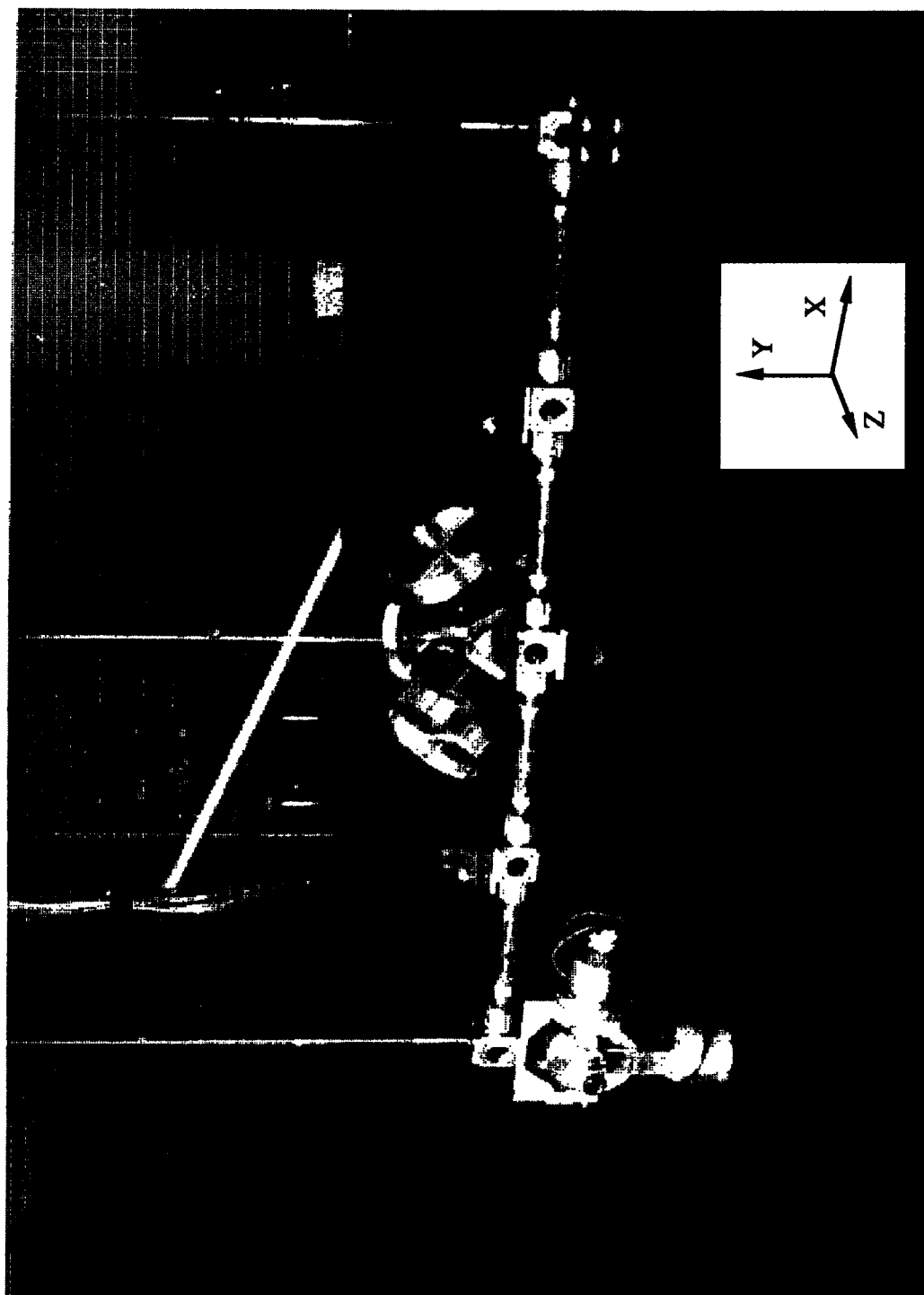
FIGURE 3.1: The MACE Development Model

miscellaneous hardware being stored in the area, but it can most certainly accommodate a test article 76" (1.9m) long. Maximum height of the middeck is about 88" and maximum depth is about 60". This restricted the outer dimensions of MACE. The flight plan also calls for the MACE hardware being stowed in a middeck locker with about two cubic feet of volume. This necessitated the need for a modular design such that the structure could be taken apart and reassembled easily by the shuttle crew. Other restrictions on power, weight, and safety dictated much of the design. The MACE hardware is shown in figure 3.1.

The main science objective is to investigate the extent to which closed loop behavior of an on-orbit dynamic system can be predicted on earth. It is impossible to reasonably simulate on the ground the environment that the test article would see in space. The prediction, thus, must come from a combination of theoretical modeling and test results in a 1-g environment. During the flight mission, three types of control strategies will be used. The first will be the control derived and tested on Earth. The second will be derived from a theoretical 0-g model, and the third will be one derived during the flight and uploaded after dynamic tests have been made on the test article. These experiments will explore how accurately closed loop systems can be tested on earth before being put into space.

The control objectives focus on the accuracy of the inertial angle of the pointing payloads. The performance objectives are threefold:

- Pointing accuracy of one payload in the presence of disturbances.
- Tracking accuracy of one payload in the presence of disturbances.
- Accuracy of both payloads while both simultaneously point and track.

Pointing accuracy may involve a telescope that needs to point to a star light years away. One can easily imagine how important the accuracy is. Tracking accuracy may be necessary on a structure like EOS, where sensors would scan the earth's surface. The payload would then need to move in a smooth continuous motion.

3.3   Current Research

The current MACE hardware is in the first of three hardware phases. The Development Model, which is located at MIT, is the first iteration of the hardware. The second iteration will be called the Engineering Model, and the third iteration is the flight hardware. There are currently various parallel research projects being conducted on different aspects of MACE. Saarmaa [19] has conducted thorough open loop testing of the hardware and the suspension system. These tests have then been compared to the NASTRAN finite element model. Miller, Sepe, Rey, Saarmaa, and Crawley [14] have incorporated gravity and suspension effects into a finite element model of the development hardware. This study showed that low fundamental frequency, multiple payload devices such as MACE exhibit significant suspension and gravity coupling. The 1-g FEM models displayed much better correlation to experimental data than the 0-g models. Miller, Saarmaa, and Jacques [13] have used measurement based models in deriving SISO (single input single output) and SITO (single input two output) controllers using Linear Quadratic Gaussian design. They used a nonlinear curve fitting routine to derive an analytical model based on experimental frequency response data. These controllers proved to be

effective in rejecting broad band disturbances. An order of magnitude improvement in pointing accuracy was achieved. Other current research efforts involve developing a three dimensional nonlinear model of MACE, and the use of classical control techniques to achieve more robustness in control design
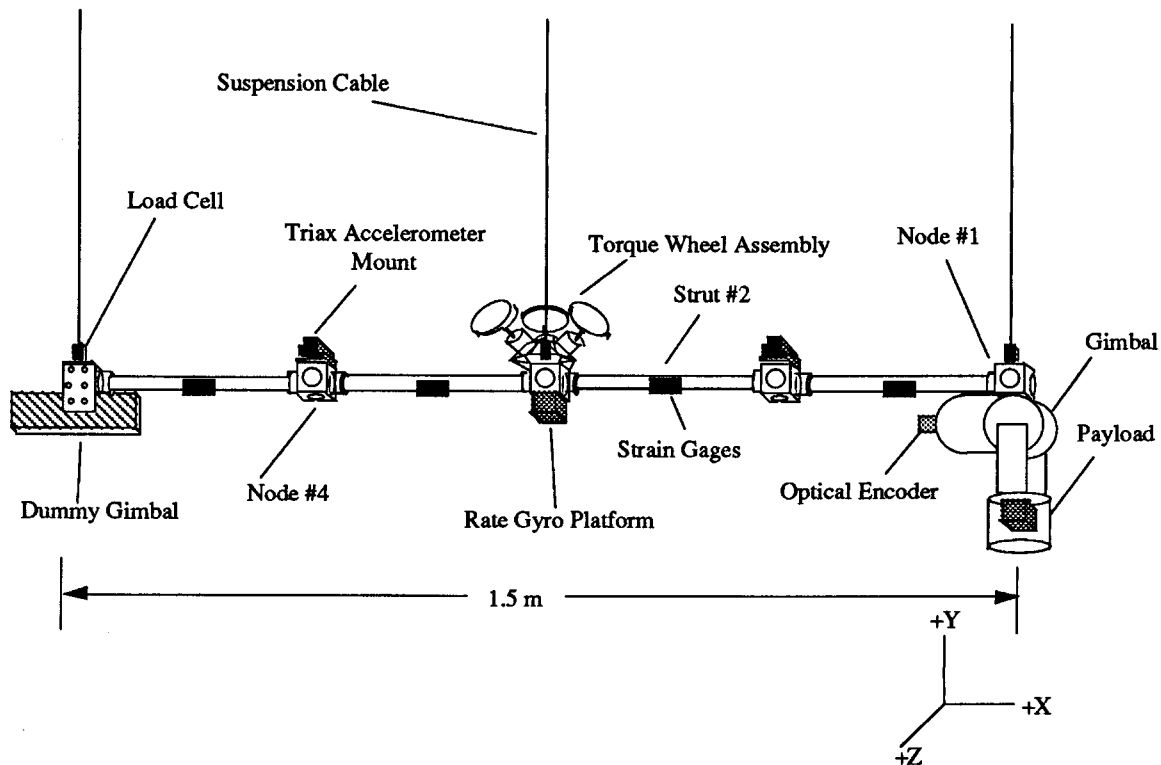
FIGURE 3.2: MACE Development Model Schematic.

3.4   Development Model Hardware

MACE consists of a long flexible bus, a three-axis torque wheel assembly, and a two-axis gimbal payload. There are also various sensors mounted on the assembly. The entire system is attached to a sophisticated pneumatic suspension system at three points along the bus. A diagram of the hardware and its components are shown in figure 3.2.

The specifications for the hardware dictated a structure that is very flexible yet durable for long-term testing. For this reason, the bus struts are made out of hollow Lexan. There are four struts connected by aluminum collars to the five nodes. These collars allow for easy manual assembling and disassembling of the bus. The nodes are machined with four threaded holes on each side for mounting of actuators and sensors. The bus is approximately 1.5 meters long.

The torque wheel assembly is used to control the attitude of the bus in space. Three inertia wheels are mounted orthogonally on a triangular base which is attached to node three. When the wheels accelerate, they exert a reaction torque on the structure. With precise control of the three wheels, attitude stability in all three axes can be achieved. The unit can exert torques of 40 oz.-in. for up to five seconds. and the Aerotech 1017 servo motors can drive the wheels up to 6000 RPM.

A single gimbal actuator is attached at node one. A mass of steel acts as a dummy gimbal on the other side of the bus at node five while the Engineering Model gimbal is under development. The two-axis actuation is achieved through a yolk design where one gimbal stage is contained within the other. The Inland RBE 03000-B50 brushless DC torque motors directly drive the payload in both axes. These motors are sized to exert 2000 oz.-in of torque and to have a pointing accuracy of 1 arcmin. A picture of the gimbal without the payload can attached is shown in figure 3.3.

There are also plans for attaching piezoelectric actuators at strut two to provide more options for control. This active strut could be used to dampen

vibration in the structure.   As of this writing, these struts were under development.
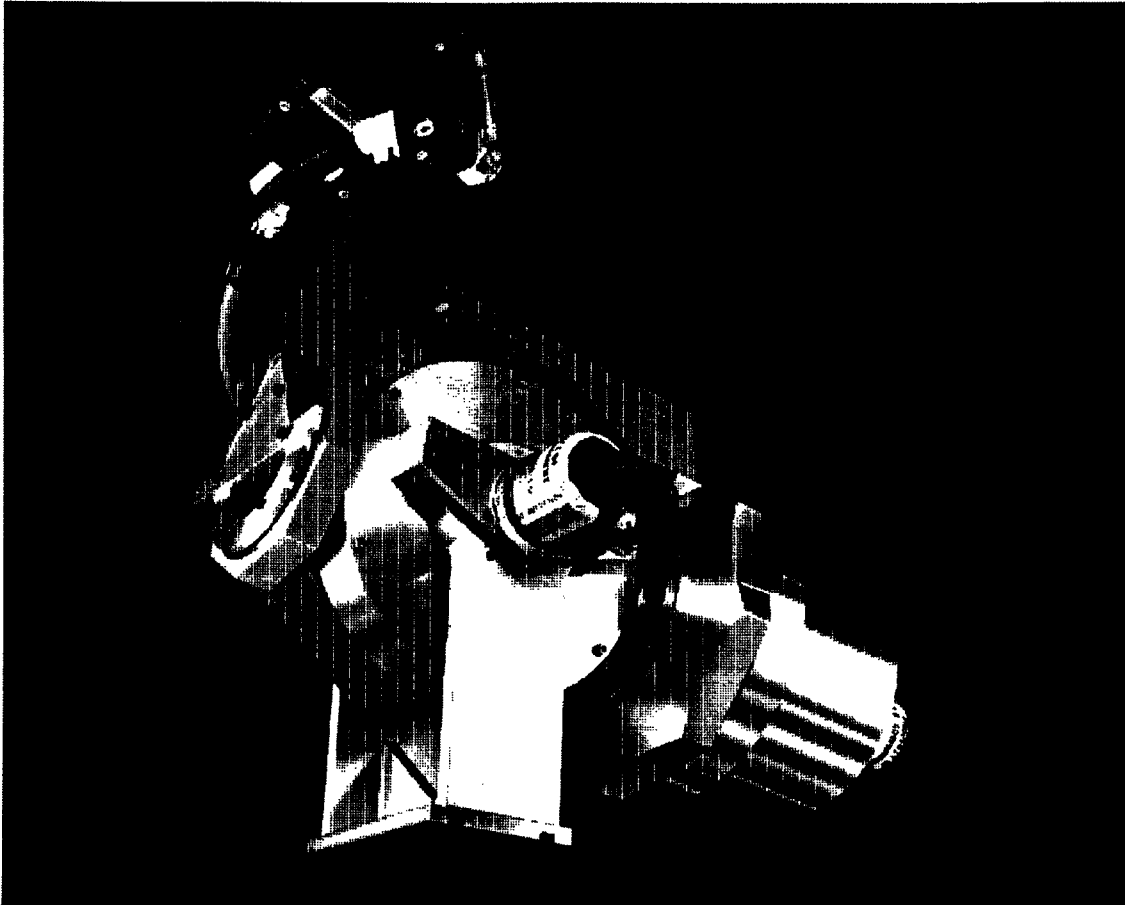
FIGURE 3.3: A two-axis gimbal actuator.

There are currently 28 sensors attached at various points on MACE. Sixteen strain gauges (two pairs at each strut) measure the bending deflection in two directions on the bus. There are also two three-axis rate gyros; one mounted underneath the torque wheels at node three, and the other inside the payload can. These measure inertial velocity in the three directions, and the signal can be stably integrated to acquire the inertial position. There are three single axis load cells at the connections to each suspension cable, which measure the amount of force being transmitted

from the suspension system to the structure. Canon laser rotary encoders are attached to each motor shaft of the gimbal to measure the relative angle between the bus and the payload. Finally, five accelerometers are attached to nodes two and four (two at node two and three at node four) to measure acceleration in all three axes. All of these sensors are routed through a breakout panel of various sensor amplifiers and conditioners.

The structure is supported by CSA Engineering's Zero-G Suspension System which connects to MACE at nodes 1, 3, and 5. These nodes were chosen to off-load the three high mass locations along the bus. The suspension system employs pneumatic pistons and a feedback loop to actively control the vertical position of each node. It allows the structure to move .0635m in the vertical direction friction-free. The plunge mode of the pneumatic suspension system is variable and usually set to about 0.2Hz. The cable length was determined such that the pendulum frequency of the suspension system would not affect the dynamics of the plant. Rule of thumb demands that this frequency be less than an order of magnitude of the first bending mode. Space limitations constrained the cables to be no longer than 4.6m. This translates to a pendulum frequency of approximately 0.23Hz, reasonably close to one tenth of the predicted bending mode at around 1.8Hz. The torsional pendulum mode is also low ($\approx$ 0.24Hz). There are also horizontal plane suspension frequencies and violin modes of the cables , however, which have higher frequencies and may affect the dynamics of the structure. Also, only the points where the suspension attaches to the structure are suspended. Other points in the structure are still in a gravity field. As this analysis illustrates, a sophisticated

suspension system can be employed, but there are still numerous problems in trying to simulate a zero gravity environment on earth.

All of the control and time data acquisition was done through Integrated System's AC-100 real time controller. The AC-100 system is comprised of a DEC3100 workstation, the hardware interface and processor board box, and the required compilers and development software. The system has eight encoder inputs, 8 D/A channels, 16 A/D channels, 2 fast analog channels, and 32 parallel digital I/O's. The main processor card is an 80386 with a Weitek 3167 math co-processor. Integrated Systems has provided an interface between their MatrixX control analysis software package and the processor board such that the user may do her programming in the SystemBuild section of MatrixX. This simplifies the coding process in that the user can work in a higher level language (block diagrams), to create the download files to the processor board. Another advanced feature of the AC-100 is the interactive animation. Users can directly interface with the hardware through the computer screen. Values from the sensors can be displayed in real time and the user can also input commands from the screen with the mouse. This removes the need for extra monitoring or input devices. The user interface is often convenient and very easy to learn but not very powerful in trying to code complicated control algorithms.

3.5   Dynamic Analysis

Extensive testing of the development model has been done to identify the dynamic characteristics of the structure. All of the data was taken using a Tektronix Spectrum Analyzer which fed broad band white noise into the

gimbal motor amplifiers. The sensor readings were read, amplified and fed back to the spectrum analyzer where a transfer function was calculated. This data was then analyzed using STAR ID software to determine the resonant frequencies and damping ratios. The gimbal motor to node four vertical accelerometer transfer function is shown in figures 3.4 - 3.5. The fundamental bending frequency is at 1.72Hz. Some of the modes, such as the ones at 3.45 and 4.58Hz were seen more in the horizontal plane. This may indicate that they are either horizontal or torsional modes. A summary of the predominant vertical modes for the first 50Hz is given in Table 3.1.

FREQUENCY (Hz)	DAMPING RATIO
1.72	.023
6.70	.017
8.92	.006
9.26	.008
13.45	.007
13.84	.009
36.04	.012
41.69	.013

TABLE 3.1: A summary of the modal frequencies and damping ratios
of the MACE test article in the vertical plane.

OPEN LOOP TRANSFER FUNCTION
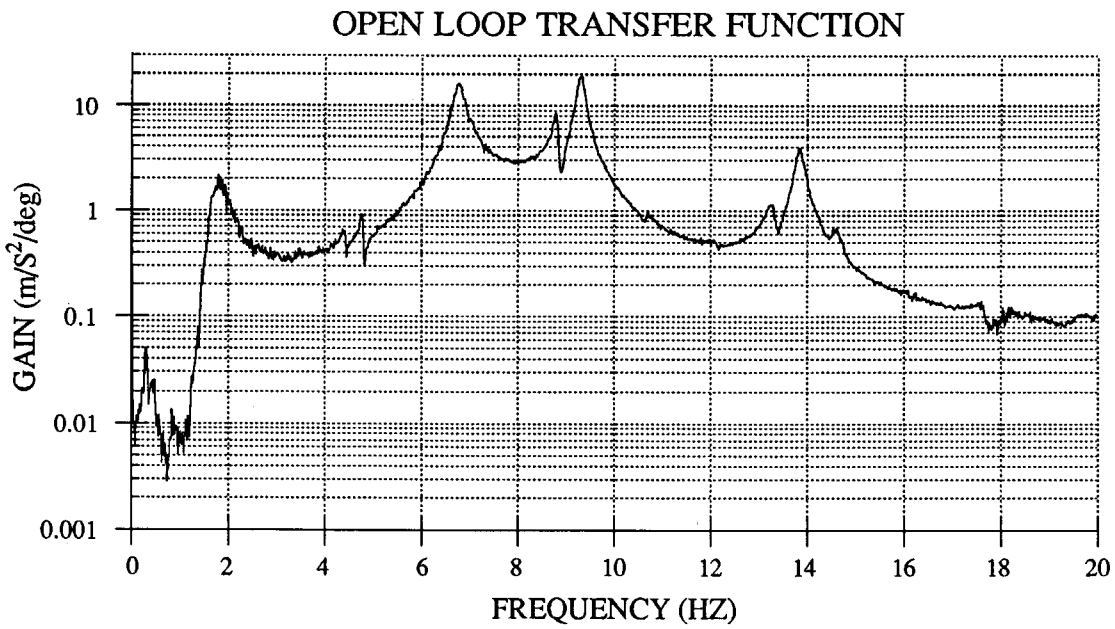
FIGURE 3.4: Outer gimbal stage to node four accelerometer open loop
gain transfer function.

OPEN LOOP PHASE TRANSFER FUNCTION
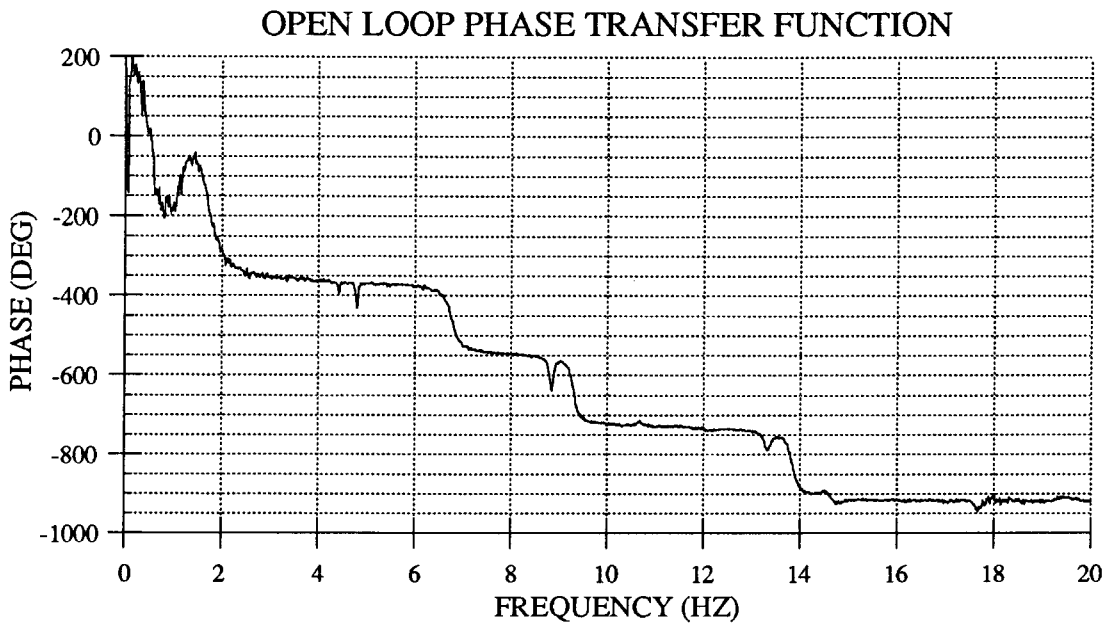
FIGURE 3.5: Outer gimbal stage to node four accelerometer open loop
phase transfer function.

MACE Development Model

First Vertical Mode
(1.72 Hz)

Second Vertical Mode
(6.70 Hz)

Third Vertical Mode
(8.92 Hz)
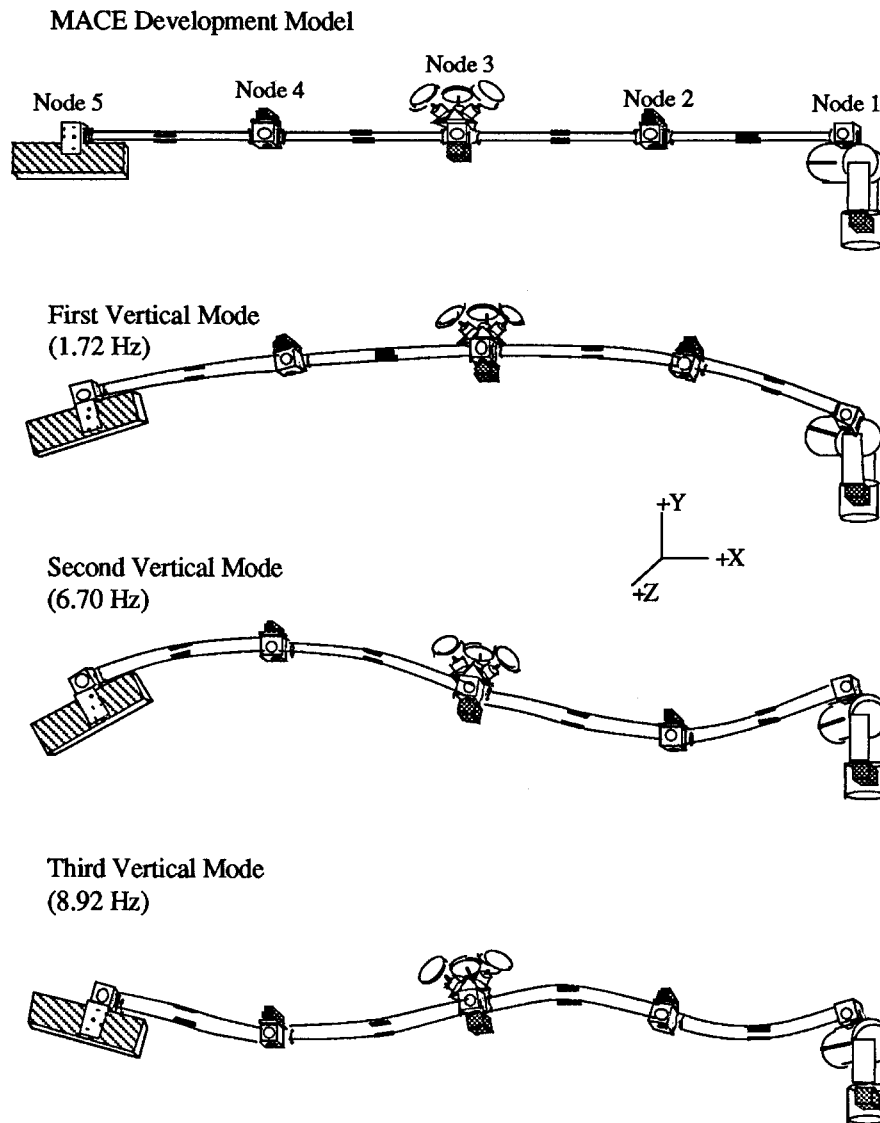
FIGURE 3.6: An illustration of the first three vertical bending
modes of the MACE development model.

The mode shapes of these frequencies can be predicted by looking at the
phase of each mode and also by comparing them to those derived from finite
element models. An illustration of these mode shapes is given in figure 3.6.

The frequency identification experiments show that MACE is a highly
flexible system with many excitable modes with small damping ratios. The
first bending mode is under 2Hz and the three next bending modes are

under 10Hz. These dynamic characteristics make MACE an ideal testbed for active control experiments, both closed loop and open loop , i.e. impulse shaping.

3.6   Gimbal Control

The gimbal actuator was detached from the bus and mounted on a test base to investigate the characteristics of the gimbal. The goal was to identify the modal frequencies and to design a slewing controller around the system. The specifications for the original gimbal design require that the gimbal assembly be capable of achieving a bandwidth of 30Hz. There were certain challenges in designing the controller. Some of the issues are dealt with in this section.

The outer gimbal stage was modeled as a rigid pendulum in a linear gravity field. The gimbal is only capable of slewing $\pm 30°$, and gravity is linear to $\pm 4\%$ in this region. The gimbal payload arm is made of a wide piece of aluminum and very stiff in the outer stage. Its resonant frequency is expected to be over 100Hz so it was omitted from the model. The dynamics of the motor and amplifier were assumed to be fast enough to be modeled as constant coefficients. This assumption was verified by the vendors specs and the successful experiment results. The parameters for the pendulum model of the gimbal are listed in table 3.2.

some overshoot was seen because the integrator places a zero near the closed loop poles. Attempts to increase the bandwidth with this method failed due to unmodeled dynamics.

Further testing revealed that there were three different causes of instability at higher gains with the simple PID control. The first was the resonant mode of the structural mount that holds the gimbal. This mode was observed at around 60Hz. It was identified as the mount because the manual stabilizing of the mount deleted the resonance at that mode. Also, the addition of viscoelastic material to parts of the test mount resulted in a shifting of that frequency. A second order notch filter was designed to temporarily erase the problem. A second unstable mode with very high gain was found at around 460Hz. This mode was a structural mode of the gimbal, most likely the encoder shaft torsional mode. The shaft on the outer stage is rather long due to the yolk shape of the design. Since this is such a high frequency, a low pass filter was deemed satisfactory for the problem. An analog eighth-order Bessel lowpass filter with a corner frequency of 100Hz was placed in the loop to neutralize the instability. The Bessel filter has a linear phase function, and therefore causes a constant time delay for all frequencies. This time delay was calculated to be 0.003 seconds.

The third cause of instability was the most problematic. A dynamic analysis of the computer showed that the processor delay is on the order of 2.7 cycle periods. At a servo rate of .001 seconds, this translates to a delay of .0027 seconds for each feedback signal to go through the processor. At the desired bandwidth frequency of 30Hz this delay is a phase loss of 29°. The phase lag causes marginal modes to go unstable very quickly. The time delay induces a linear phase loss so the higher frequencies lose more phase

margin.   Along with the newly acquired .003 seconds of delay from the lowpass filters, this added up to be the overwhelming cause of instability at high gains.   Since it is unreasonable to filter out all the unstable modes, it was decided to include the computer and filter delays in the system model.

A discrete state space model was formulated that includes the computer delay and the new lowpass filter delay. The continuous model was modified using the z-transform method to derive a finite difference form of the state matrix equations.   We start with the continuous form of a system model that includes a delay in control action:

$$\dot{x}(t) = Fx(t) + Gu(t - \lambda)$$
$$y = Hx$$

(3.3)

where x is the state variable, F is the dynamic matrix, G is the input matrix, H is the output matrix, and λ is the number of sampling periods that the controller delays. As described in Franklin[9], we can then derive the discrete form of this model:

$$x(k + 1) = \Phi x(k) + \Gamma_1 u(k - l) + \Gamma_2 u(k - l + 1)$$
$$y(k) = Hx(k)$$

(3.4)

where k is an integer increment in time, Φ is the z-transform of the dynamic matrix, and H is the output matrix. Γ_1 and Γ_2 are weighted sums of the z-transform input matrix Γ. The values of the matrices are determined by the non-integer part of the delay λ. For example, if the system delay were a whole number such as 1 cycle period, Γ_1 would equal Γ

and Γ_2 would equal zero. This weighting works to account for non-integer system delays. For these equations to actually come to realization, we need to introduce l new variables as states, one for each sampling period of delay. The matrix structure of the equations now looks like the following.

$$
\begin{bmatrix} \mathbf{x}(k+1) \\ x_{n+1}(k+1) \\ x_{n+2}(k+1) \\ \vdots \\ x_{n+l}(k+1) \end{bmatrix} = \begin{bmatrix} \Phi & \Gamma_1 & \Gamma_2 & 0 & \cdots & 0 \\ 0 & 0 & 1 & 0 & \cdots & 0 \\ 0 & 0 & 0 & 1 & \cdots & 0 \\ \vdots & \vdots & \vdots & \vdots & & 1 \\ 0 & 0 & 0 & 1 & \cdots & 0 \end{bmatrix} \begin{bmatrix} \mathbf{x}(k) \\ x_{n+1}(k) \\ x_{n+2}(k) \\ \vdots \\ x_{n+l}(k) \end{bmatrix} + \begin{bmatrix} 0 \\ 0 \\ 0 \\ \vdots \\ 1 \end{bmatrix} u(k)
$$

$$
y(k) = \begin{bmatrix} \mathbf{H} & 0 \end{bmatrix} \begin{bmatrix} \mathbf{x} \\ x_{n+1} \\ x_{n+2} \\ \vdots \\ x_{n+l} \end{bmatrix}
$$

(3.5)

What is happening is that each new state variable x is storing a past input command and then passing that input command to the variable above it at every time step. When this input gets to the "top" of the matrix, it is then multiplied by Γ_1 and Γ_2 to be used to evaluate the new state matrix. The augmented states are simply serving as buffers which hold past inputs in its memory.

The gimbal model was transformed into this format with $\lambda=5.7$ cycle periods (2.7 + 3.0). The second order model has now grown to an eighth order model. A full state controller was then designed on this discrete model. The eight feedback gains obtained illustrate an unorthodox but effective method of dealing with system time delays in control systems. The first two feedback gains are from the two original states of the system, the angle and angular velocity of the encoder output. The next six feedback gains are from the augmented states which represent the six past input values. The control law now takes the form:

$$u_k = -Jx_k - \sum_{i=1}^{l} g_i u_{k-i} \qquad (3.6)$$

where J is the proportional and derivative gains, and G is the vector of augmented state gains. The implementation of these states is similar to the discrete modeling of them. The calculated inputs are fed back into the control loop and queued in another discrete state space system for the appropriate number of cycle periods before they are released. They are multiplied by their corresponding gain values once they leave the delay state space system. This "buffer" type of control feature deals directly with the phase loss involved with system delays. A block diagram of the control algorithm is shown in figure 3.7. The inputs are the encoder counter and three command inputs from the user which indicate the two angles that she wants to slew between. The output from the controller is the command voltage into the gimbal motor amplifier. This voltage is cut off at ±10 volts to avoid saturation.

A bandwidth of 15Hz was obtained using this strategy. Subsequent experimentation with notch filters obtained the 30Hz specification bandwidth. The transfer functions for the 15Hz bandwidth controller with the buffer delay function are shown in figures 3.8 - 3.9. These are compared to the theoretical results predicted from the discrete augmented state model. Notice that the unmodeled modes have altered the bandwidth somewhat. There is still noticeable phase loss due to delays, but the delay states have yielded an improvement over the previous phase plot. The implementation of the buffers had a realizable stabilizing effect on the controller. A summary of the gains for the 15Hz bandwidth controller is shown in table 3.2.

MatrixX SystemBuild Diagram
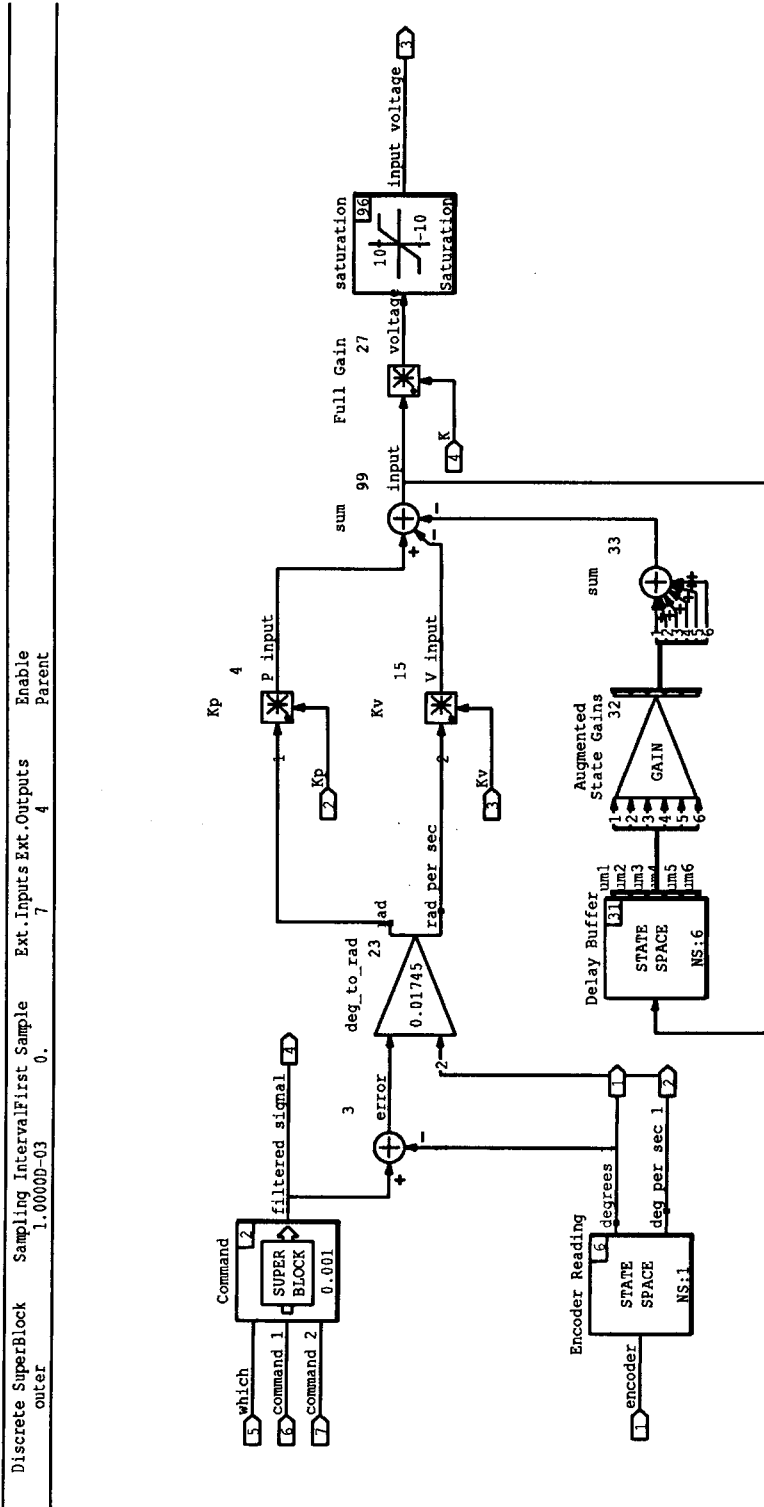
FIGURE 3.7: A block diagram of control algorithm for a PD controller with augmented delay buffer states.

CLOSED LOOP GAIN TRANSFER FUNCTION
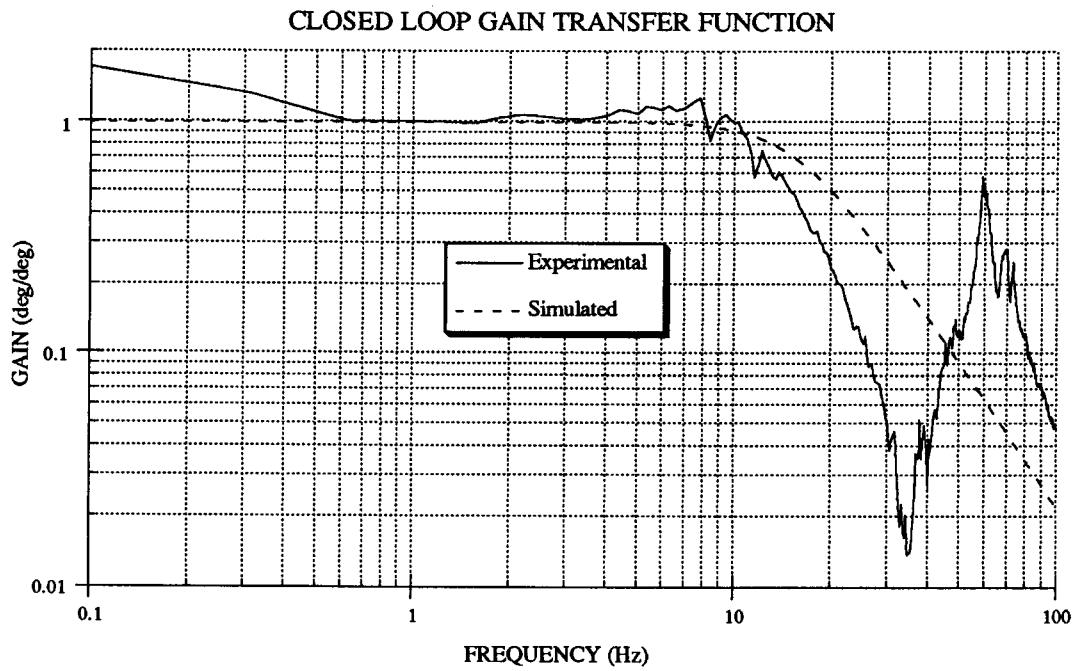
FIGURE 3.8: Closed loop gain transfer function of command to
encoder angle.

CLOSED LOOP PHASE TRANSFER FUNCTION
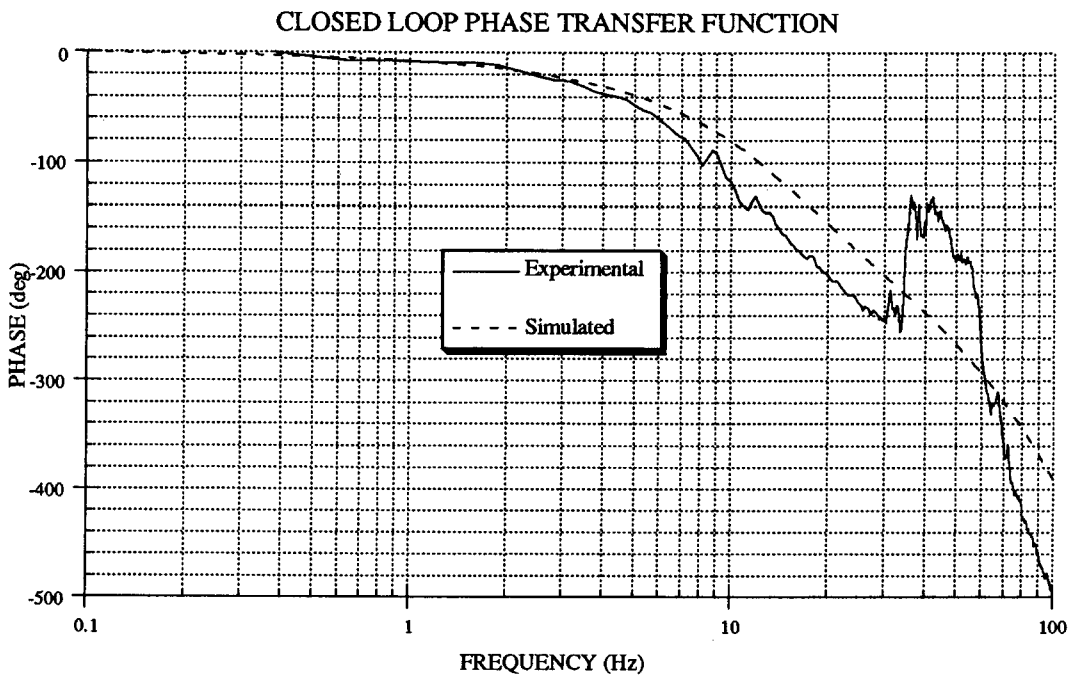
FIGURE 3.9: Closed loop phase transfer function of command to
encoder angle.

GAIN	VALUE
Kp	552 volts/rad
K_V	11.6 volts/rad/sec
g1	0.180 volts/volt
g2	0.249 volts/volt
g3	0.237 volts/volt
g4	0.224 volts/volt
g5	0.212 volts/volt
g6	0.200 volts/volt

TABLE 3.3: A summary of the parameters for 15Hz bandwidth controller with delay buffer states.

3.7 Difficulties Encountered and other Considerations

Dealing with computer and filter delays was a good exercise in control theory but an unnecessary one. Further research on the MACE test article will demand much more computing power and will tolerate less delay than these initial experiments. Higher order controllers will require more computation and may decrease the servo rate. Since the processor delay is a function of the servo rate, it will become increasingly more troublesome. Plans for a new processor board may help the situation. Also, the instability at 460Hz is a design oversight that needs to be resolved. A solution may erase the need for a filter in the loop and cause less phase loss. This may come about in the second generation Engineering Model gimbal which has taken this into consideration.

There are some other control issues for the gimbal that were not covered. An integrator feedback was not used because a reasonable method of modeling the integrator in the augmented state model was not found. However, ad hoc methods of prediction and trial and error may prove to be an effective way to add an integrator term to the control law. Another method of reducing the steady state error is to use a gravity compensator. This was also examined but neglected due to the problems with system delays. Two methods of implementation are possible. A feedback method would read the encoder angle and transmit the right amount of current into the motor to hold the gimbal steady at that angle. A feedforward method would translate the input command into a voltage corresponding to that angle and feed it directly into the gimbal. Both of these methods would increase pointing accuracy and would work in addition to the controller in place. A more legitimate method of control derivation may be to model the unstable structural modes of the gimbal and the testing mount, rather than filtering them. This would result in a more complicated model and a higher order controller that may further tax the computer. The controllers implemented in this section were found to be sufficient for the required slewing and pointing applications.

3.8   Closure

In this chapter we have covered the Middeck Active Control Experiment as the testbed for the experiments presented in this paper. MACE is a NASA funded project whose purpose is to develop the hardware and science specifications for experiments on board the Space Shuttle during the summer of 1994. The goal of the project is to investigate issues concerning

active control on a flexible structure in a zero gravity environment. The Development Model (DM) hardware located at MIT has been discussed in detail. The suspension system was seen as an advanced tool for simulating a zero gravity environment, but not sufficient as to be able to ignore gravity effects. Some results of open loop testing were given to describe the dynamic characteristics of the DM. Finally, a detailed description of the procedure for deriving the controller for the gimbal actuator was presented.

Impulse shaping is one of many different parallel research efforts going on at the Space Engineering Research Center. MACE will provide a vehicle for the impulse shaping technology to gain credibility by securing real on-orbit test results. The goals and specifications of the MACE project are congruent with those of my research. It is a most suitable platform for advanced experiments on impulse shaping.

THE SIMULATION: DISCOS

Chapter 4

4.1 Introduction

There were two reasons we wanted to utilize simulation as a tool in this research. The first is that impulse shaping had been verified in simple systems and linear models, but nonlinearities had not been addressed. We wanted to present a comparison between the linear and nonlinear simulations. The hope was to gain some insight into how impulse shaping affects nonlinear systems. Second, simulation was a method of verifying our algorithms before applying them to the hardware. Nonlinear simulation was a tool that was available before the hardware. This chapter will briefly describe the DISCOS simulation code and the corresponding model of MACE. We will end the chapter with some results of dynamic analysis and impulse shaping results. Bodley [3] should be consulted for a more in depth review of DISCOS.

4.2 What is DISCOS?

DISCOS stands for Dynamic Interaction Simulation of Controls and Structure. It is a fairly large program written in FORTRAN developed by Martin Marietta and Goddard Flight Center in the 1970's. Its purpose is to provide a tool for studying the nonlinear behavior of large, multiple-body, flexible space structures. It formulates and calculates time domain solutions to the nonlinear differential equations of motion. It also has a linearization capability for frequency domain and control stability analysis. Some features which allow it specifically to be used in space systems are the inclusion of gravity gradients, thermal gradients, solar pressure, and drag. It is an ideal program for analyzing large satellites or space vehicles. We decided to use it to simulate MACE.

The MACE model input into DISCOS is derived from an early version of an ADINA finite element model developed at SERC. The details of the derivation of this model are described in Padilla [17]. DISCOS sees a system as a collection of bodies connected by hinges. The bodies may be flexible or rigid and the hinges can be defined as clamps, pins, rollers, or spring damper systems. MACE was modeled as three bodies, two rigid payloads and a flexible bus connected by pins. A schematic of the MACE model is shown in figure 4.1.

The bus, two gimbals, and torque wheels are modeled as one long beam with concentrated masses at the actuator locations. At the center of the bus is an actuator point where outside torques and forces can be applied. This is how we'll simulate the action of the torque wheels. The gimbal actions will be simulated by a hinge torque between the bus and the payloads. A sensor is

placed at the hinge between payload two and the bus to provide a measurement of vibration.

MACE DISCOS model schematic
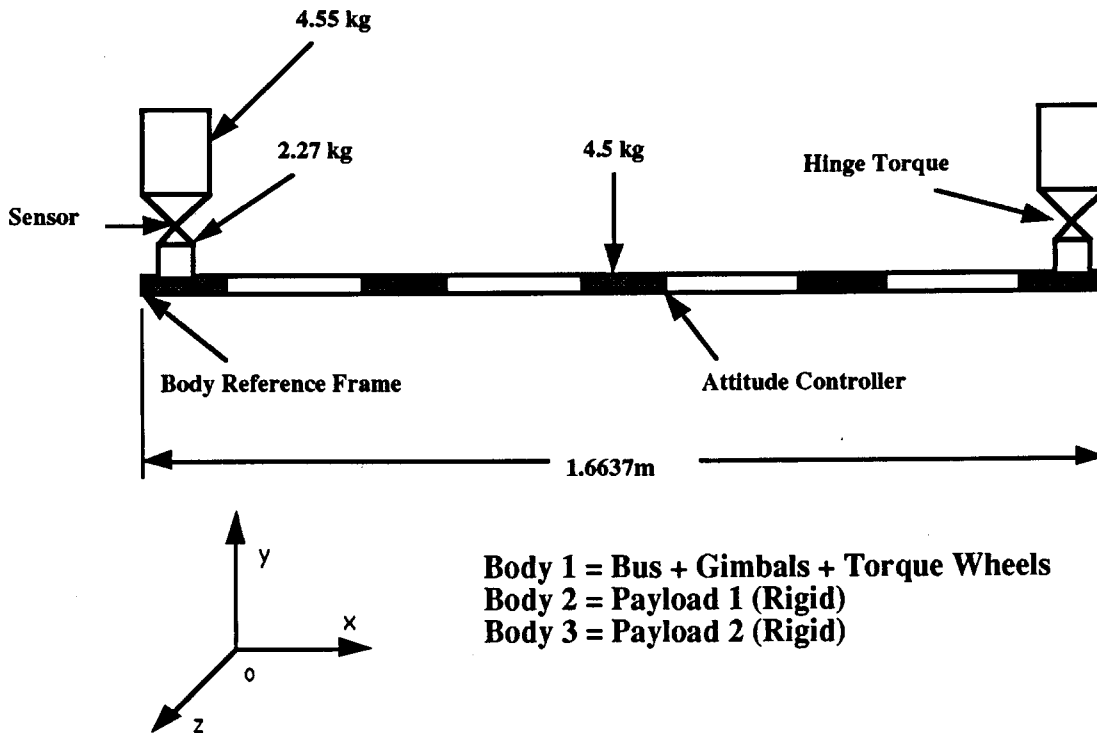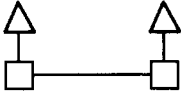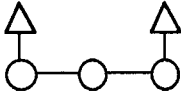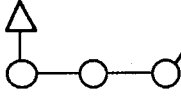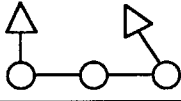
FIGURE 4.1: A schematic of what MACE looks like in DISCOS.

The flexibility in the bus is modeled as a set of elastic displacement coordinates projected onto the inertial axis which are derived from the vibration modal information from the FEM model. These modes, along with the mass and inertia information for each point on the bus, are defined kinematically in DISCOS with respect to the body-fixed reference frame on the bus. The first nine modes of the system were modeled.

4.3 Dynamic Analysis

To find the modal frequencies of the full model in different configurations, frequency identification tests were performed. Wide band white noise was generated from the computer and used as input into the payload one gimbal. In DISCOS, this was translated as a hinge torque between bodies one and two. The sensor output from the sensor between the bus and payload two was read. Ten simulations were completed and an average of the Fast Fourier Transform of the runs was analyzed to identify the resonant modes. Several configurations were tested to distinguish the differences in modal frequencies. PD controllers were added at both payloads and at the attitude controller to provide a closed loop analysis as well. A summary of the modal information for different configurations is given in figure 4.2.

MACE CONFIGURATION	ANGLES (deg)	FREQUENCY 1 (Hz)	FREQUENCY 2 (Hz)	FREQUENCY 3 (Hz)
	0 / 0	1.65	5.4	6.9
	0 / 0	1.85	7.5	15.5
	0 / 20	2.01	7.5	16.5
	0 / -20	1.80	6.9	14.5

KEY: ○ CONTROLLER △ PAYLOAD □ LOCKED

FIGURE 4.2: DISCOS model modal frequencies in four different configurations.

The parameters used in this model come from an earlier design of MACE. Therefore, the dynamic characteristics may be slightly different from the actual hardware. The closed loop frequencies are also different because the controllers are altered along with the system. The first three open loop bending frequencies of the DISCOS model were 1.65Hz, 5.4Hz, and 6.9Hz. The real modal frequencies were 1.72Hz, 6.70Hz, and 8.92Hz.

The kinematic nonlinearities in the DISCOS equations allow the identification of the shifts in the modal frequencies. These shifts in frequency were a focus in the analysis of the simulations. We can see how the first four frequencies change with the different configurations. It was not clear how effective impulse shaping would be as the frequencies change during a large angle slew. Also, verification of the impulse shaping algorithm was sought in a nonlinear formulation of the equations of motion. An impulse shaper only seeks the modal information from a system (ω and ζ). Since this assumption comes from fundamental linear theory, it was desired to see its effectiveness on a nonlinear system.

4.4 Simulation Results

The first set of tests completed were open loop. The payloads were clamped in the vertical position to the bus. The attitude controller was used as the actuator of the torques on the bus. A bang-bang type of input was used to torque the system to an angle and stop it. The inertial angle of the bus was used as an indicator of the system vibration. The input was then shaped using a three impulse sequence for the first mode at 1.65Hz. The first mode dominated the response of the system and the suppression of that frequency

TORQUE INPUT SHAPED FOR 1 MODE
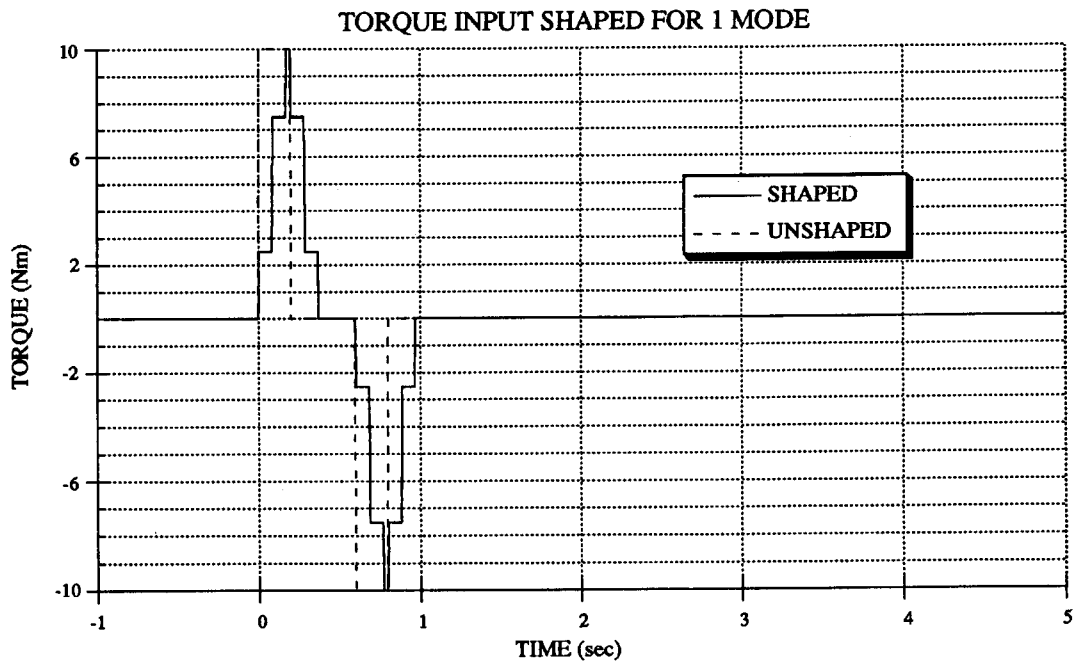
FIGURE 4.3: Shaped and unshaped torque inputs into attitude
controller. 1 mode (1.65 Hz)

BUS ANGLE RESPONSE TO UNSHAPED TORQUE
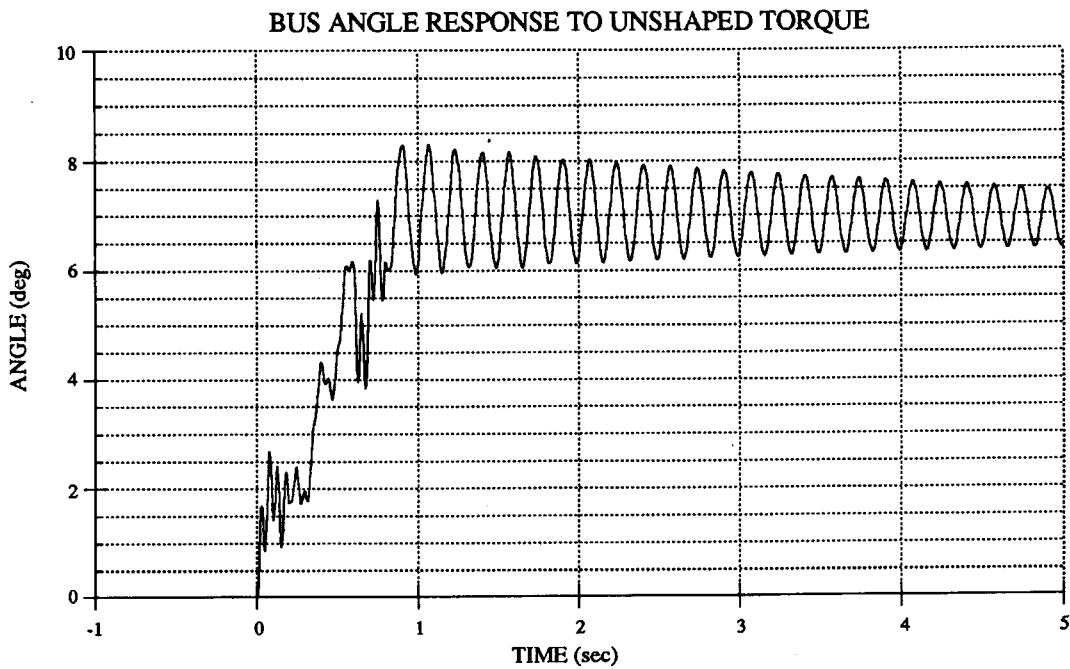
FIGURE 4.4: Bus inertial angle response to unshaped torque
input into attitude controller.

BUS ANGLE RESPONSE TO SHAPED TORQUE
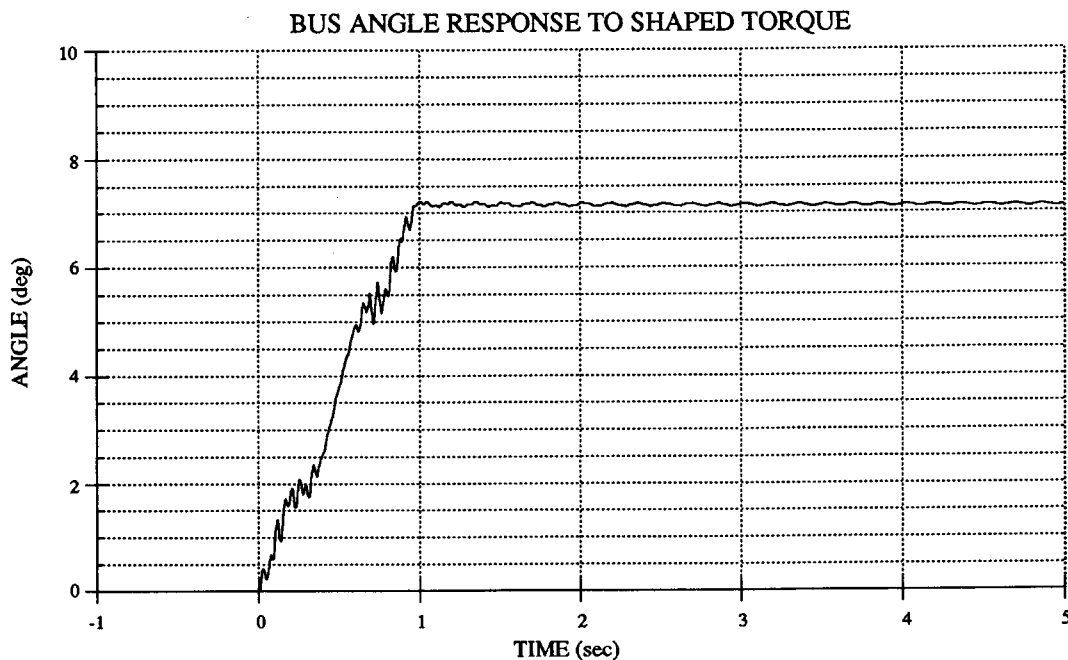
FIGURE 4.5: Bus inertial angle response to shaped torque input into attitude controller (1.65Hz)

would cancel most of the vibration. The same output was recorded and compared to the unshaped case. A summary of the results is given in figure 4.3 - 4.6.

The unshaped response shows the multiple mode behavior of the system. It is clear that the bang-bang input has excited much vibration in the bus. The shaped response shows a vast improvement over the unshaped response. There is almost no visible residual vibration in the first mode. Notice how the input is now staircased for the three impulses in the sequence. The time delay incurred from the shaping is about 0.606 seconds. The settling time of the vibration however is almost zero.

A closed loop simulation was the goal of the next test. PD controllers at the three actuators provided a configuration that is more like what will happen on the test flight. Payload one was given a position command that moved from -20° to +20°. The deflection in the Y direction was read from the sensor mounted at payload two. The command was then shaped for a direct solution sequence for the first three modes. A summary of the results is given in figures 4.7-4.8. Notice that the sensor reads motion relative to the body-fixed reference frame of the bus and hence the steady state deflection is zero. The deflections are small due to the actions of the control system.

PAYLOAD ANGLE RESPONSE TO SLEW
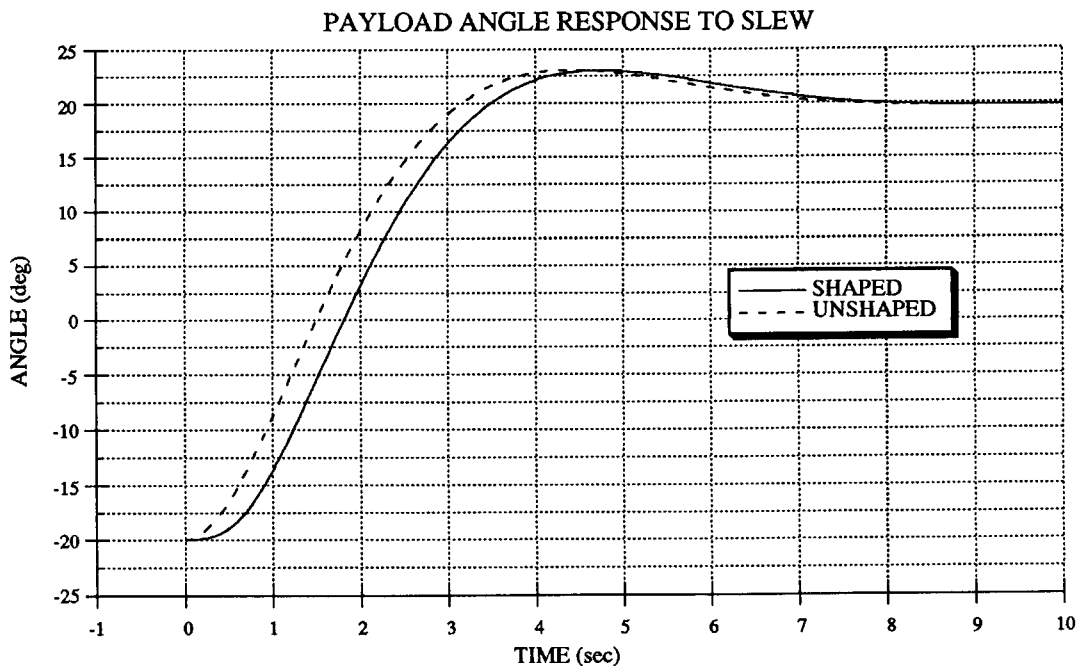
FIGURE 4.6: Payload angle response to 40° shaped and unshaped slews. 3 modes (1.85, 7.5, 15.5 Hz).

ENDPOINT DEFLECTION TO UNSHAPED SLEW
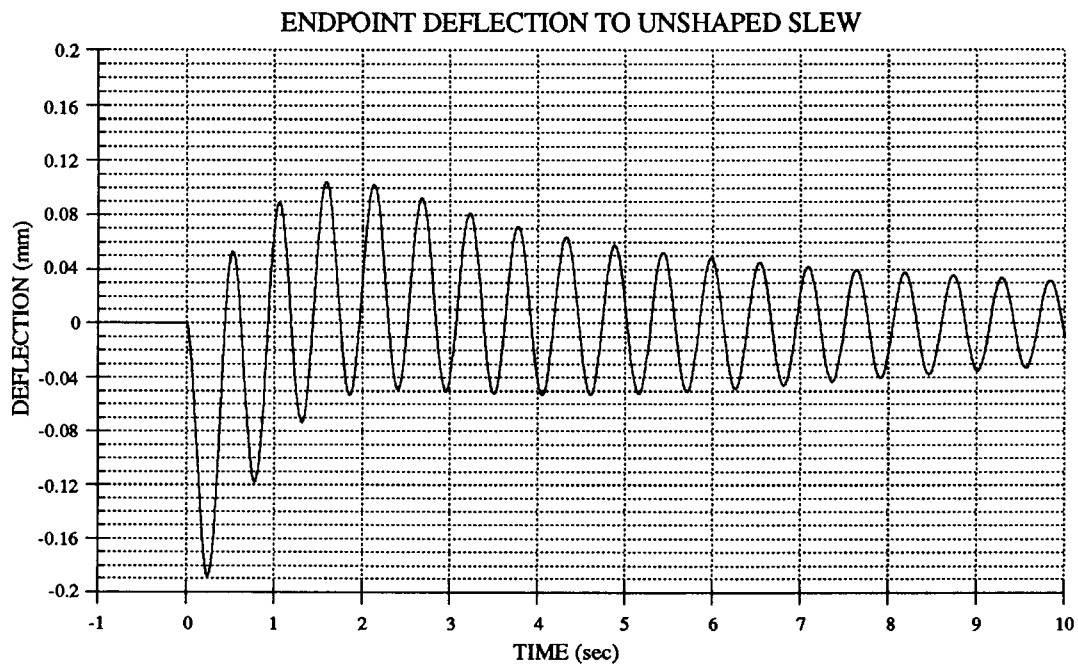
FIGURE 4.7: Sensor deflection in y direction for unshaped
40° slew.

ENDPOINT DEFLECTION TO SHAPED SLEW
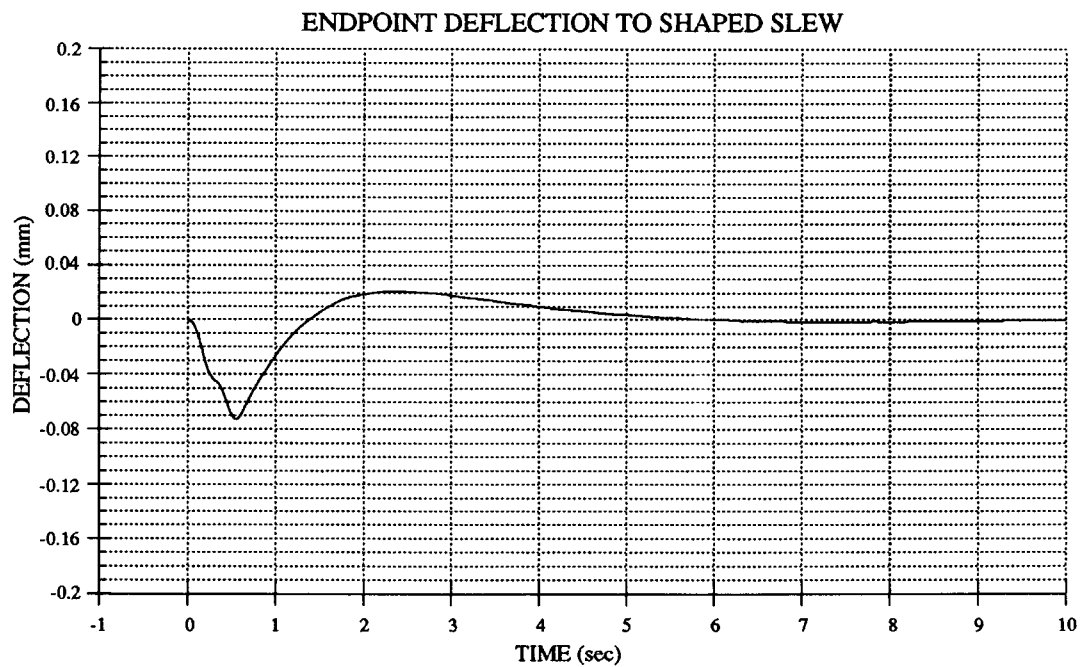
FIGURE 4.8: Sensor deflection in y direction for shaped
40° slew. 3 modes (1.85, 7.5, 15.5 Hz)

The results are similar to that of the open loop tests. The shaped response shows a clear improvement in vibration response. However, a closer look at the responses will reveal that the vibration response is not absolutely zero. We notice that in the slew from -20 to +20 degrees the first modal frequency has shifted from 1.80Hz to 2.01Hz. The shaper has been designed for the vertical configuration with the first mode at 1.85Hz. The changes in frequency due to the kinematic nonlinearities are causing a slight decrease in the effectiveness of the impulse shaper.

Although the shaper did not meet the absolute zero vibration constraints set by the original equations, it did show a significant improvement in the vibration response over unshaped moves. It wasn't expected that the nonlinear model would conform completely to impulse shaping. More analysis of the nonlinearities will be discussed in the hardware experiments. These simulation experiments have proven that impulse shaping can be effective on nonlinear systems. This will serve as a basis for the results from hardware tests presented in the next chapter.

EXPERIMENTAL RESULTS

Chapter 5

5.1 Introduction

Data from the MACE hardware was sought in order to verify the impulse shaping effects on a real system. We also wanted to address the issues that would arise from implementation. The experiments presented in this chapter are from the MACE Development Model and its supporting electronics and suspension system. This chapter will also provide an analysis of the data, its implications, and how to deal with some of the problems.

5.2 Defining Input Shaping Effectiveness

Before we can start evaluating experimental results, we need to define what we're looking for. There needs to be a performance metric to gauge the effectiveness of a shaper in reducing vibration. This performance

metric, of course, depends on the particular application and is a function of, among other variables, the percentage of vibration reduction.

The MACE flight plan calls for the pointing of one payload while the other slews to a different position. The stability of the first payload is crucial since the payload is likely to be a precise telescope or laser pointing at a far away target. The primary goal then is to design a regulator that rejects all the disturbances caused by the slew. We are not concerned with that here. The secondary goal is to be able to slew the second payload without causing much disturbance to the other end of the bus. This is where impulse shaping is employed.

The appropriate sensor needs to be chosen to evaluate the relevant response of the system. The vertical accelerometer at node four on the other end of the bus (figure 3.2) was chosen as it relates closely to the amount of force that is exerted on the other payload. It also shows good amplitude for the mode shapes of those modes under 10Hz. Notice that unless a sensor is mounted on a node point of a particular mode shape, the same resonances should be seen at any sensor on the structure. There may be additional zeroes in the transfer function to some sensors, but the poles do not change. Singer has shown that numerator dynamics do not matter in impulse shaping. So, the choice of sensors just allows us to more closely examine a certain point on the structure; it does not determine the validity of the results. Other sensors were observed to verify the accuracy of the first.

MACE was designed to have many lightly damped modes under 20Hz as seen in section 3.5. In vibration control, we are mostly concerned with low frequency modes. Generally speaking, the slow modes tend to last longer

and have higher amplitudes, and hence, cause more of a delay by increasing the settling time. We arbitrarily decided to concentrate on those modes under 10Hz, ignoring the higher modes as less significant. In a typical slew, these modes were the most visible and the cause of most of the vibration problems. In the vertical plane, 6 modes were identified under 10Hz, and it was felt that was a suitably complex problem for the impulse shaping calculation methods available.

The performance metric becomes, then, the amount of vibration a certain shaper can suppress in the vertical acceleration at the other end of the bus for the modes within the first 10Hz of the MACE test article. As a general rule, we will describe "good" performance as 5% residual vibration. We then weight the amount of vibration suppression against the complexity of the impulse sequence and the length of time delay caused by the sequence. The time delay is a cost since a very slow move regardless of shape will always cause little vibration. The solution complexity is still an issue because the formulation of the sequences has not been fully resolved.

5.3   Open Loop Results and Discussion

The first set of tests done on MACE were open loop. An entered user command was converted to a current command that was directly input to the motor. Theoretically, the controller state of the plant does not matter in impulse shaping. As seen in the DISCOS simulations in Chapter 4, shapers can be just as effective for open loop slews as for closed loop slews. The open loop shaping results in actual hardware, however, were very poor and showed little improvement in residual vibration. This was due to the

hardware inconsistencies which were too severe to overcome with an open loop control scheme. The slew profiles and the plant responses were both very inconsistent from run to run. An impulse shaper requires very precise movement of the actuator to be effective. A shaped command tends to be more irregular than the original commanded move and thus requires more precision from the actuator. There are many factors in the setup that hinder this accurate movement. There is a lot of steady state error in the gimbal movement. The brushless motor also has problems doing consistent moves for a given input current. There are also other factors such as friction, cogging torque, amplifier dynamics, etc. A more precise actuator should produce just as consistent results as the closed loop experiments which are covered next.

5.4   Closed Loop Frequency Response

5.4.1   Experimental setup

A 10Hz bandwidth PD loop similar to the one that was designed in Chapter 3 was implemented on the gimbal as mounted on the bus. It should be noted that this is no longer a full state feedback compensator and there are many unmodeled modes of the bus within the bandwidth of the controller that are not being controlled. The compensator was found to be stable and robust, however, and adequate for the slewing application.

This loop was closed and a transfer function was then taken from the command gimbal input to the vertical acceleration at node four. The setup for this experiment is shown in figure 5.1. White noise is generated from a Fourier analyzer and input into the real-time controller. This voltage is
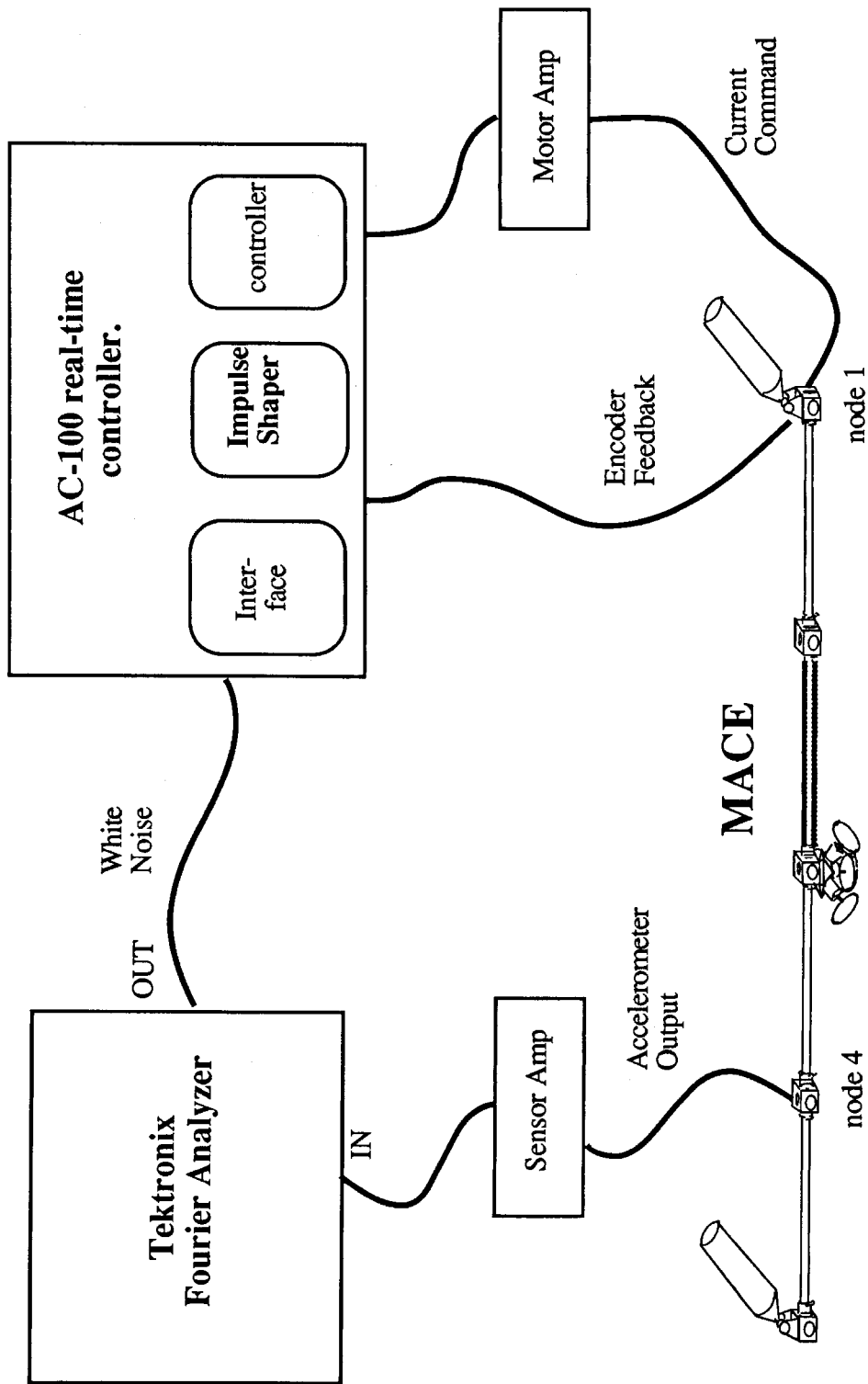
FIGURE 5.1: Diagram of Experimental Setup

translated to angle commands into the control loop. This then drives the gimbal, causing a response in the bus and the node four vertical accelerometer. The accelerometer signal is amplified and input into the Fourier analyzer. The analyzer then calculates ten averages of the Fast Fourier Transform of the accelerometer output divided by the transform of the white noise, resulting in a closed loop frequency response of the plant.

This loop was closed and a transfer function was then taken from the command gimbal input to the vertical acceleration at node four. The setup for this experiment is shown in figure 5.1. White noise is generated from a Fourier analyzer and input into the real-time controller. This voltage is translated to angle commands into the control loop. This then drives the gimbal, causing a response in the bus and the node four vertical accelerometer. The accelerometer signal is amplified and input into the Fourier analyzer. The analyzer then calculates ten averages of the Fast Fourier Transform of the accelerometer output divided by the transform of the white noise, resulting in a closed loop frequency response of the plant.

The results are shown in figures 5.2 - 5.3. We note the similarity to the open loop transfer functions shown in Chapter 3. The amplitudes are different because the units have changed from $m/s^2/volt$ to $m/s^2/deg$. The peaks, however, retain the same shapes. This is due to the large relative size of the bus compared to the gimbal actuator. We can imagine that adding a controller is similar to adding a small spring and damper at the first node. This new stiffness has caused certain modes to change. Two of the visible alterations are the smaller amplitude and sharper peak of the first mode and the larger amplitude of the fifth. The second vertical mode
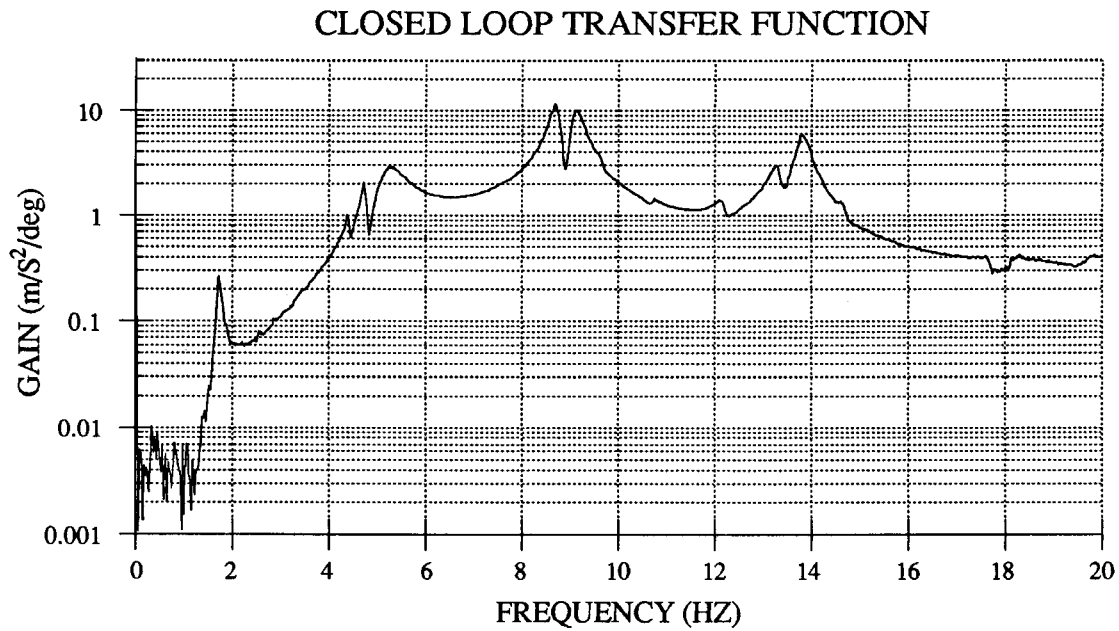
CLOSED LOOP TRANSFER FUNCTION

FIGURE 5.2: Closed loop gain transfer function from commanded gimbal angle to vertical acceleration at node 4.

CLOSED LOOP PHASE TRANSFER FUNCTION
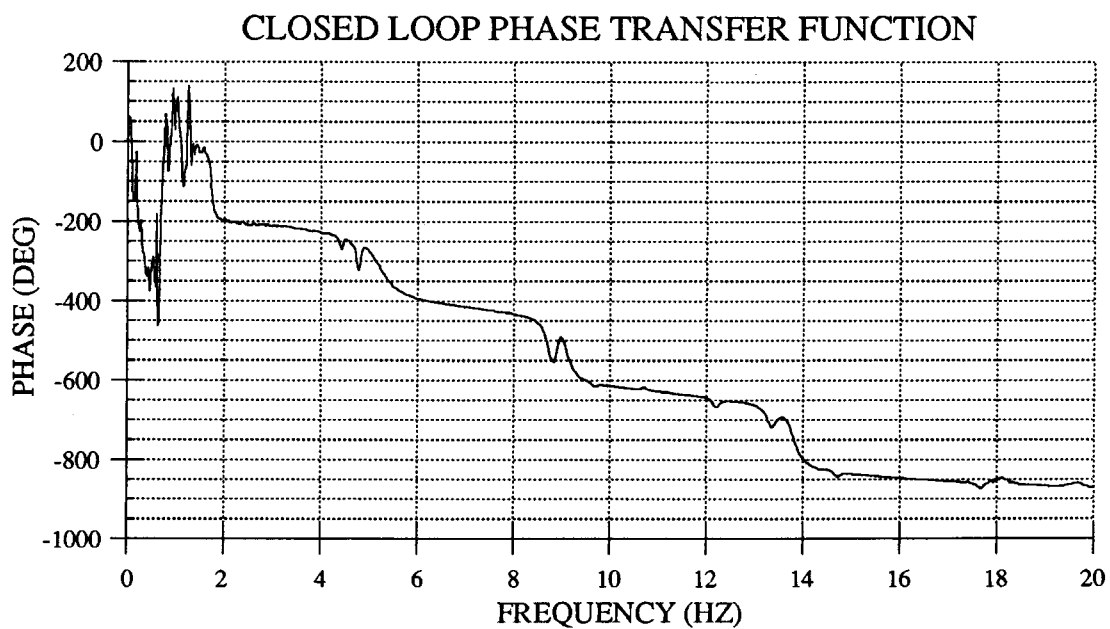
FIGURE 5.3: Closed loop phase transfer function from commanded gimbal angle to vertical acceleration at node 4.

at 5.23Hz has been most affected by the controller as it has shifted from its prior 6.82Hz.

5.4.2 Shaped response

The experiment was then repeated with an impulse shaper placed in between the Fourier analyzer and the controller to examine the shaping effects on the system in the frequency domain. The shaper is programmed into the microprocessor and designed to convolve any input with the impulse sequence in real time. The white noise is now shaped before it enters the control loop and the shaper becomes a part of the plant whose transfer function is being taken. The shaped closed loop transfer function is then acquired as shown in figures 5.4 - 5.5. Results for two different shapers are shown: a three impulse shaper for the first mode at 1.75Hz and a nine impulse direct solution sequence for the first, fourth, fifth, and sixth modes (1.75, 5.23, 8.68, and 9.13Hz). These shapers were chosen to suppress vibration at the slowest mode, and then the next three with the highest amplitudes. The second and third modes were omitted because they are primarily horizontal modes as shown in section 3.5.

We can immediately see what the shaper is doing. The three impulse sequence for the first mode has cut the amplitude of vibration in that mode by almost two orders of magnitude. Moreover, we can see that the areas around that mode are also suppressed as well. This robustness is even more evident in the direct solution sequence. We see that most of the area under the curve between around 5Hz and 13Hz has been destroyed. We also notice from these plots the repeating nature of these shapers. They happen to cancel modes which are multiples of the ones being shaped. For

SHAPED CLOSED LOOP TRANSFER FUNCTION (1 MODE)

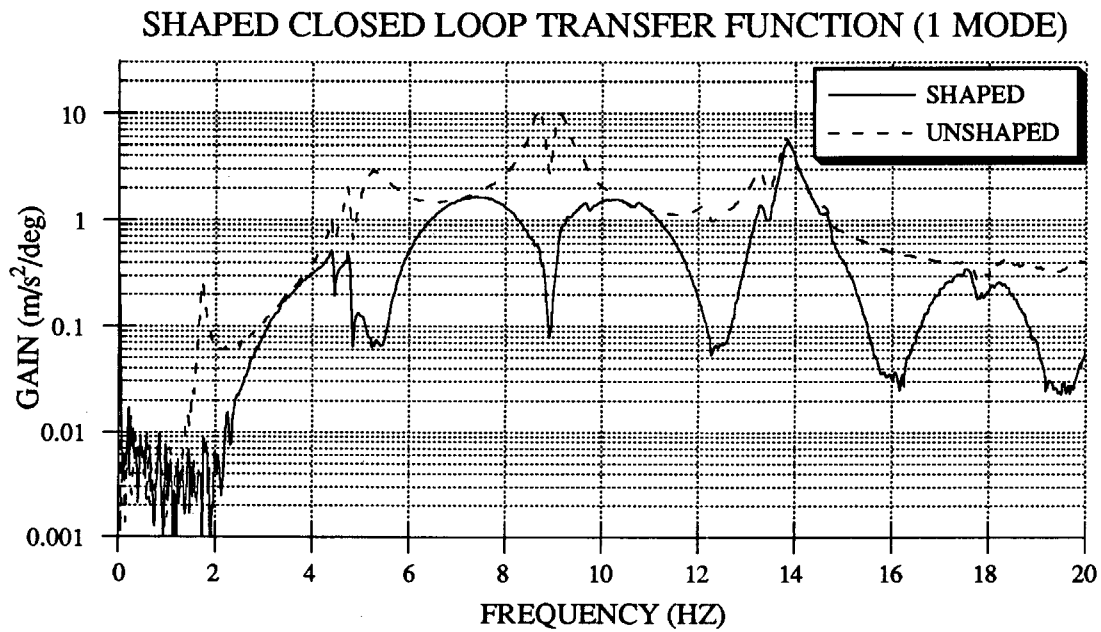**FIGURE 5.4**: Closed loop transfer function with 1 mode, 3 impulse shaper (1.75Hz)

SHAPED CLOSED LOOP TRANSFER FUNCTION (4 MODES)
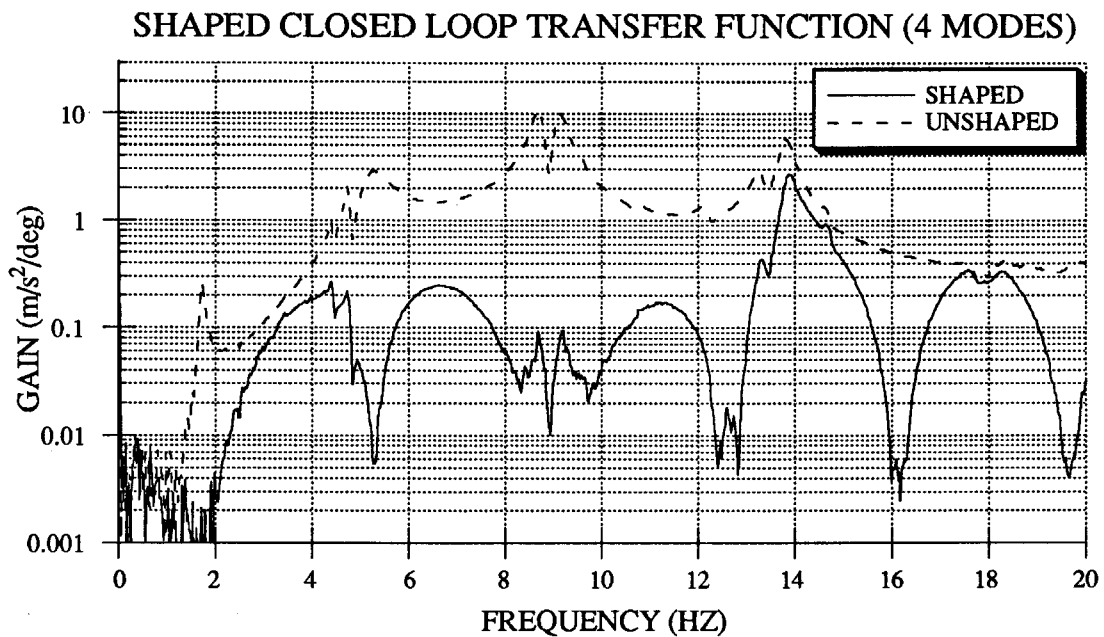
FIGURE 5.5: Closed loop transfer function with 4 mode direct solution sequence (1.75, 5.23, 8.68, 913Hz).

example, in the three impulse one mode shaper, by coincidence we have also canceled most of the fourth, fifth, and sixth modes as well. It is not yet quite understood where the direct solution sequences will repeat, but it is clear that they have a unique pattern of repetition. Although we don't cancel as much amplitude or achieve as much robustness in higher modes by using technique, we will see later that it can be just as effective as independently shaping for those modes.

5.4.3 Experimental insensitivity curves

Recall how we calculate an insensitivity curve. It is a measure of the amplitude of vibration response, at each frequency on the x axis, to a given shaped move as a percentage of the response to an unshaped move. An amplitude of one would mean that the shaped move causes the same amount of residual vibration at that frequency as the unshaped move. The transfer functions we have taken have enough data on them to produce experimental versions of these insensitivity curves. By dividing at each point in frequency the amplitude of the shaped response by the amplitude of the unshaped response, we get a measure of the percentage of vibration that the shaped excitation has left relative to the unshaped excitation. The resulting curve is in effect a plot of the amount of vibration a shaper can cancel for a range of frequencies. This can be directly correlated to the theoretical insensitivity curves that have been produced using the impulse response equations. The experimental insensitivity curves for both the one mode three impulse sequence and the four mode direct solution sequences are shown in figures 5.6 - 5.7.

EXPERIMENTAL INSITIVITY CURVE (1 MODE)
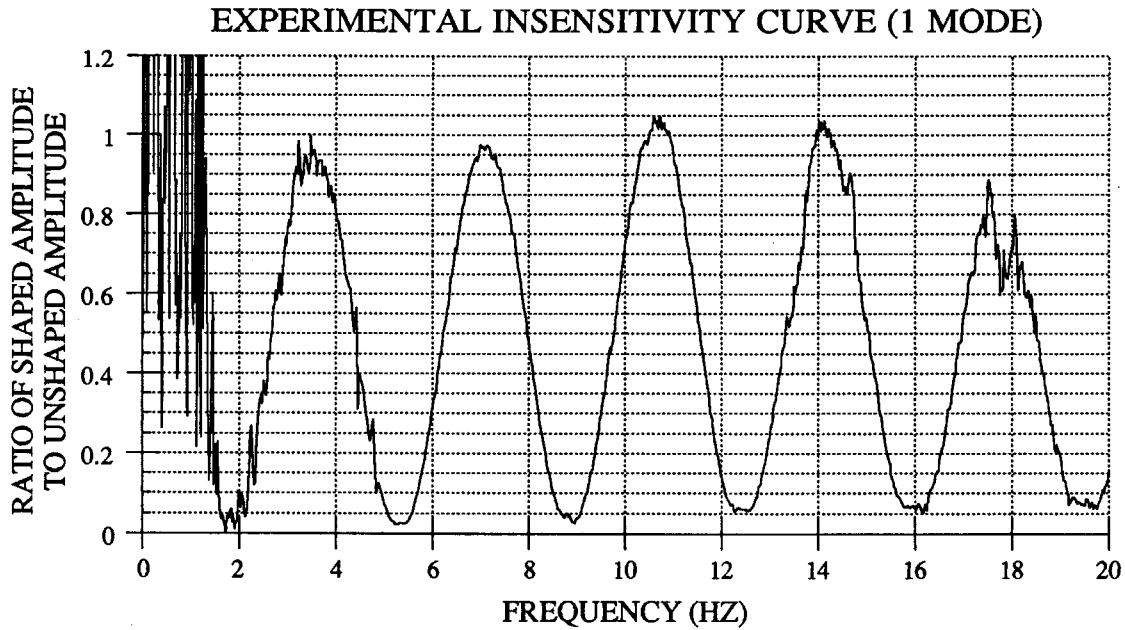

FIGURE 5.6: Insensitivity curve for three impulse shaper for 1 mode (1.75Hz).

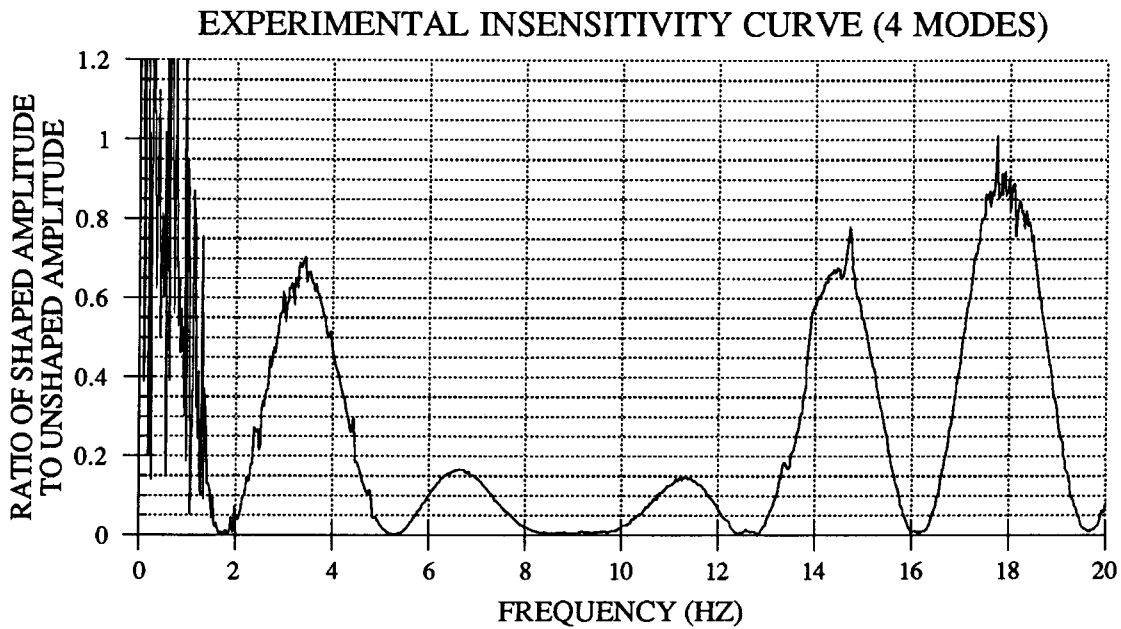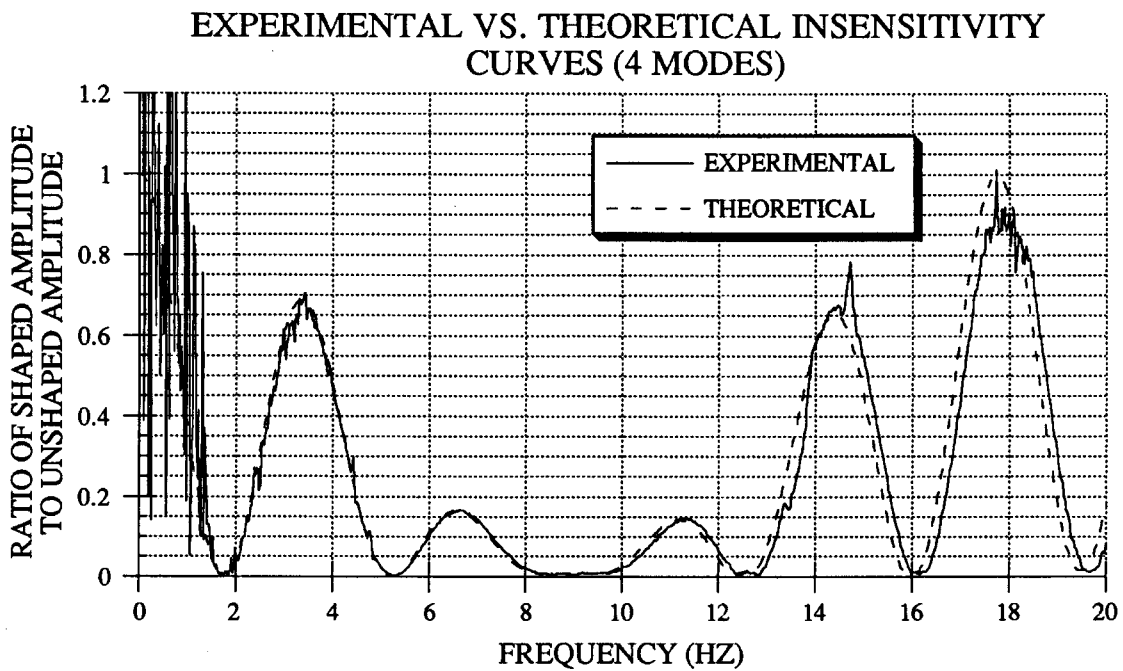## EXPERIMENTAL INSENSITIVITY CURVE (4 MODES)

FIGURE 5.7: Insensitivity curve for 4 mode direct solution sequence (1.75, 5.23, 8.68, 9.13Hz).

These curves provide a more visual measure of the robustness of these shapers to errors in plant parameter estimation. For the first mode, we can see we're within 5% vibration error in the range of 1.5Hz to 2.0Hz. We also see the repetition of the zero vibration constraint at odd multiples of 1.75Hz. The loss of effectiveness at higher modes is a result of the digitization of the impulse sequence (we can only approximate the times of the impulses as accurately the servo rate of the controller allows; in this case .001 sec). The effect of digitization is seen more in the higher repeated modes as can be seen in the figures. In the four mode direct solution plot, we see the same robustness in the 1.75Hz range, and we see even more robustness in the 8 to 10Hz range where we have shaped for two modes. This is a case where the robustness of the shaper for two modes which are close together "overlap" and cause a large region to be very robust. That whole region appears to have close to zero percent vibration. We also note that the robustness of the 5.23Hz region is about the same as that of the 1.75Hz region. As discussed in Chapter 2, this is due to the direct solution formulation. A convolved sequence would show approximately three times more robustness in the 5.23Hz range. For the time savings gained from the direct solution method, however, this sequence seems to be a more efficient one.

When the experimental results are compared to the theoretical data, we see a very close correlation. Equation 2.3 is used to calculate at each point in frequency the amplitude of vibration to obtain the theoretical insensitivity curves for the particular sequences. Both sets of data are shown in figures 5.8-5.9. The theoretical data has also been calculated using the digitized sequences. We see that the experimental data not only follows the trends of the theoretical data, but even mimics the small details, such as the tiny

EXPERIMENTAL VS. THEORETICAL INSENSITIVITY CURVE (1 MODE)

FIGURE 5.8: A comparison of experimental versus theoretical insensitivity curves for 1 mode 3 impulse shaper (1.75Hz)

EXPERIMENTAL VS. THEORETICAL INSENSITIVITY CURVES (4 MODES)

FIGURE 5.9: A comparison of experimental versus theoretical insensitivity curves for 4 mode direct solution sequence (1.75, 5.23 8.68, 9.13Hz).

hump at 12.5Hz for the four mode direct solution sequence. The experimental data obtained through this procedure indicates a good correlation between the theoretical model and the actual hardware.

5.4.4 Why does it work so well?

Any time experimental data looks this good, one must question why it does so. The theoretical data is based on a linear representation of the plant. It is derived from the second-order linear response of a system to a series of impulses. We can deduce from the experimental data that the system behaves like the linear system described, or a close approximation of one. There are a couple of reasons that MACE may look linear in this configuration.

When the frequency data is being taken, the plant does not move much. The white noise amplitude is kept small due to the amplifier constraints and there is no DC offset, so there is no rigid body movement. There is enough movement to induce vibration in the bus, and enough amplitude to see high coherence in the frequency response data. However, the envelope of vibration in the bus is small and the gimbal angle displacement is minimal ($< \pm 1°$). Typically, Dynamic systems that have small angles or displacements can be modeled as linear systems. So the small amplitudes of the test lend itself to exhibiting very linear behavior.

Another reason for the good correlation is the lightly damped modes of MACE. When the impulse sequences and the insensitivity curves were calculated, we assumed that every mode had zero percent damping. This is

because, in order to calculate the response of a frequency to the impulse sequence, we need to know the damping ratios at each frequency. This is difficult to know, so we generally assume that the damping ratios at each frequency are the same as that of the most lightly damped mode being shaped. The modes within the first 20Hz of MACE are very lightly damped; all under 2% damping. So the zero percent damping was a good assumption in this case. Each frequency under 20Hz for MACE behaved very closely to zero percent damping as the results suggest.

5.4.5 Why shouldn't it work so well?

We have reasoned why the experimental data should follow the theoretical data, but we can also reflect on why it shouldn't. Although the plant is not moving very much, it is still a real-life nonlinear system with all its unpredictable characteristics. There are many real hardware hurdles that this test overcomes: there is friction and stiction in the actuator and in the joints of the bus; the computer, amplifiers, and filters all have dynamics of their own; energy migrates between frequencies as in all real systems; and the MACE suspension system adds funny dynamics to the structure including the plunge modes, the pendulum modes, and the violin modes of the rods. All of these factors are not accounted for in the theoretical formulation. Although the test experiences all of these "non-linearities," the frequency response data still follows closely what we would predict from a simple linear model. We will see in the next section that once we start slewing large angles, this linearity assumption becomes less valid.

5.5 Closed Loop Time Histories

5.5.1 Slew profile and limitations

All the slew calculations were done in real time with user inputs. The slew profile was originally derived from scaled slews of what a larger size pointing payload would do, such as a telescope on the EOS platform. This was determined to scale to an angle of 120 deg ($\pm 60°$), a velocity of 50 deg/sec, and an acceleration of 125 deg/s^2. The slew angle of the gimbal is governed in actual hardware, however, by the limitations of the suspension system. The suspension system travel does not allow for any slews larger than 20 degrees as the pressure pistons bottom out for larger moves. The move was then transformed for a 20 deg slew that kept that same maximum velocity. The slew has a trapezoidal velocity profile which has a 1-2-1 ratio of acceleration - constant velocity - deceleration. The profile in shown in figure 5.10. This profile was used as a typical slew for a pointing payload in our experiments. The slew formulation was programmed into the real-time computer to convert a user step input command into this type of profile. Since this smoothing function manipulates inputs, it can also be considered a type of real-time input shaping. It does, though not very efficiently, filter out unwanted high frequency content from the input.

5.5.2 Unshaped response

A summary of the unshaped 20 degree slew is shown in figures 5.11 - 5.13. We can see that the controller follows the move fairly closely with a bit of time lag and some steady state error, as we would expect from a PD
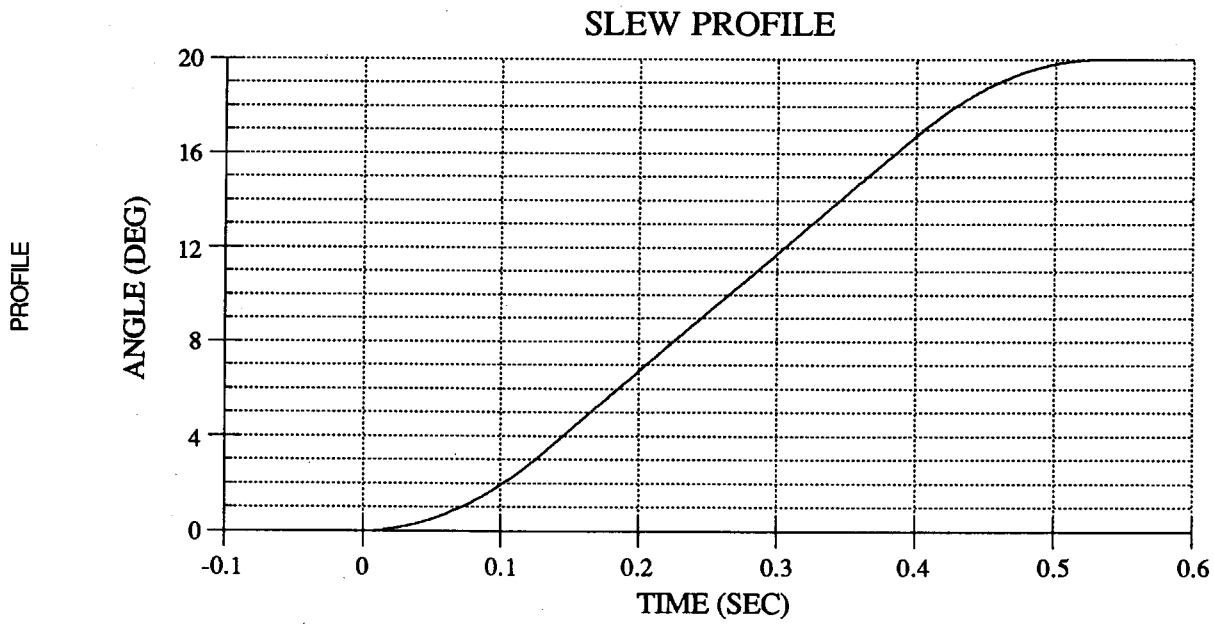
SLEW PROFILE

FIGURE 5.10: Profile of gimbal angle command

GIMBAL ANGLE RESPONSE TO 20° UNSHAPED SLEW

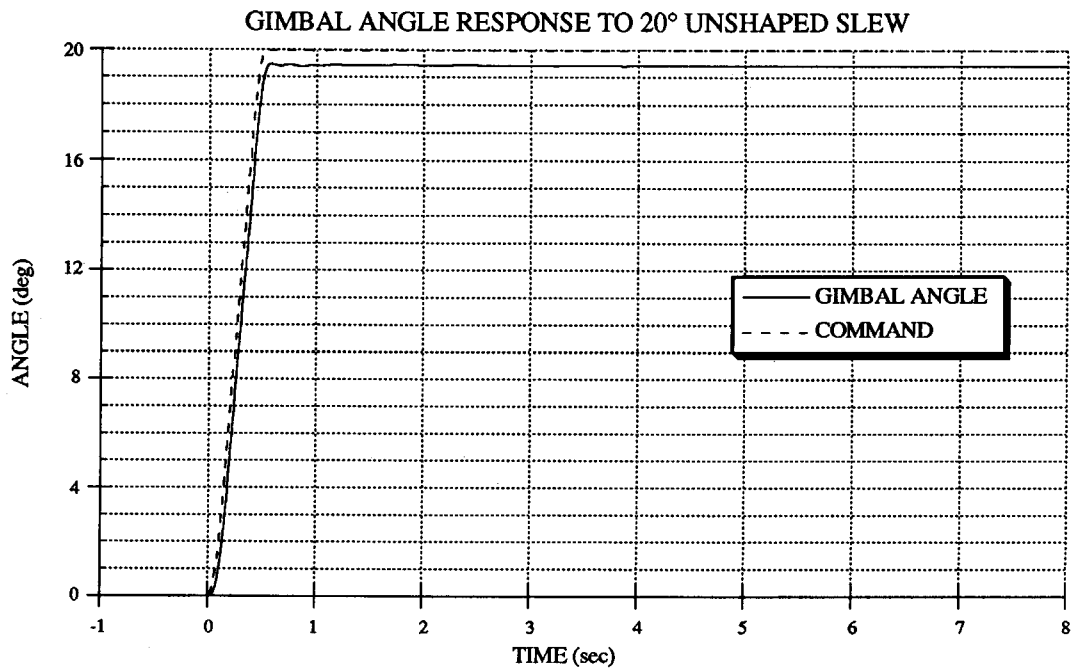**FIGURE 5.11**: Gimbal angle command and response for a smooth 20° slew.

GIMBAL ANGULAR RATE RESPONSE TO 20° UNSHAPED SLEW
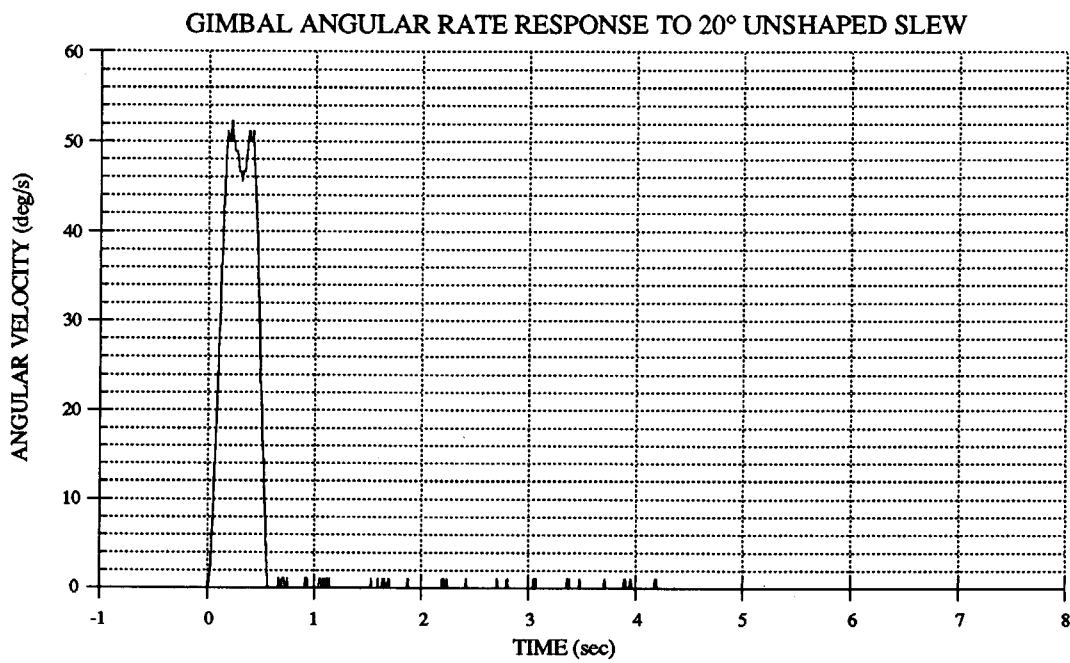
FIGURE 5.12: Gimbal angular rate response to smooth
20° slew.
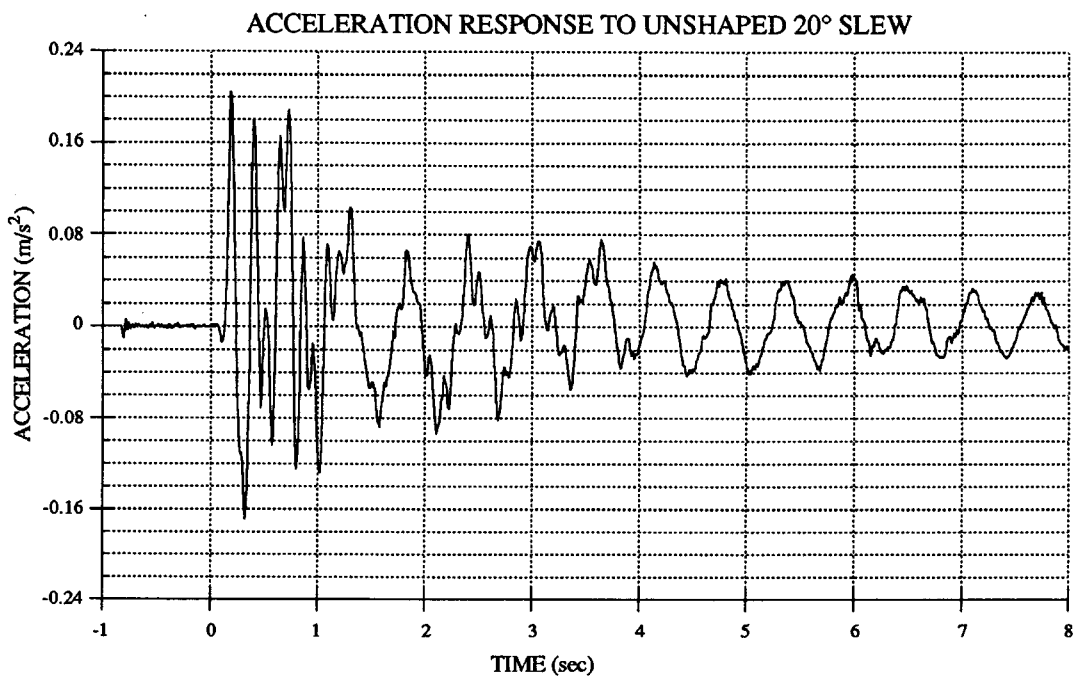
ACCELERATION RESPONSE TO UNSHAPED 20° SLEW

FIGURE 5.13: Node 4 vertical acceleration response to smooth
20° slew.

controller. The slew is smooth enough such that there is no visible overshoot or settling time in the gimbal angle response. The velocity plot shows the trapezoidal profile that the gimbal is following. There is a bit of overshoot in the velocity curve which shows up as a dip at the top of the trapezoid. The maximum velocity is around 50 deg/sec. The accelerometer output shows the response at the other end of the bus. The acceleration plot shows the multiple mode behavior of the response, and that most of the amplitude is governed by the first bending mode of the system (1.75Hz). We can also note from the plot the slight 0.2Hz plunge mode of the suspension system. This will become more evident in the shaped responses. As discussed in Chapter 3, this mode is an order of magnitude below the first resonance of the bus and it should have little effect on the dynamics of the plant. The vibration in the acceleration response is large and lasts for quite a while, begging the need for a vibration control scheme.

5.5.3 Shaped Response

5.5.3.1 One mode shaped

Figures 5.14 - 5.15 show a summary of what the slew looks like when it is convolved with a three impulse shaper for the first bending mode. A close look at the slew profile reveals that the shaped slew reaches the end position about .57 seconds (1/1.75Hz) later than the unshaped move in figure 5.11. This is the time delay cost or the length of the shaper. The acceleration response exhibits a significant reduction in the vibration amplitude. The first mode, which is the most visible and the longest lasting, is almost unnoticeable. In the nine seconds of data that is taken, we can see most of

GIMBAL ANGLE RESPONSE TO 20° SHAPED SLEW (1 MODE)
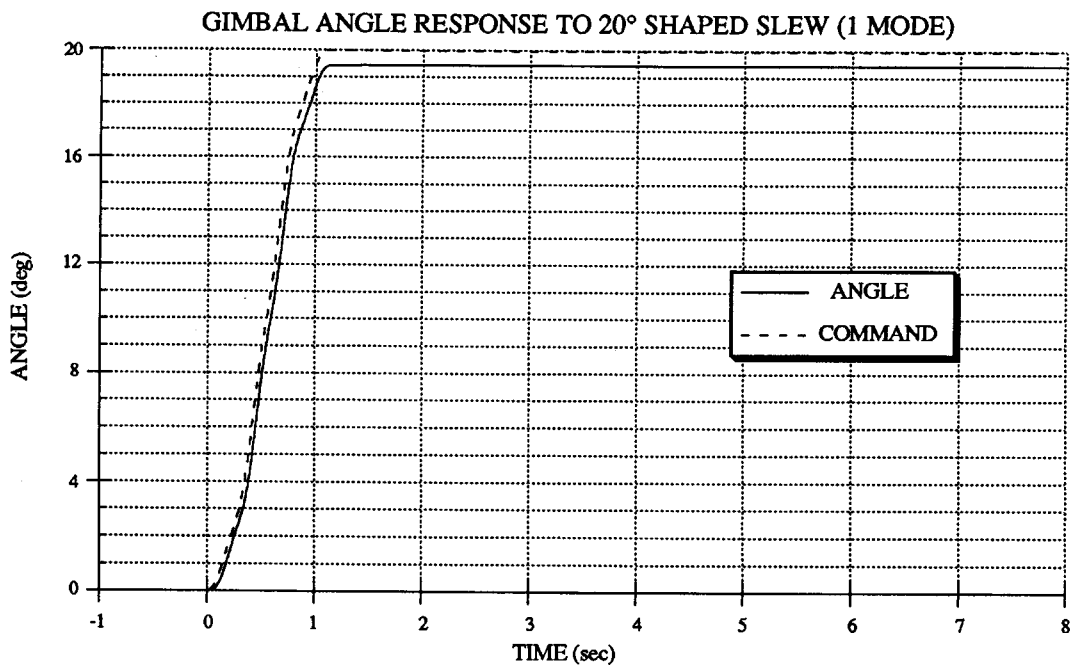

FIGURE 5.14: Gimbal angle command and response for a 20°
slew shaped for one mode (1.75Hz).

ACCELERATION RESPONSE TO SHAPED 20° SLEW (1 MODE)
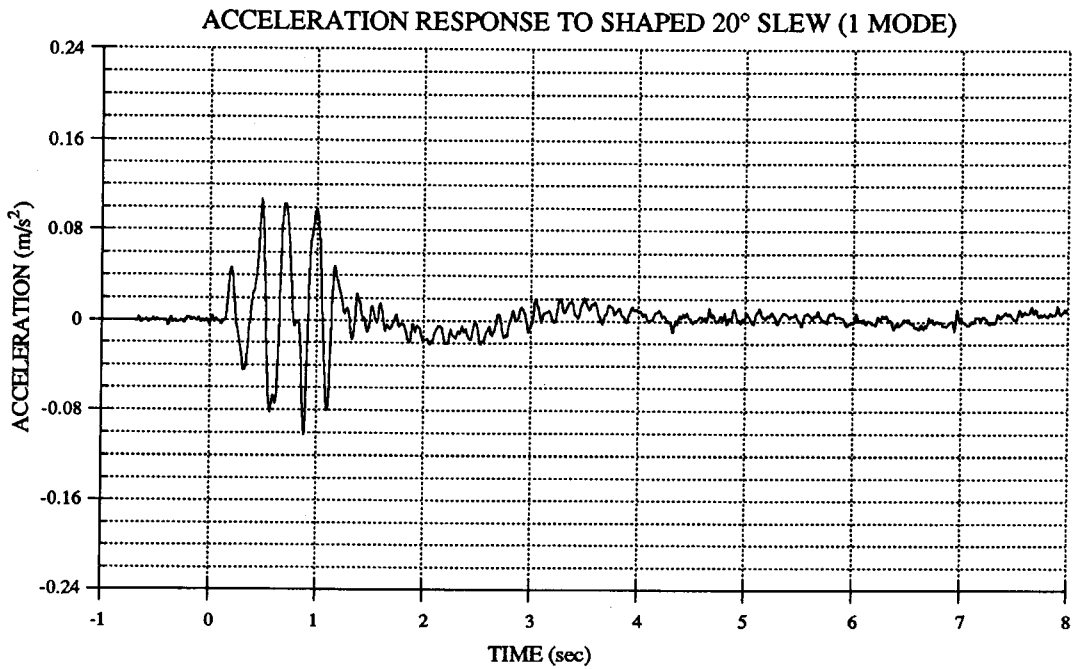
FIGURE 5.15: Node 4 vertical acceleration response to 20° slew
shaped for one mode (1.75Hz).

FAST FOURIER TRANSFORM OF SHAPED 20° SLEW (1 MODE)
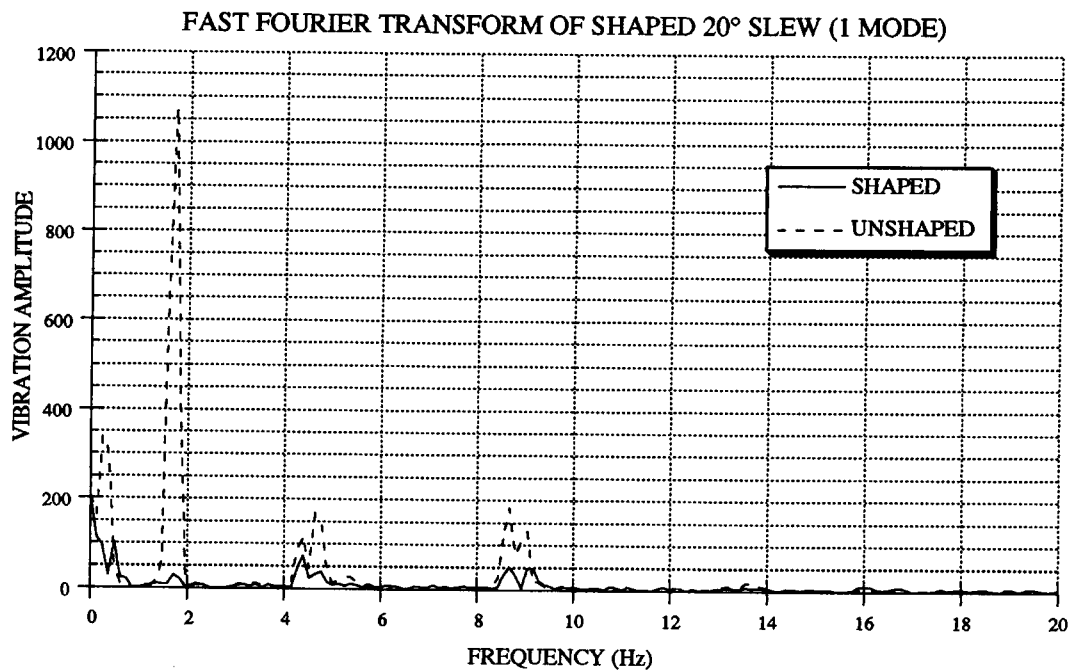
FIGURE 5.16: Fast Fourier Transform of residual vibration at node
4 accelerometer for 20° slew shaped for 1mode (1.75Hz).

the vibration in the other modes settle as well. A more quantitative way to view this data is to take an FFT (Fast Fourier Transform) of the data to get a frequency spectrum over a range of frequencies. To measure the residual vibration, we need only to FFT the data after the move has been completed, which in this case is at about 1.1sec (.53+.57). Five runs were taken and averaged to plot the data shown in figure 5.16. The amplitude of the vibration is plotted on a linear-linear scale for the 0-20Hz range. We can see the reduction of the peak at 1.75Hz. This corresponds to an effective vibration reduction of 97%. We also see that substantial vibration has been canceled in the third, fifth, and sixth modes. None of those modes were canceled to a satisfactory level, but it is interesting to note the consequence of the repeating nature of the impulse shaper. This shaper is a very

effective one for the first mode and correlates closely to the results shown in the frequency response experiments. We see in the next section that the higher modes are more difficult to suppress.

5.5.3.2 Four modes shaped

We now move on to the data taken with the four mode direct solution impulse shaper. The same plots as in the previous section are shown in figures 5.17 - 5.18. We notice that the cost in shaper delay is slightly higher (around .676 seconds). The acceleration response plot shows an improvement over the one mode sequence. This is a slower move than the one mode sequence, so we see less vibration during the move also. Almost all of the visible vibration is gone by 8 seconds into the move. The FFT data in figure 5.19 shows in more detail the improvement over the unshaped move and the one mode shaped move. The reduction in the first mode is practically unchanged. The vibration reduction is about 96%. The peaks at 8.9Hz and 9.13Hz have been further reduced. However, their amplitudes are still very visible. In the time traces, we can see that the move has ended at about 1.2 seconds, but there is still very visible vibration with a frequency of around 9Hz. The percentage reductions here were only 69% and 85% respectively. This is inconsistent with the theoretical and experimental insensitivity curves which showed almost zero percent vibration over the whole range between 8 and 10Hz. These are highly excitable modes and that may contribute to their sensitivity, but we would expect the robustness of this 4 mode sequence to overcome any tendency for those modes to vibrate.

In the next section, we try using more robust shapers to cancel the vibration in this region.

5.6 Using More Robust Sequences

We need now to address why the 4 mode direct solution shaper is not as effective for the higher modes at 8.9 and 9.13Hz as it was for the 1.75Hz mode. The problem lies in the fact that impulse shaping is based on linear theory and here it is being applied to a nonlinear system. We saw hints of linearity in the frequency response data and we may expect that the time histories would be somewhat close to that, if not the same. But it is not. The movement of the gimbal over a large angle induces unmodeled effects that
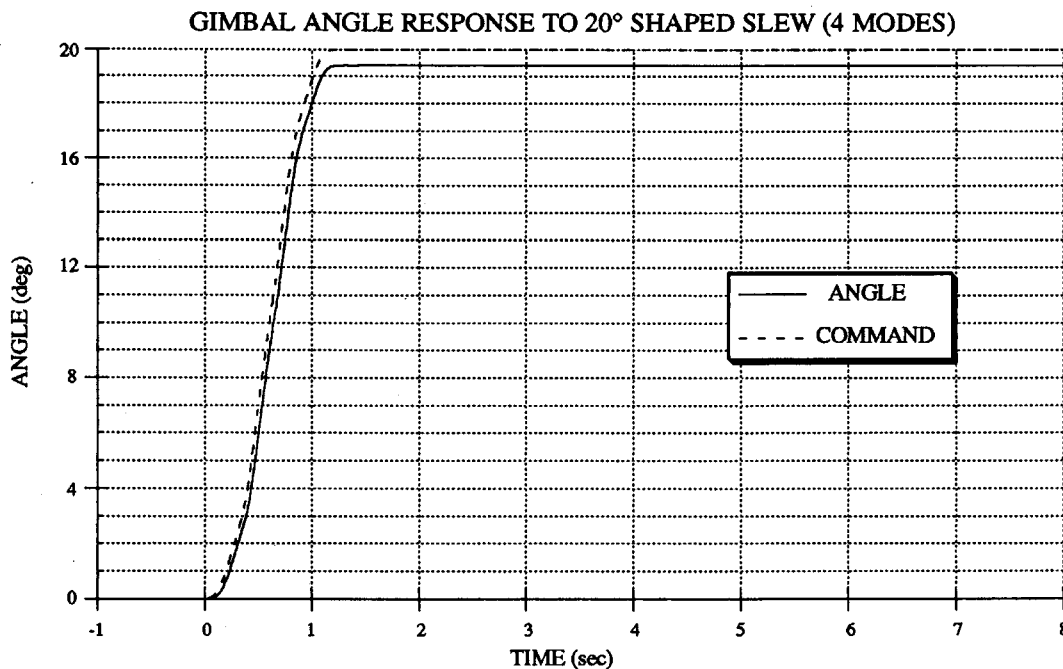
FIGURE 5.17: Gimbal angle command and response to 20° slew shaped
for 4 modes (1.75, 5.23, 8.68, 9.13Hz).

ACCELERATION RESPONSE TO SHAPED 20° SLEW (4 MODES)
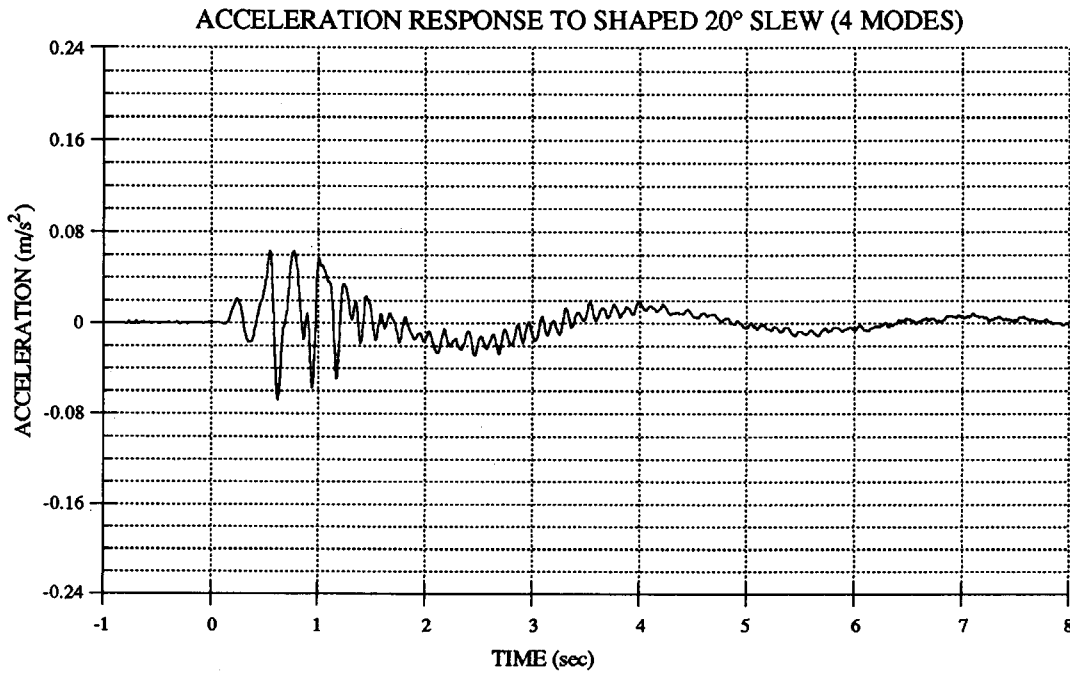

FIGURE 5.18: Node 4 vertical acceleration response to 20° slew shaped
for 4 modes (1.75, 5.23, 8.68, 9.13Hz).

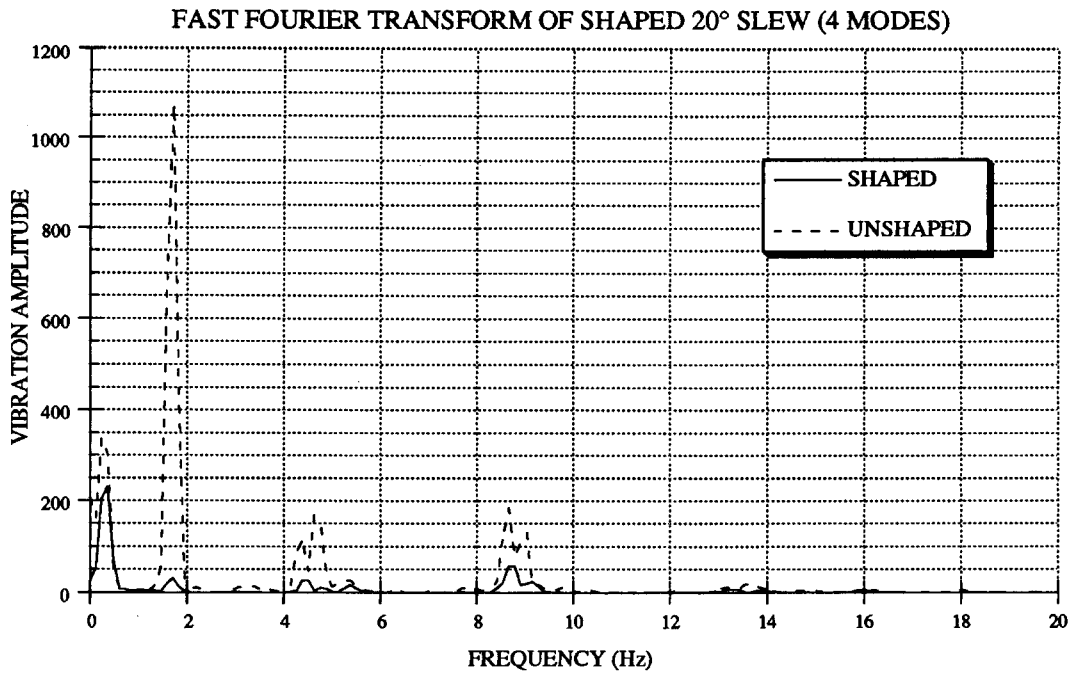FAST FOURIER TRANSFORM OF SHAPED 20° SLEW (4 MODES)

FIGURE 5.19: Fast Fourier Transform of residual vibration at node 4
accelerometer for 20° slew shaped for 4 modes.

disable the impulse shaper from canceling higher frequency modes. We will from here on call these unwanted effects "nonlinearities." We now want to determine if a more robust sequence can overcome these non-linearities and cancel the remaining residual vibration in the 8.9Hz and 9.13Hz modes.

As mentioned in Chapter 2, the direct solution method loses some robustness in higher modes when compared to the convolution method. Seeking more robustness in the 8 to 10Hz region, a convolved sequence of the two modes around 9Hz was formulated. Four impulse sequences were also considered, adding another derivative constraint to the zero vibration equations. Two new four impulse sequences were calculated; one sequence for the frequency in between the two modes (8.9Hz), and the second, a convolved sequence for both modes. Both convolution and second derivative constraints add substantially to the length of the sequences. For example, a direct solution sequence using two impulses per mode for the two frequencies at 8.68 and 9.13Hz yielded a sequence 0.112 seconds long where a convolved four impulse sequence is 0.337 seconds long. What we lose in time delay, we are gaining in robustness. The new sequences concentrate on the modes in the 9Hz area, foregoing canceling vibration at the other modes. An exhaustive list of impulse sequences were implemented in an attempt to cancel the vibration at these frequencies. However, none of them were successful. The results of the slews with the different shapers are shown in figures 5.20 - 5.21. All of these plots are averages of five runs and contain 164 points in the 0-20Hz region. This plots are not intended to show the exact amplitudes of the individual shaped moves. There is too much data here to show. It does reveal the trends in the data; that no matter what

shaper was used, the response was always pretty much the same in that region. Even the convolved four impulse sequence, which contains 16 impulses and is extremely robust in the 8-10Hz range, failed to effectively cancel those modes. Interestingly, the shaper we would least expect to be effective, the three impulse sequence for the first mode, performed about median among all the other shapers.

The results show that a more robust sequence cannot cancel the remaining 30% or so vibration left in the fifth and sixth modes. In fact, there was very little deviation in the residual vibration for all the shapers that were implemented It follows to reason that the resulting vibration is caused by something other than what impulse shaping theory would predict. This "nonlinear" effect is evident in the higher frequencies when we slew large angles. From the results of these experiments, we may say that nothing in the domain of impulse shaping seems to be able to overcome the nonlinearities associated with large angle movement to effectively suppress vibration in the higher frequency modes.

COMPARISON OF FFT's OF DIFFERENT SHAPERS

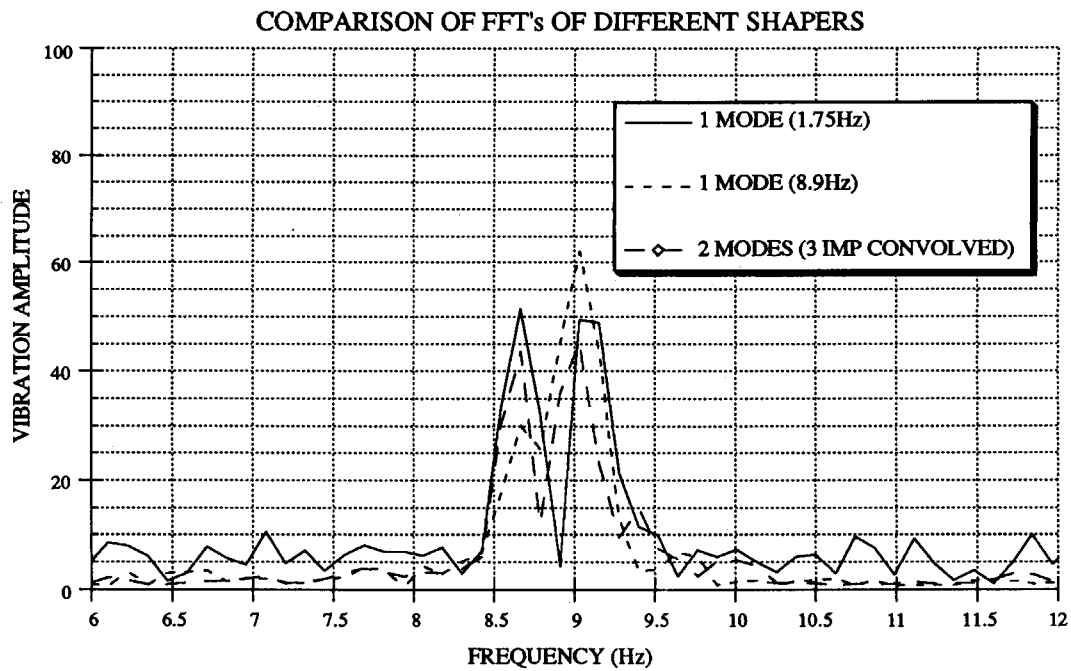
FIGURE 5.20: A close-up view of FFT of residual vibration amplitude
for 3 different impulse shapers.

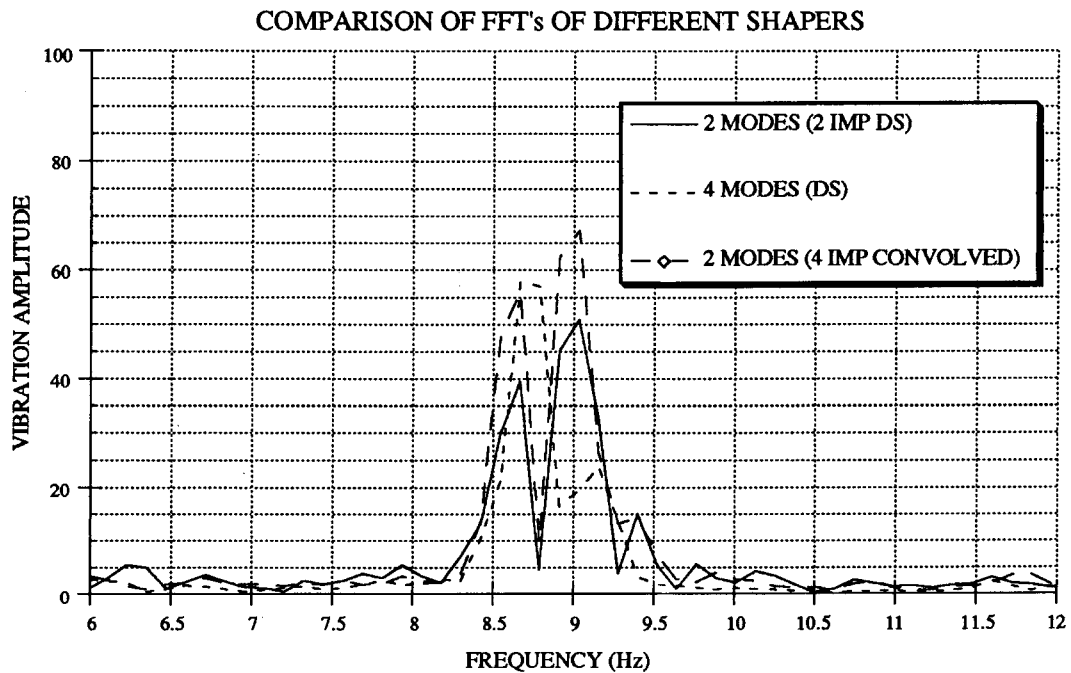COMPARISON OF FFT's OF DIFFERENT SHAPERS

FIGURE 5.21: A close-up view of FFT of residual vibration amplitude
for 3 different impulse shapers.

5.7 Identifying Nonlinearities

It is difficult to determine which particular nonlinearity causes most of the vibration in this region. Most likely, it is a combination of many different things. We have identified some nonlinearities as being small from the success of the frequency response experiments. For example; amplifier/computer/filter dynamics, friction, stiction, digitization, and the suspension effects were all found to be negligible factors. Of course, the slew experiments induce different amplitudes of these factors, but we wouldn't expect any one of them to be the major contributing factor to the residual vibration.

Some other nonlinearities can be examined as well. Centripetal acceleration is caused when the gimbal slews large angles. This, however, is found to be very small. For a maximum velocity of 50 deg/sec, this translates to a centrifugal force of less then .007 lbf. And this is applied for only a fraction of the slew time. The effect on the dynamics of the system is minimal. There is also a kinematic nonlinearity of frequencies shifting as the configuration of the plant changes as discussed in Chapter 4. In hardware, this was found to be small, as a transfer function of the plant with the gimbal at 20° showed less than 1% change in all the frequencies under 10Hz. The gimbal is small in mass and in length compared to the bus, so its movement causes little change in the frequency characteristics of the whole structure. The gravity torque was also an issue. This is a very important issue in terms of space-borne systems such as MACE, since gravity is a factor only during the ground testing phase. The gravity is pretty linear in the ±20° range however. Its effect on the motor was found to be linear to ±2% in this region. Moreover, the inclusion of a gravity

compensator, as mentioned in Chapter 3, did not remedy the problem. All of these factors were considered as contributors to the remaining vibration, but not one of them was found to be major.

The severity of the nonlinearity does seem to be a function of the size of the slew. Different size slews of the same maximum velocity were used in a series of experimental runs with the same impulse shaper. The slews have been scaled in both time and angle to retain the same velocity profile for the smaller angle slews. So, a slew to 10° would have the same shape as the 20° slew but would finish its move in half the time. A plot of the amplitude of vibration in the 8-10Hz range for the various angle slews with the two mode three impulse convolved sequence is shown in figure 5.22. We can see that the residual vibration is more severe with the 20° move and is the least visible in the 1° move. This is despite the fact that the unshaped smaller angle moves are actually putting more energy into these modes because they are more abrupt, sharper moves. This was done to accent the higher frequency modes for the smaller angle slews. Small angle slews done in the same time as the 20° run would have caused little vibration and provided little insight into the nonlinearity of large angle slews.

The data suggests that the nonlinear effect is linked to the size of the move. As mentioned in the frequency response analysis in section 5.4, linear approximations are generally valid in systems with small amplitudes. Larger amplitudes tend to cause to system to act more nonlinearly and thus less responsive to impulse shaping. The slews done here have much higher amplitudes than the frequency response experiments. More energy from the amplifiers causes the structure to

COMPARISON OF FFTs OF DIFFERENT SIZE SLEWS

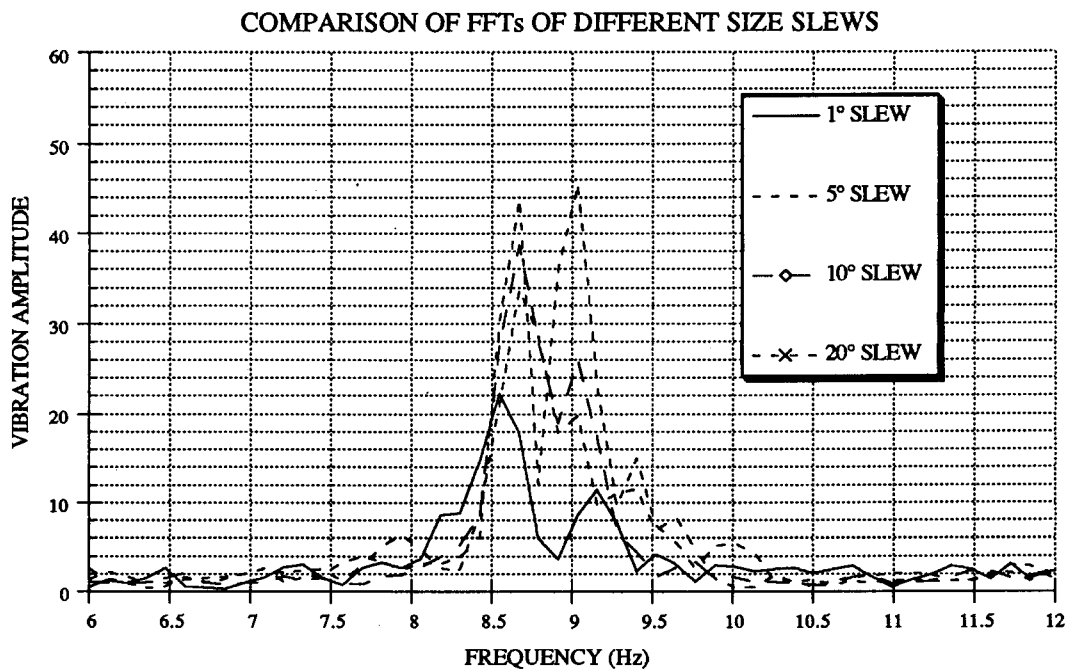FIGURE 5.22: A comparison of FFTs of residual vibration amplitude for four different size slews, all shaped for 2 modes (8.68, 9.13Hz).

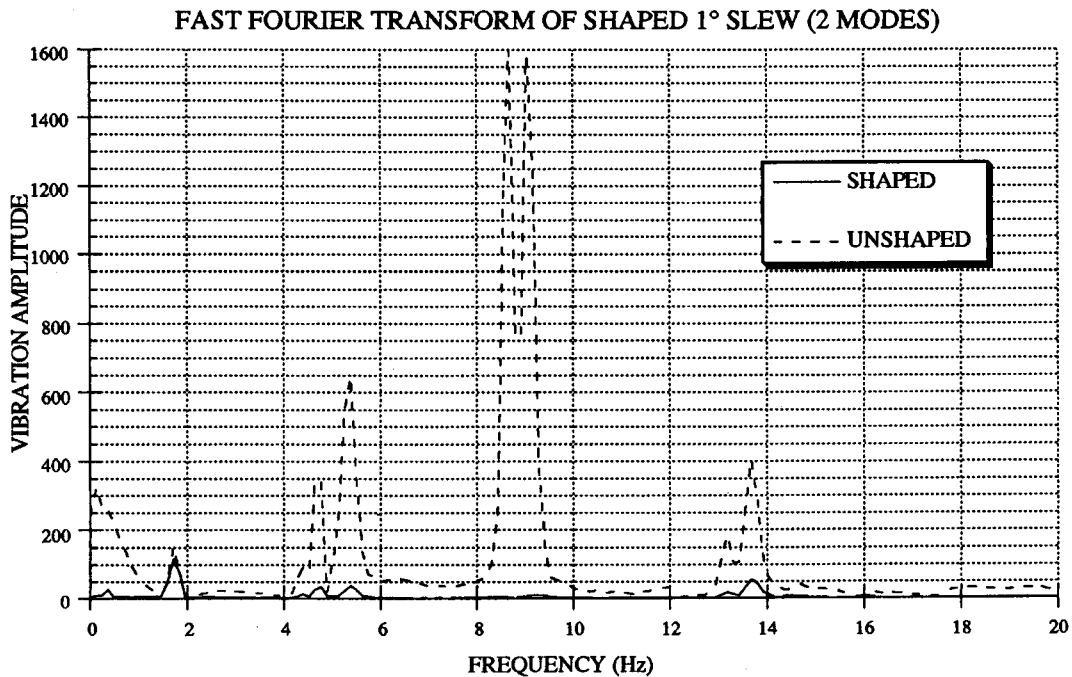## FAST FOURIER TRANSFORM OF SHAPED 1° SLEW (2 MODES)

FIGURE 5.23: Fast Fourier Transform of residual vibration amplitude for 1° slew shaped for 2 modes (8.68, 9.13Hz).

physically deform more. What we are observing is a system which acts linearly only for small angle displacements (<1°).

An example of a small angle move is shown in figure 5.23. This 1° move shows similar effectiveness as that was seen in the frequency response plots. The move is short and abrupt and causes a lot of amplitude in the 8-10Hz range. The shaped response cuts that amplitude by 99%. The resulting vibration is even less than that left by the 20° slew which had much less unshaped vibration amplitude. Although the 20° slew puts less energy into the higher modes, it puts more total energy into the system than the smaller slews and causes much more amplitude during the move time. The larger amplitude of vibration and the greater change in plant configuration contribute to the nonlinearity of the system and cause the impulse shaper to be less effective.

We can conclude that the a good portion of the nonlinear effect is caused by the large vibration amplitudes and change in configuration due to large angle slews. Many other nonlinearities were explored as possibilities, but not one was found to be a major factor. It is likely that a combination of all of them contribute to the nonlinearity of the whole system. The size of the move was seen to have the most correlation to the amount of vibration that was canceled by the impulse shaper.

5.8 Using Different Controllers

5.8.1 Breaking with impulse shaping assumptions

Impulse shaping only assumes the plant eigenvalues in the system it is trying to control. The plant is seen as a black box with some unique second order poles associated with it. The type of controller determines where these poles are, and in some cases can even add poles to the system. An impulse shaper is concerned only with these closed loop poles and tries to minimize the energy put into those frequencies. The black box, however, has components which cannot be ignored. In this section, we will show that the controller inside the system is an important factor in determining the effectiveness of an impulse shaper.
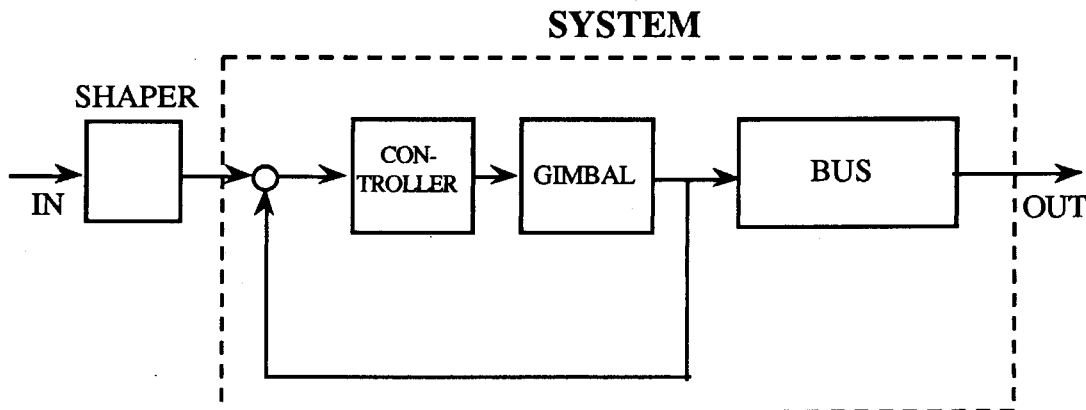
A block diagram of MACE may look like the following:

FIGURE 5.24: A system diagram of MACE

The system that the shaper is trying to affect consists of the gimbal actuator, its controller, and the bus. The gimbal and bus can be seen as decoupled here because of the large relative size of the bus and the

configuration of the gimbal sensor (the encoder). The gimbal as the actuator has much authority to induce vibration in the bus, but there is not much feedback from the bus to the gimbal angle. Of course, both components are part of the same system and the same resonances are seen on both components, but the large vibration that the gimbal can cause in the bus is not significant in the angle amplitude of the gimbal. This is due to the fact that the encoder is an angle sensor where most of the vibration induced in the bus is vertical. This is also partly the reason a PD loop was able to be successfully closed on the gimbal.

The system configuration is one closed loop system (gimbal) which excites an open loop system (bus). The sensor that we're trying to control (the accelerometer) is not a part of the closed loop system. This presents an interesting challenge in that the controller now becomes an integral part of how much vibration is induced in the bus. The torque that the controller applies at the gimbal is in effect the input into the plant since the majority of the dynamics is in the bus. In impulse shaping theory, this can still be seen as a black box with unique resonances. The controller only determines where and how large the poles are. However, the controller is important in terms of impulse shaping because it determines how much authority the actuator has over the dynamics of the bus.

Controllers tend to act like low-pass filters in that the gain rolls off past the bandwidth frequency of the controller so that the high frequency amplitudes are minimal. For example, the current PD controller of the gimbal could not follow a 20Hz sine wave very well. It would have trouble with any move that has frequency content greater than its bandwidth. This is the reason that the controller is usually designed with the types of likely

command inputs in mind. Similarly, a low bandwidth controller will not be able to follow the precise and quickly changing path demanded by a complicated impulse shaper. This will be more true when higher modes are being shaped and the impulses are closer together. For the shaper to be most effective, the path of the command needs to be followed closely. This ensures that the vibration induced during the move will be canceled by the impulses of the shaper. Also the move needs to be consistent. Deviations at irregular times during the move can render the shaper ineffective. This is the reason the bandwidth of a controller is a factor in how effective a shaper can be. One may argue that a low bandwidth controller won't put high frequency energy into the system in the first place, so that canceling vibration at those frequencies is not an issue. If the gain at that frequency were zero, then this would be true. However, this is never the case, and modes that have very high gains do not need much excitation to cause a lot of vibration. We will see in the next section that for highly excitable modes, such as the fifth and sixth modes of MACE, the vibration is still an issue even for low bandwidth controllers.

The bandwidth of the controller determines how closely an actuator can follow a command and determines the consistency of the move. A higher bandwidth controller will be more able to follow high frequency moves since its frequency response will be higher in those frequency ranges. Also it will be more able to overcome inconsistencies of the system (friction, disturbances, etc.). This makes for a more robust and consistent move. This is also very important in the precise implementation of impulse sequences. It follows, then, that the bandwidth of the gimbal controller can determine how effective a shaper is in reducing residual vibration. Since

the gimbal is the cause of the vibration in the bus, a stiffer gimbal controller will more precisely apply inputs to the bus. Because the impulses require very precise amplitudes, this determines then how much vibration we can cancel in the higher modes. We will now look at results from shaping experiments done with different controllers.

5.8.2 Designing different bandwidth controllers

The controller used in the experiments thus far was designed to have a bandwidth of 10Hz as mounted to a rigid frame. This means that the gain of the closed loop transfer function is .707 at 10Hz. Bandwidth becomes an ill-defined term for a PD controller once the gimbal is attached to the rest of MACE because there are now unmodeled modes which are within the bandwidth. The controller was designed for the gimbal itself, not for the gimbal mounted to the bus assembly. If we look on the transfer function plot for the 10Hz bandwidth controller (figure 5.25), we see the peaks and valleys before the 10Hz point. In this case, the closed loop transfer function crosses the .707 point more than once, so it is difficult to define bandwidth here. Moreover, the dynamics of the system have changed such that the previous .707 crossing point at 10Hz has shifted due to the addition of a zero. Thus, we will use the term bandwidth as a measurement of the relative strength or stiffness of the controllers.

Both a 3Hz bandwidth and 20Hz bandwidth controller were designed in addition to the old 10Hz bandwidth controller. A summary of the parameters of the 3 existing controllers is shown in table 5.1.

All three are basically PD controllers with some stabilizing features in the loop. The 3Hz bandwidth controller did not require a delay buffer as there was enough gain and phase margin to account for the delay of the computer processor board. This controller is very weak but also very stable. The 20Hz controller employed the delay buffer and also required a notch filter in the loop. A mode at 85Hz crossed the gain margin in closing the loop and went unstable. A second order Butterworth notch filter with corner frequencies at 80Hz and 90Hz proved to be an effective solution to the problem. This controller is stable and very stiff. The closed loop transfer functions from the angle command to the encoder angle output are shown in figure 5.25 for all three controllers.

Parameters	3Hz Bandwidth	10Hz Bandwidth	20Hz Bandwidth
K_p (volts/rad)	20	260	975
K_v (volts/rad/s)	1.7	7.3	16.8
Delay Buffer	no	yes	yes
Notch Filter	no	no	yes

TABLE 5.1: Summary of three different bandwidth controllers

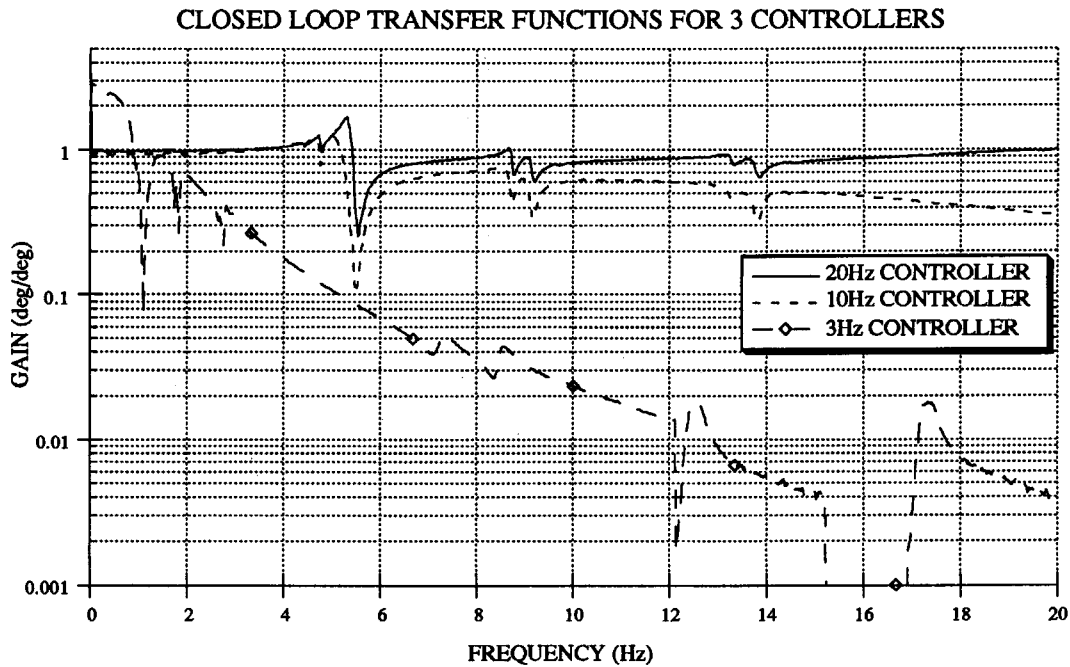CLOSED LOOP TRANSFER FUNCTIONS FOR 3 CONTROLLERS

FIGURE 5.25: Closed loop transfer functions of commanded angle to encoder output for three different controllers.

5.8.3 Effectiveness of shaping on different controllers

As we have discussed, the bandwidth of the controller can determine how effective a shaper is in canceling vibration. This is because the higher bandwidth controller follows the move more closely and is more true to the command that the shaper demands. The same inputs, unshaped and shaped, were employed with all three controllers. The original .53 second 20° slew was used. Five runs of the data were recorded for each controller, and the Fast Fourier Transform of the residual vibration was taken for each and averaged. The results for the three controllers are shown in figures 5.26 - 5.28. The 10Hz controller response is one we've already seen.
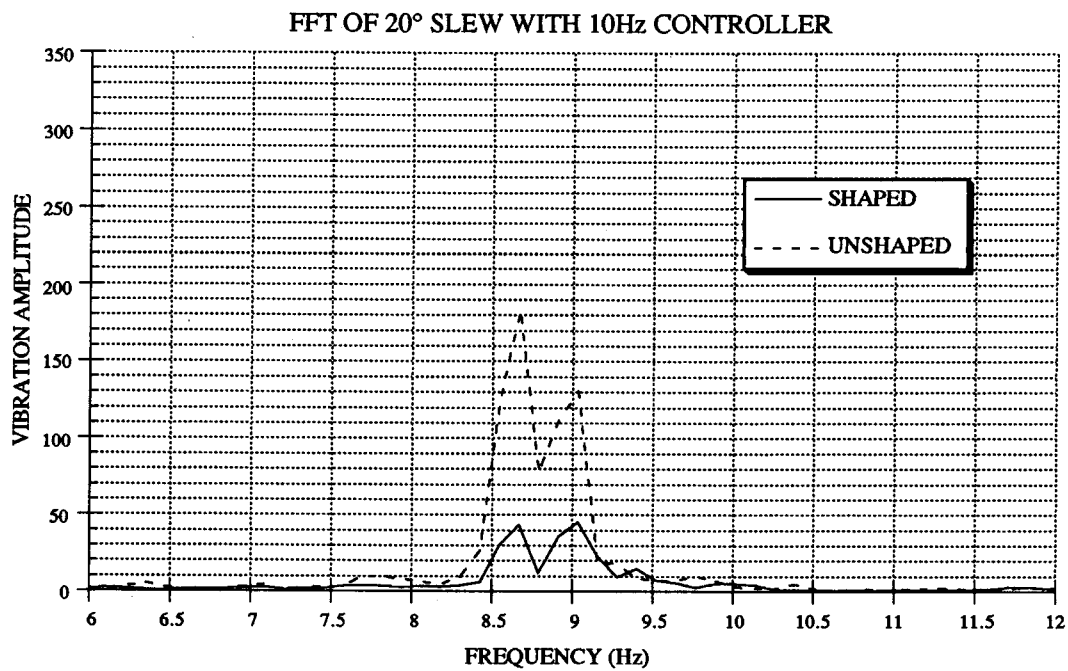
FFT OF 20° SLEW WITH 10Hz CONTROLLER

FIGURE 5.26: Closeup view of FFT of residual vibration for 10Hz
controller. 20° slew is shaped for two modes (8.68, 9.13Hz).

FFT OF 20° SLEW WITH 3Hz CONTROLLER
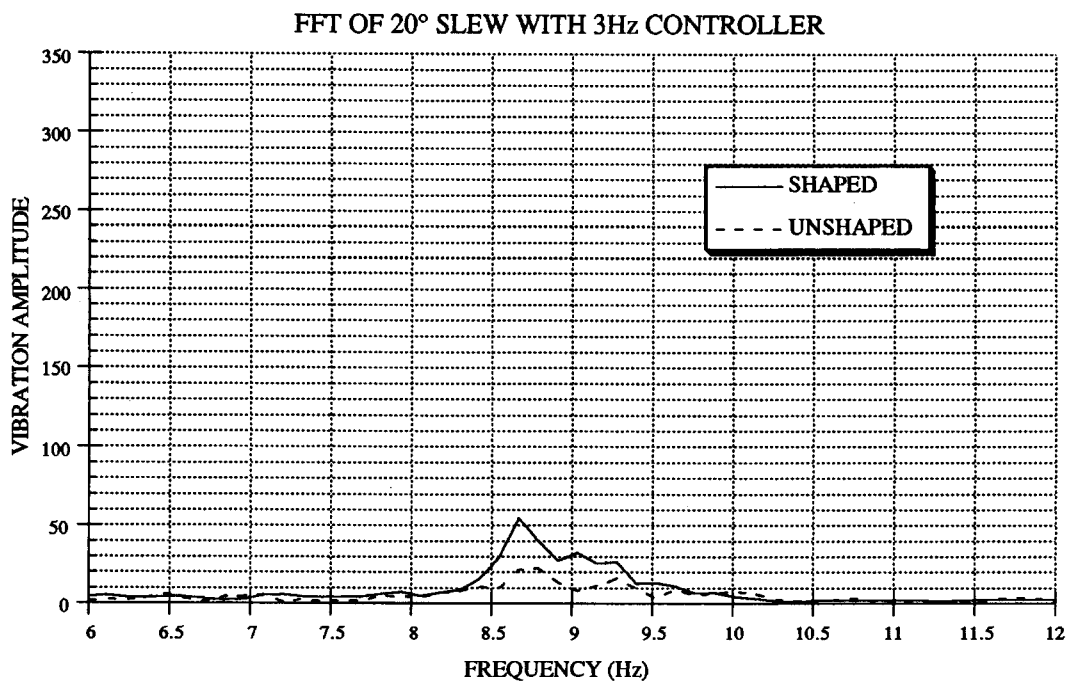

FIGURE 5.27: Closeup view of FFT of residual vibration for 3Hz
controller. 20° slew is shaped for two modes (8.68, 9.13Hz).

FFT OF 20° SLEW WITH 20Hz CONTROLLER

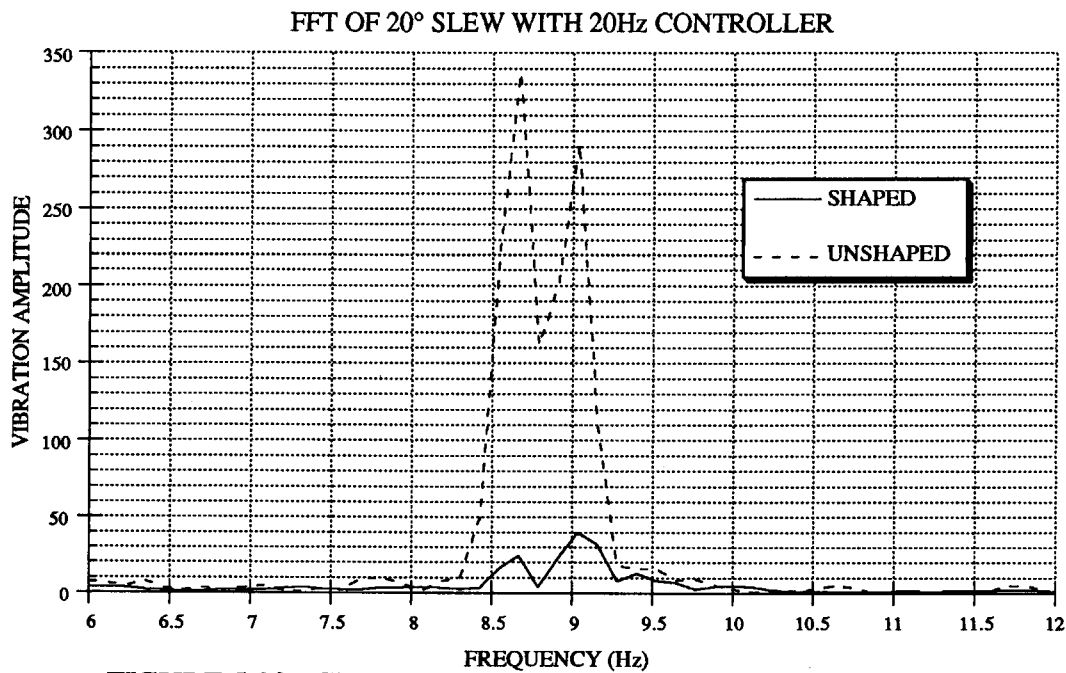**FIGURE 5.28**: Closeup view of FFT of residual vibration for 20Hz
controller. 20° slew is shaped for two modes (8.68, 9.13Hz).

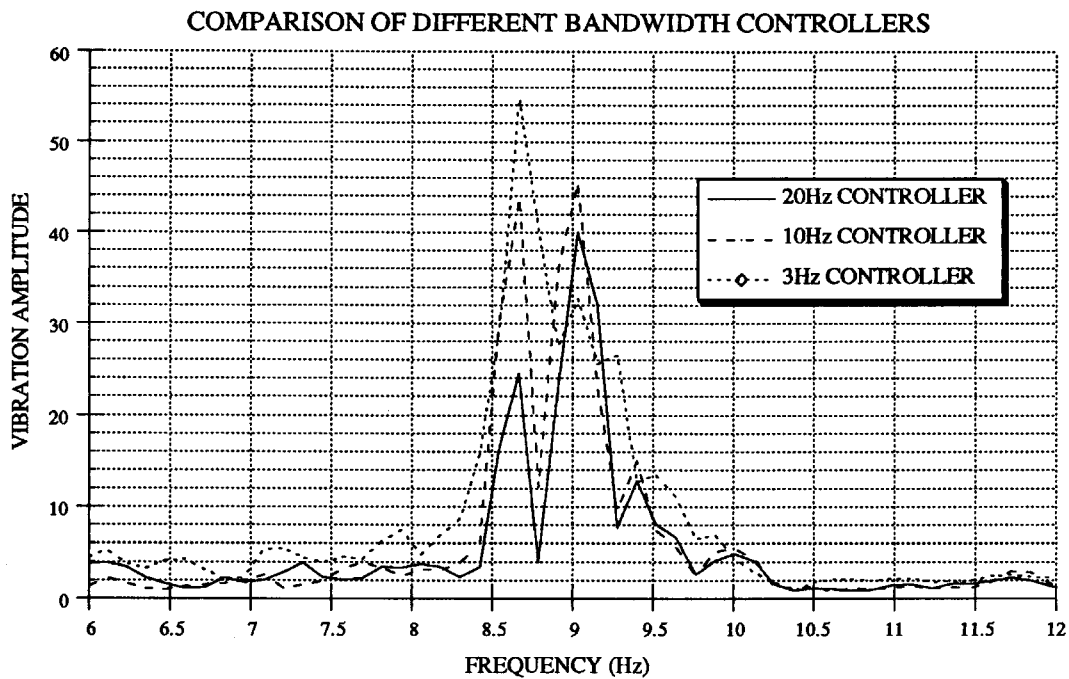COMPARISON OF DIFFERENT BANDWIDTH CONTROLLERS

FIGURE 5.29: A comparison of residual vibration amplitudes in
the 6 to 12Hz region for three different controllers. Same 20° slew
is shaped for two modes in each case (8.68, 9.13Hz)

It is interesting to note that, in using the 3Hz bandwidth controller, we actually incur more vibration in the 8-10Hz range when the move is shaped. This is a case where the controller, as seen, has very little authority to put energy into these modes whether shaped or unshaped. The frequency response of the controlled plant is very low in this range. However, the amplitude of these modes are very high, and are nevertheless excited by the 3Hz controller. The controller has a hard time trying to follow the shaped move because of its low feedback gains. In fact, for a 20° command, the controller can only push the gimbal up to a steady state angle of 16°. Therefore, the unshaped move shows little vibration in this range. It is a noteworthy fact, however, that the shaped move has a detrimental effect on the vibration cancellation. We can conclude that the controller could not follow the move closely enough to have any impact on those modes at all. The extra vibration comes from the fact that the move is longer and more inconsistent. This gives more chance for system disturbances or inconsistencies to add high frequency energy to the resulting output.

The 20Hz bandwidth controller shows more promising results. As shown in the figure, the fifth and sixth modes have higher unshaped amplitudes than the other controllers. This is due to the same reason that a shaped move puts less energy into higher modes. The move is quicker, crisper, and faster such that the profile has more high frequency components. The frequency response of the controller in this range is nearly 1 for this controller, so it can follow the shaped moves fairly closely. The shaped amplitudes are about 7% and 14% of the unshaped amplitudes in the fifth and sixth modes. This is still not the level of performance that we saw on the frequency response experiments, but it constitutes a

significant improvement over the lower bandwidth controllers. Although the controller is more true to the demanded shaped move, there are still the nonlinearities associated with a 20° slew such that all the vibration cannot be canceled.

Not only is the higher bandwidth controller an improvement in terms of percentage vibration reduction, but it also has the absolute least residual vibration. A close-up of the 8-10Hz region for the FFT's of the shaped responses of the three controllers is shown in figure 5.29. The plot reveals that, even in absolute terms, the 20Hz controller performed the best out of the three. This is despite the fact that the unshaped slew caused much more vibration. The 20Hz controller is a win in both percentage cancellation and absolute residual amplitude.

5.8.4 Conclusions

We have just touched on a topic that has been mostly ignored in past research on input shapers. That is the role of the controller in determining the effectiveness of a shaping algorithm. We have seen here through experimental results that the controller does determine how effective an impulse shaper can be in this application. The 20Hz bandwidth controller was shown to be more effective in canceling vibration in the 8-10Hz range than either the 3Hz or 10Hz bandwidth controllers. The 3Hz controller even showed a slight detrimental effect on the shaped response. Thus far we have only dealt with bandwidth of PD controllers. Most likely, higher order controllers will also have an effect on the shaper effectiveness. The more consistently and precisely a shaped command is input into the system, the

more effective an impulse shaper can be. A more sophisticated pointing controller for the MACE gimbal should show an improvement in vibration cancellation.

5.9 Closure

In this chapter, we have looked at various hardware experiments to determine the effect of an impulse shaper on the residual vibration of the MACE test article. We began by defining the performance metric. We then went on to look at frequency response data with the shaper in the system. These proved to be very effective in canceling unwanted vibration and followed the theoretical data very closely. The time histories of slews to 20° showed less success in percentage vibration reduction. The first bending mode was effectively canceled, but the higher modes, specifically the fifth and sixth modes between 8 and 10Hz showed significant amplitude even in the shaped runs. A look at more robust impulse shapers showed that nothing in the realm of linear impulse shaping seemed to be able to overcome the nonlinearity associated with a large angle slew. The most simple impulse shaper was just as effective as any of the more complicated and more robust sequences. Slews done for different angles at the same maximum velocity showed that this nonlinearity is a function of the size of the slew. For a one degree slew, the response looked similar to that of the transfer function data.

We then looked at how the controller in the system can change the effectiveness of an impulse shaper. Three different bandwidth controllers were designed and tested with the same set of slews. The results showed

that a higher bandwidth controller is more effective in canceling vibration at higher frequencies. This is because higher bandwidth controllers will more accurately and consistently follow the move demanded by the impulse shaper, which tends to be more irregular and have high frequency content. The 20Hz bandwidth controller was found to be most effective in percentage reduction and even in absolute terms in leaving the least amount of residual vibration.

CONCLUSIONS AND FUTURE WORK

Chapter 6

6.1 Conclusions

We have investigated the issues involved with implementing impulse command shapers on a large flexible space structure. There was a need to do this because of a lack of real experimental data to verify the effectiveness of impulse shaping on complex multiple mode systems. My contribution to the field of input shaping has been to answer some questions about which qualities of impulse shaping work well and which ones don't. I also suggest ways in which to make shaping more effective in implementation.

In Chapter 2, we discussed the theoretical background of the impulse sequences. The zero vibration constraint equations are derived from the response of second order systems to impulses. Derivative constraints are added to give the sequence more robustness to variations in frequency and damping ratio. We discussed methods of generating sequences for multiple mode systems and contemplated the tradeoffs between the convolution

method and the direct solution method. Some suggestions were then made on finding the most efficient sequence for particular applications. The variables that were considered are: the number of modes to shape, direct solution versus convolution, and the number of impulses per mode. These can be used in our favor to find the sequence that best suits a particular application.

The testbed for the experiments, MACE, was discussed in Chapter 3. MACE is a NASA/MIT active control experiment that is scheduled to fly on the space shuttle in the summer of 1994. Its goal is to provide a platform for investigating zero gravity dynamics of a large space structure which utilizes Controlled Structures Technology. A description of the Development Model hardware was provided. Some results from dynamic testing were presented and a modal description of the test article was presented. We then went on to detail some of the controller issues in the gimbal actuator and the AC-100 computer system. The MACE test article was found to be a very suitable testbed for the goals of this research.

Non-linear simulation was the topic of Chapter 4. DISCOS was used as a tool for verifying the effectiveness of input shaping on both open loop and closed loop configurations of MACE. The kinematic non-linearity due to changes in the configuration of the plant was discussed. The frequency change in the structure was shown to be a hindrance in the canceling of the first mode.

The experimental data was presented in Chapter 5. It was found that in frequency response tests, impulse shaping worked nearly to the level predicted by theory. Insensitivity curves for both experimental and theoretical data were shown to correlate well. Time histories of smooth

profile slews showed, however, that the shaping did not work as well for higher modes when the angle of the slew became large (> 1°). Many "nonlinearities" were analyzed to be the cause of the extra vibration, but not one was found to be a large factor. It was concluded that the large amplitudes of the slew cause the structure to no longer act linearly. The larger slews introduce more total energy into the system and cause the structure to deflect to amplitudes that take it out of the linear approximation range. We then ended the chapter by discussing the effect of higher and lower bandwidth controllers on the shaping method. It was determined that the shaped inputs require more precision from the actuator, and therefore the higher bandwidth controller was much more effective in implementing the impulse shaper. The lower bandwidth controller was not only ineffective, but contributed more amplitude to the residual vibration at higher frequencies.

The conclusions drawn in Chapter 5 will have the most impact on impulse shaping technology. We have always been weary of how impulse shaping would work on complicated nonlinear systems. It has been shown here how effective it can be. It certainly shows an improvement over unshaped moves in most configurations especially in the lower frequencies But as can be seen from higher frequency results, it doesn't meet expectations for large angle slews. The effectiveness of the shaper was directly correlated to the slew angle. We saw that a 1° slew showed similar effectiveness to that shown by small angle frequency response experiments. Larger slews exhibited more shaped residual vibration. Also, a correlation was found between the bandwidth of the controller and the effectiveness of shaping. A good rule of thumb we may take away from this is that the bandwidth of controller should be as high as the frequency we're trying to cancel. A 3Hz bandwidth

controller was found to have no effect on trying to cancel a 9Hz mode, while a 20Hz controller was more effective.

Also, we have seen a comprehensive review of the present status of impulse shaping theory. The tradeoffs between the different methods are described, and suggestions on how find the most efficient shaper are given. This paper will hopefully stand as a resource for users to review the options available in implementing impulse shaping.

6.2 Suggestions for MACE Project

I regret not being able to stay on the MACE project to see it to completion. Seeing years of work come together would have been a gratifying experience. I am comforted by the fact that the project is in the hands of some very competent and talented people at SERC. I would like to leave my impressions and suggestions for the MACE project, however.

As discussed in chapter 3, there were some problems with the gimbal hardware and the AC-100 computer. The gimbal had structural frequencies whose amplitudes were high enough to require a lowpass filter in the control loop. Hopefully, this problem will be solved in the second generation gimbal design. The AC-100 computer, although a very user friendly environment, may present problems with processing delay when dealing with multi-input, multi-output systems. For example, two encoders could not be read at the same time at the current 1KHz servo rate. Also, some of the more complicated direct solution impulse sequences could not be implemented because of processing delay. A new processor board or some further investigation by Integrated Systems would be welcomed. As MACE moves on

to higher order controllers, the stability of the computer will become more crucial. Also, the original specifications for the slewing size of the gimbal have not been met. Presently, the gimbal is constrained to move ±30° by its own design. The suspension system constrains that movement further once the gimbal is attached to the bus to < ±20°. A larger slewing angle can be more useful in studying the non-linearity of the system and the gravity effects of a cantilevered payload. Considerations for a new suspension system or a lighter payload should be given.

As far as impulse shaping, much can be learned from the results in chapter 5. As discussed, a high bandwidth controller is more responsive to the needs of impulse shaping, and hence will yield more of the vibration reducing characteristics of the shaper. Since thorough dynamic testing of the test article will be done both on earth and in space, the modal frequencies can be identified fairly accurately. Also, the frequencies do not seem to shift very much from move to move, at least in the range of motion that is possible. This may suggest a shorter sequence in exchange for lack of some robustness. A direct solution sequence for the first four vertical modes plus one for the two horizontal modes around 4.7Hz is an effective and relatively short sequence that can be used. Of course, these frequencies will shift as different controllers are implemented. If the structure were to go into orbit with the current controller, which it probably will not, this is the impulse sequence that should be used. The direct solution sequence is shown below.
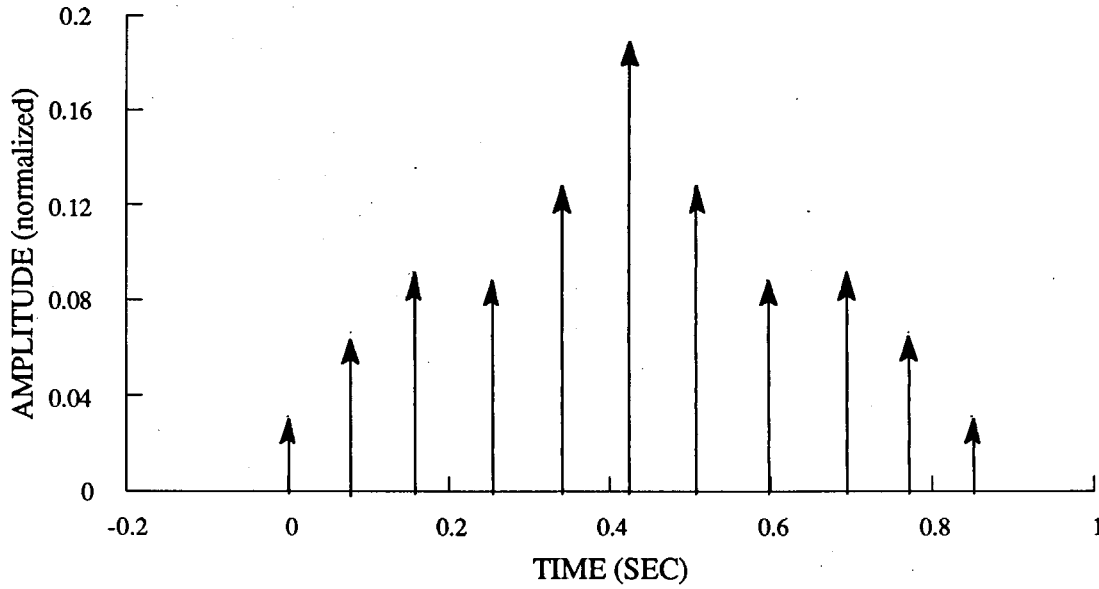
FIGURE 6.1: A five mode direct solution sequence for the MACE
Development Model. (1.75, 4.7, 5.23, 8.68, 9.14 Hz).

TIME (sec)	AMPLITUDE
0	0.0313472
0.0784381	0.0665015
0.155516	0.0916246
0.253105	0.088278
0.340187	0.127523
0.424599	0.189451
0.509011	0.127523
0.596093	0.088278
0.693681	0.0916246
0.770759	0.0665015
0.849198	0.0313472

TABLE 6.1: Listing of impulse times and amplitudes for
impulse sequence in figure 6.1.

Most of all, experimental data needs to be continually gathered on various combinations of shapers and controllers. Although many megabytes of data have been recorded, there are so many variables to tune that it's hard to imagine that a full optimization has been achieved.

6.3 Future Work

My research has answered many of the questions in the impulse shaping field. There is much room for more research on the topic. Some suggestions are presented here

As shown in this work, the controller is something that must be dealt with in implementing shapers. Further investigation into this topic may reveal a method of integrating the design of the controller with the capabilities of the impulse shaper. For example, more overshoot from the controller may be tolerated because of the vibration reducing characteristic of the shaper. A framework can be created in which the design of the filter and the controller can be simultaneously addressed. An even further extension of this topic may be to incorporate the shaper inside the control loop. Currently this is not possible due to the phase lag inherent in an impulse shaper. A closed loop implementation will work not only to cancel vibration caused by the move, but also vibration caused by disturbances in the system.

Impulse shapers work to cancel residual vibration but do not affect the vibration during the move. In tracking applications in space, the vibration during the move is equally important. A new formulation of the shapers that addresses this issue could be helpful to the MACE project.

An investigation into a non-linear extension of impulse shaping would be a rewarding research area. The results from chapter 5 showed that non-linearities limited the effectiveness of the shaper for higher frequency modes. Although some suggestions were made to help the problem, the non-linearities were not directly addressed. A non-linear formulation of the vibration constraint equations or an extension of the existing theory to approximate non-linear behavior would be a worthy study.

Further investigation of the formulation of direct solution multiple mode sequences is needed. The complexity and sometimes inability of the method to generate solutions makes it difficult to use for some applications. A closed form solution of this method would prove very beneficial.

Finally, more comparison studies need to be conducted to illustrate the advantages of impulse shaping over other types of input shaping. This examination could lead to developments of shaping algorithms that utilize many types of input shapers. A shaper that applies impulse shapers for low modes and digital notch filters for high modes is an example. It is clear that the good attributes of the different types of input shaping can be brought together to maximize the efficiency.

REFERENCES

[1] **Asada, Haruhiko, Ma, Zheng-Dong, Tokumaru, Hidekatsu,**
"Inverse Dynamics of Flexible Robot Arms for Trajectory Control,"
Modeling and Control of Robotic Manipulators and Manufacturing
Processes Session, ASME Winter Annual Meeting, 1987.

[2] **Aspinwall, D. M.,**
"Acceleration Profiles for Minimizing Residual Response." *Journal of
Dynamic Systems, Measurement, and Control,* Vol. 102, March1980.

[3] **Bodley, C.S., Devers, A. D., Park, A. C., and Frisch, H. P.,**
"A Digital Computer Program for the Dynamic Interaction Simulation
of Controls and Structure (DISCOS)," NASA Technical Paper No. 1219,
1978.

[4] **Christian, Andrew D.,**
"Design and Implementation of a Flexible Robot," MIT Masters of
Science Thesis and MIT Artificial Intelligence Laboratory Technical
Report #1153, August 1989.

[5] **Crawley, E. F., de Luis, J., and Miller, D. W.,**
"Middeck Active Control Experiment (MACE): Phase A Final Report,"
MIT Space Engineering Research Center #16-90-R, June 1989.

[6] **Eisler, G. R., Segalman, D. J., and Robinett, R. D.,**
"Approximate Minimum-Time Trajectories for Two-link Flexible
Manipulators," American Control Conference, San Diego, California,
May 1989.

[7] **Ewins, D. J.,**
Modal Testing: Theory and Practice, Research Studies Press Ltd.,
Taunton, England, 1984.

[8] **Farrenkopf, R. L.,**
"Optimal Open-Loop Maneuver Profiles for Flexible Spacecraft,"
Journal of Guidance and Control, Vol. 2, No. 6, Nov.-Dec. 1979.

[9] **Franklin, Gene F., Powell, J. David, and Workman, M. L.,**
Digital Control of Dynamic Systems, Addison-Wesley Publishing
Company, Inc., Reading, MA, 1990.

[10] **Hyde, James, M.,**
"Multiple Mode Vibration Suppression in Controlled Flexible Systems,"
MIT Masters of Science Thesis and MIT Artificial Intelligence
Laboratory Technical Report #1295, May 1991.

[11] **Kienholz, David A.,**
"A Pneumatic/Electric Suspension System for Simulating On-Orbit
Conditions," American Society of Mechanical Engineers Winter
Annual Meeting, Dallas, Texas, November 1990.

[12] **Meckl, Peter H.,**
"Control of Vibration in Mechanical Systems Using Shaped Reference
Inputs," MIT PhD Thesis and MIT Artificial Intelligence Laboratory
Technical Report #1018, January 1988.

[13] **Miller, David W., Saarmaa, Erik, and Jacques, Robert N.,**
"Preliminary Structural Control Results from the Middeck Active
Control Experiment (MACE)," AIAA Dynamics Specialist Conference,
Dallas, Texas, April, 1992.

[14] **Miller, David W., Sepe, Raymond B., Rey, Daniel, Saarmaa,
Erik, and   Crawley, Edward F.,**
"The Middeck Active Control Experiment (MACE)," Fifth NASA/DOD
Controlled Structures Interaction Technology Conference, Lake Tahoe,
Nevada, March 1992.

[15] **Murphy, Brett R., and Watanabe, Ichim,**
"Digital Shaping Filters for Reducing Machine Vibration," *IEEE
Transactions on Robotics and Automation*, Vol. 8, No. 2, April 1992.

[16] **Nurre, G. S., Ryan, R. S., Scofield, H. N., and Sims, J. L.,**
"Dynamics and Control of Large Space Structures," *Journal of
Guidance and Control*, Vol. 7, No. 5, Sept.-Oct. 1984.

[17] **Padilla, Carlos E.,**
"Mid-deck Active Control Experiment (MACE): Nonlinear modelling
Simulation, and Preliminary Control of the Baseline Test Article,
Final Report," MIT Space Engineering Research Center, August 1990.

[18] **Prucz, Z., Soong, T. T., and Reinhorn, A.,**
"An analysis of Pulse Control for Simple Mechanical Systems,"
Journal of Dynamic Systems, Measurement, and Control, Vol. 107,
June 1985.

[19] **Saarmaa, Erik,**
"MACE DM Dynamic Testing & Modelling," MIT Space Engineering
Center, October 17, 1991.

[20] **Singer, Neil C.,**
"Residual Vibration Reduction in Computer Controlled Machines,"
MIT PhD Thesis and MIT Artificial Intelligence Laboratory Technical
Report #1030, February 1989.

[21] **Singhose, William,**
"Shaping Inputs to Reduce Vibration: A Vector Diagram Approach,"
MIT Bachelor of Science Thesis and MIT Artificial Intelligence
Laboratory Memo No. 1223, March 1990.

[22] **Smith, O. J. M.,**
Feedback Control Systems, McGraw-Hill Book Company, Inc., New
York, NY, 1958.

[23] **Swigert, C. J.,**
"Shaped Torque Techniques." *Journal of Guidance and Control*, Vol. 3,
No. 5, Sept.-Oct. 1980.

[24] **Thorne, James,**
"Design of a Two Axis Precision Gimbal," MIT Bachelor of Science
Thesis, February 1991.

[25] **Turner, James D., and Junkins, John L.,**
"Optimal Large-Angle Single-Axis Rotational Maneuvers of Flexible
Spacecraft," *Journal of Guidance and Control*, Vol. 3, No. 6, Nov.-Dec.
1980.

[26] **Tzes, Anthony P., Englehart, Matthew J., and Yurkovich,
Stephen,**
"Input Preshaping With Frequency Domain Information For Flexible-
Link Manipulator Control," AIAA Guidance, Navigation and Control
Conference, August 1989.

[27] **Tzes, Anthony P., and Yurkovich, Stephen,**
"Application and Comparison of On-Line Identification Methods for
Flexible Manipulator Control," *Proceedings 1989 International
Conference on Advanced Robotics*, Columbus, OH, June1989.

This blank page was inserted to preserve pagination.

REPORT DOCUMENTATION PAGE

1. AGENCY USE ONLY (Leave blank)	2. REPORT DATE	3. REPORT TYPE AND DATES COVERED
	June 1992	technical report

4. TITLE AND SUBTITLE

Shaping Inputs to Reduce Vibration in Flexible Space Structures

5. FUNDING NUMBERS

N00014-86-K-0685

6. AUTHOR(S)

Kenneth Wonuk Chang

7. PERFORMING ORGANIZATION NAME(S) AND ADDRESS(ES)

Artificial Intelligence Laboratory
545 Technology Square
Cambridge, Massachusetts 02139

8. PERFORMING ORGANIZATION REPORT NUMBER

AI-TR 1368

9. SPONSORING / MONITORING AGENCY NAME(S) AND ADDRESS(ES)

Office of Naval Research
Information Systems
Arlington, Virginia 22217

10. SPONSORING / MONITORING AGENCY REPORT NUMBER

AD-A279877

11. SUPPLEMENTARY NOTES

None

12a. DISTRIBUTION / AVAILABILITY STATEMENT

Distribution of this document is unlimited

12b. DISTRIBUTION CODE

13. ABSTRACT (Maximum 200 words)

A theoretical background of impulse shaping is presented along with some insight into the methods of calculating multiple mode sequences. The Middeck Active Control Experiment (MACE), an MIT/NASA space shuttle experiment, is then described as the testbed for the experiments. A nonlinear simulation is used to verify the effectiveness of these shapers on a model of MACE. Finally, hardware experimental results are presented and analyzed.

Some conclusions were derived from the results of testing. First, it was found that the shaper was effective in canceling the slowest frequency of the structure, but was less successful in the higher modes. Second, large angle movements decreased the effective vibration cancellation. Third, although methods exist which can increase the robustness of an impulse shaper, none were found to aid in canceling the effects of nonlinearities caused by large angle moves. Fourth, the bandwidth of the controller was found to be closely associated with the effectiveness of the shaper.

14. SUBJECT TERMS (key words)

shaping, mace, vibration, discos, modes

15. NUMBER OF PAGES

130

16. PRICE CODE

17. SECURITY CLASSIFICATION OF REPORT	18. SECURITY CLASSIFICATION OF THIS PAGE	19. SECURITY CLASSIFICATION OF ABSTRACT	20. LIMITATION OF ABSTRACT
UNCLASSIFIED	UNCLASSIFIED	UNCLASSIFIED	UNCLASSIFIED

Scanning Agent Identification Target